Differential pairings of MAT1-1-1 and MAT1-2-1 protein variants with heteromorphic tertiary structures produced simultaneously by *Ophiocordyceps sinensis* strains

Xiu-Zhang Li [1], Yu-Ling Li [1], Wei Liu [2], Jia-Shi Zhu [1]*

[1] State Key Laboratory of Plateau Ecology and Agriculture, Qinghai Academy of Animal and Veterinary Sciences, Qinghai University, Xining, Qinghai 810016, China

[2] Institute of Immunology, Army Medical University, Chongqing, 400038, China

* Corresponding author

E-mail: zhujosh@163.com (JSZ)

Abstract

The MATα_HMGbox domain in the MAT1-1-1 protein and the HMG-box_ROX1-like domain in the MAT1-2-1 protein play essential roles in DNA binding and regulating the transcription of genes that control sexual reproduction in *Ophiocordyceps sinensis*. Previous studies have documented differential occurrences, differential transcription, and alternative splicing of the *MAT1-1-1* and *MAT1-2-1* and pheromone receptor genes in *Hirsutella sinensis* (Genotype #1 among 17 genome-independent *O. sinensis* genotypic fungi). This study further revealed that the DNA-binding domains of the paired MAT1-1-1 and MAT1-2-1 proteins derived from each of the 20 *O. sinensis* strains exhibit heteromorphic tertiary structures, as predicted by AlphaFold 3D structural modeling. The differentially paired mating proteins, characterized by different truncations, 1–4 amino acid substitutions at distinct sites, altered hydrophobicity and secondary structures, and heteromorphic tertiary structures, indicate divergency in the fungal origins of the mating proteins within the mycologically and genetically impure *O. sinensis* strains. These findings support the hypothesis of *O. sinensis* self-sterility and are likely ensure the fidelity and genetic diversity of heterothallic or hybrid reproduction throughout the lifecycle of the *Cordyceps sinensis* insect–fungal complex.

Keywords: MATα_HMGbox domain of the MAT1-1-1 protein; HMG-box_ROX1-like domain of the MAT1-2-1 protein; heteromorphic primary, secondary, and tertiary structures of proteins; *Ophiocordyceps sinensis* strain; the *Cordyceps sinensis* insect−fungal complex; sexual reproduction; heterothallism; hybridization

1. Introduction

Natural *Cordyceps sinensis*, also known as Chinese cordyceps (non-Latin term) or DōngChóng XiàCǎo 冬虫夏草 in Chinese, exists only in high-altitude alpine meadows (3,000−5,000 m), which contributes to its natural scarcity. It has a centuries-long history of clinical application in health maintenance, characterized by the dual reinforcement of "*YIN* 阴" and "*YANG* 阳", as well as in disease amelioration, postillness and postoperative recovery, and antiaging therapy [1−4]. Modern science is increasingly allowing researchers to elucidate the complex biochemical mechanisms (*e.g.*, immunomodulation, anti-inflammatory activity, antioxidant activity, organ protection, hormone-like activity supporting libido and fertility, metabolic (glucose and lipid) regulation, and the enhancement of energy–vitality–stamina, etc.) that underpin these traditional applications, proving its status as a valuable

therapeutic resource, despite the complexity and rarity of this medicinal resource. This natural substance, with its unique therapeutic significance, embodies a remarkable fusion of nature's ingenuity and traditional medicinal wisdom; however, its high value has led to overharvesting, making it a Level-II protected natural substance [5].

Natural *C. sinensis* comprises the fruiting body of *Ophiocordyceps sinensis* and the remains of mummified *Hepialidae* moth larva, which retain a thick body wall with numerous bristles, intact larval intestine, head tissues, and fragments of other larval tissues [6−13]. Dual-fluorescence microscopy has revealed multicellular heterokaryotic microstructures of *C. sinensis* ascospores and hyphae, containing mono-, bi-, tri-, and tetra-nucleate cells [14]. Natural *C. sinensis* exhibits apparent genetic heterogeneity, harboring >90 fungal species from at least 37 fungal genera, as well as 17 genomically independent genotypes of *O. sinensis* that differentially naturally co-occur, the abundance of which undergoes dynamic alterations in different compartments of *C. sinensis* during maturation [6, 9−10,12−13,15−44]. Thus, the Chinese Pharmacopoeia defines this medicinal microecosystem as an insect–fungal complex.

Among the numerous intrinsic co-occurring fungal species [20,31−33,40−41], *Hirsutella sinensis* has been postulated to be the sole anamorph of *O. sinensis* [45], although this hypothetical claim needs to be validated based on all 4 criteria of Koch's postulates. In terms of validation, Wei *et al*. [46] reported a successful artificial cultivation project conducted in an industrial product-oriented setting. Unfortunately, they reported a species contradiction that arose between the anamorphic inoculants of 3 *H. sinensis* strains (GC-biased Genotype #1 of *O. sinensis*) inoculated on *Hepialidae* moth larvae and the genome-independent, sole teleomorphic AT-biased Genotype #4 of *O. sinensis* identified in the fruiting body of cultivated *C. sinensis*.

Since the 1840s, the Latin name *Cordyceps sinensis* has been indiscriminately applied to both the teleomorph/holomorph of the fungus *C. sinensis* and the wild insect–fungal complex, disregarding Edward Doubleday's original identification in 1842 that the insect portion of the natural material belongs to *Agrotis* [47]. This imprecise use of the Latin name has blurred the distinction between the fungus, its host, and the insect−fungal complex, resulting in ambiguity in the scientific literature, commercial trade in the mass market, and governmental regulations worldwide. The fungus was renamed *O. sinensis* in 2007, and *H. sinensis* strain EFCC7287 (GC-biased Genotype #1 of *O. sinensis*) was used as the nomenclatural reference [6,9−10,48−51]. Zhang *et al*. [52] have improperly implemented the "One Fungus=One Name" nomenclature rule set by the International Mycological Association (IMA) and replaced the anamorphic name *H. sinensis* with the teleomorphic name *O. sinensis* according to the

international rule [53−54]. They interpreted *O. sinensis* as a single fungus to fulfill the prerequisite of "One Fungus" of the international rule but did not fully consider the 17 genomically independent genotypes of *O. sinensis* fungi, which differentially coexist in the different compartments of the *C. sinensis* insect–fungal complex. In the present paper, we retain the anamorphic name *H. sinensis* for GC-biased Genotype #1 among 17 genotypes of *O. sinensis* and refer to the genomically independent Genotypes #2–17 fungi as *O. sinensis* based on the taxonomic annotations used in several public depositories, including GenBank and AlphaFold, pending the formal determination and differentiation of the systematic taxonomic positions of these GC- and AT-biased Genotypes #2–17. We also maintain the long-standing use of the traditional name *C. sinensis* for both wild and cultivated insect–fungal complexes because the 2007 renaming of *C. sinensis* to *O. sinensis*, which is based on *H. sinensis* strain EFCC7287 as the nomenclatural reference, did not address the long-standing, indiscriminate application of the Latin name to the insect–fungal complex [9−10,48,53,55]. Nevertheless, this imperfect and temporarily necessary practice will likely be revised in the future through the differential use of proprietary and exclusive Latin names for the multiple genome-independent genotypes of *O. sinensis* fungi and the insect–fungal complex as a unique medicinal entity.

The sexual reproductive behavior of ascomycetes is controlled by transcription factors encoded at the mating-type (*MAT*) locus, which constitute the key regulatory mechanism governing mating type recognition and compatibility, and the development of fruiting bodies and sexual reproductive structures and cells such as ascocarps and ascospores [56−63]. The reproductive behavior of *O. sinensis* depends on the synergistic interplay of 2 core mating proteins, the *MAT1-1* and *MAT1-2* idiomorphs. The MAT1-1-1 protein harbors a mating-type alpha high mobility group box (MATα_HMGbox) domain, whereas the MAT1-2-1 protein contains the high mobility group box ROX1-like (HMG-box_ROX1-like) domain [14,51,59,64−65]. These 2 domains of mating proteins play essential roles in regulating the expression of genes associated with sexual reproduction. Li *et al*. [66−68] documented the differential occurrence, differential transcription, and alternative splicing of mating-type and pheromone receptor genes in the genomes of *H. sinensis* strains, challenging the prior self-fertilization hypothesis for *H. sinensis via* homothallism or pseudohomothallism. Instead, these discoveries support self-sterility consistent with a heterothallic or hybrid lifestyle, indicating the necessity of compatible sexual partners to complete sexual reproduction within the *Cordyceps sinensis* insect–fungus complex. Moreover, Li *et al*. [51,69] reported the heteromorphic tertiary structures of the DNA-binding domains of the full-length MAT1-1-1 and MAT1-2-1 proteins in wild-type *C. sinensis* isolates, which might be generated by either GC-biased

Genotype #1 (*H. sinensis*) or Genotype #3 of *O. sinensis*, further underscoring the complex heterothallic or hybrid sexual reproduction of *O. sinensis*.

Variations in the DNA-binding domains of the 2 mating proteins, arising from diverse amino acid substitutions, induce changes in their tertiary structures and a synergistic interaction between the 2 idiomorphic mating proteins. These proteins are derived from numerous mycologically impure, wild-type *C. sinensis* isolates [51], which were characterized by Prof. Zhang Y-J and his associates [7,52,70−72]. The N- and/or C-terminal truncations and amino acid substitutions of the mating proteins reported by Prof. Yao Y-J and his collaborators [14,36] were further analyzed in this study to clarify the protein structural basis of *O. sinensis* sexual reproduction. The changes in the primary, secondary, and tertiary structures of the MATα_HMGbox and the HMG-box_ROX1-like domains of the MAT1-1-1 and MAT1-2-1 proteins were correlated. Critically, the present study investigated the differential pairings of MAT1-1-1 and MAT1-2-1 protein variants generated simultaneously by *O. sinensis* strains to explore their possible heterospecific fungal origins within these heterogeneous *O. sinensis* strains.

2. Materials and Methods

2.1 The MAT1-1-1 and MAT1-2-1 protein sequences from the *O. sinensis* strains

The AlphaFold database provides AI-predicted 3D structural morphs for 20 truncated MAT1-1-1 proteins (AGW27517–AGW27536) and 5 truncated MAT1-2-1 proteins (AGW27543, AGW27548, AGW27552, AGW27554, and AGW27555) derived from 20 *O. sinensis* strains [14]. Li *et al*. [36] reported that 11 of the 20 strains were obtained from fresh caterpillar body specimens collected from various *C. sinensis* production regions on the Qinghai-Tibet Plateau, marked as "TS" in Table 1. The remaining 9 *O. sinensis* strains were from the cultures of monoascospores of *C. sinensis* insect–fungal complexes that were collected from a single production region (Maqên, Guoluo, Qinghai Provence of China), which are marked as "SS" in Table 1.

The MAT1-1-1 protein sequences of different lengths were encoded by the *MAT1-1-1* cDNAs that were amplified from total RNA extracted from the *O. sinensis* strains using the primer pair *m1F3/m1R3*, while the *MAT1-2-1* cDNAs were amplified using the primer pair Mat1-2F/Mat1-2R (Figures S1–S2) [14,70]. Li *et al*. [36] deposited the internal transcribed spacer (ITS) sequences into GenBank for 15 of the 20 *O. sinensis* strains, including 10 homogeneous strains shown in brown in Table 1 that reportedly harbor only the GC-biased Group-A ITS sequences and 5 other strains shown in red in Table 1 that were characterized as heterogeneous, containing both GC-biased Group-A and AT-biased Group-B ITS

sequences. The remaining 5 *O. sinensis* strains shown in black in Table 1 lack ITS sequence information in GenBank.

Table 1. *O. sinensis* strains and their tissue sources [36], GenBank accession numbers for the internal transcribed spacer (ITS) nucleic acid sequences and mating proteins, and AlphaFold UniProt codes for the truncated and full-length MAT1-1-1 and MAT1-2-1 proteins derived from the *O. sinensis* strains.

***O. sinensis* strain code**	**Source of strain**	**GenBank accession number**				**AlphaFold UniProt code for the mating protein**	
		ITS nucleotide sequence		**Protein sequence**			
		GC-biased Group-A	**AT-biased Group-B**	**MAT1-1-1**	**MAT1-2-1**	**MAT1-1-1**	**MAT1-2-1**
CS71-1219	SS	JQ900151	—	AGW27534	AGW27554	U3NE87 *	U3NEA9
CS91-1291	TS	JQ900166	—	AGW27523	AGW27543	U3N9T9 ⁋	U3N9W0
CS68-2-1229	SS	JQ900158	—	AGW27528	AGW27548	U3N9T9 ⁋	U3N9W5 ⁑
CS37-295	TS	JQ900169	—	AGW27519	AGW27539	U3N9T9 ⁋	D7F2E9 ♦
CS18-266	TS	JQ900168	—	AGW27520	AGW27540	U3N9T9 ⁋	—
CS560-961	TS	JQ900143	—	AGW27522	AGW27542	U3N6U0	D7F2E3
CS71-1218	SS	JQ900150	—	AGW27533	AGW27553	U3N6U8 †	U3N9X0
CS76-1284	TS	JQ900159	—	AGW27525	AGW27545	U3N919	—
CS561-964	TS	JQ900144	—	AGW27526	AGW27546	U3N7G5	—
CS25-273	TS	JQ900167	—	AGW27527	AGW27547	U3N6U4	—
CS71-1220	SS	JQ900152	JQ900175	AGW27535	AGW27555	U3N6U8 †	U3N9W5 ⁑
CS6-251	TS	JQ900163	JQ900180	AGW27517	AGW27537	U3N9T9 ⁋	U3N6V5
CS34-291	TS	JQ900162	JQ900179	AGW27524	AGW27544	U3N9T9 ⁋	—
CS70-1208	SS	JQ900146	JQ900172	AGW27529	AGW27549	U3NE79 ‡	—
CS68-2-1228	SS	JQ900157	JQ900178	AGW27536	AGW27556	U3N7H7	—
CS68-5-1216	SS	—	—	AGW27532	AGW27552	U3N6U8 †	U3N6W6
CS26-277	TS	—	—	AGW27521	AGW27541	U3N9T9 ⁋	D7F2E9 ♦
CS36-1294	TS	—	—	AGW27518	AGW27538	U3N9T9 ⁋	D7F2E9 ♦
CS70-1211	SS	—	—	AGW27530	AGW27550	U3NE79 ‡	—
CS70-1212	SS	—	—	AGW27531	AGW27551	U3NE87 *	—

Note: The *O. sinensis* strains shown in brown have ITS sequences of Group A; those shown in red have ITS sequences for both Groups A and B; and those shown in black do not have ITS sequences in GenBank [14,36]. "TS" indicates that the *O. sinensis* strains were isolated from the caterpillar body specimens. "SS" indicates that the *O. sinensis* strains were obtained from the cultures of monoascospores that were collected from mature *C. sinensis* insect–fungal complexes. The ITS sequences in dark blue belong to GC-biased Group A (Genotype #1) of *O. sinensis,* and those in light blue belong to AT-biased Group B (Genotype #17) of *O. sinensis* (Tables S1−S2) [10,36]. The GenBank protein accession numbers in green refer to the full-length MAT1-2-1 protein sequences, while the remaining protein accession numbers in pink refer to the truncated mating proteins. AlphaFold codes with the same suffix symbol (*, ⁋, †, ‡, ⁑, or ♦) belong to the same morphs of AlphaFold-predicted 3D structures. Those without a suffix symbol indicate unique 3D structural morphs. "—" signs indicate no recodes of ITS sequences or 3D structural models in GenBank and AlphaFold databases.

2.2 Alignment of the DNA-binding domain sequences of the mating proteins

The amino acid sequences of the MATα_HMGbox domains of the MAT1-1-1 proteins and the HMG-box_ROX1-like domains of the MAT1-2-1 proteins from the *O. sinensis* strains were aligned

using the GenBank Blastp program (https://blast.ncbi.nlm.nih.gov/ (Bethesda, MD, USA), accessed from 18 June 2025 to 31 January 2026).

2.3 Amino acid properties and scale analysis

The amino acid sequences of the DNA-binding domains of the mating proteins were scaled based on the general properties of their side chains (https://web.expasy.org/protscale/; Basel, Switzerland, accessed from 18 May 2025 to 20 October 2025) (Table 3) [51,68−69,73−77]. The MATα_HMGbox domain of MAT1-1 proteins (amino acids 51→225 of the reference sequence AGW27560 derived from the *H. sinensis* strain CS68-2-1229 [14]) and the HMG-box_ROX1-like domain of MAT1-2-1 proteins (amino acids 127→197 of the reference sequence AEH27625 [70]), with additional 9 amino acid residues extending upstream and downstream of the domains to ensure comprehensive coverage, were plotted sequentially with a window size of 9 amino acid residues using the linear weight variation model of the ExPASy ProtScale algorithms [51,68−69,73−75] to generate ExPASy ProtScale plots and predict the potential changes in the hydrophobic properties and secondary structures of proteins related to α-helices, β-sheets, β-turns, and coils. The resulting topological structures and waveforms shown in the ProtScale plots were compared to exploring changes in the hydrophobicity and 2D structural features of the DNA-binding domains of the mating proteins.

2.4 AlphaFold-based prediction of the tertiary structures of the mating proteins

For the analysis of the heteromorphic stereostructures in this study, the 3D structures of the MAT1-1-1 and MAT1-2-1 proteins from *O. sinensis* strains were predicted computationally from their amino acid sequences utilizing artificial intelligence (AI)-driven machine learning technology AlphaFold (https://alphafold.com/, Cambridgeshire, UK; accessed from 18 June 2025 to 20 October 2025) [78−88].

The AlphaFold database provides per-residue model confidence, predicts scores between 0 and 100 using the partial local distance difference test (pLDDT), and assigns a per-residue score to each individual residue [78−81,83−85]. A color-coding scheme based on the pLDDT score is used for the 3D structure to visually represent the confidence levels: residues with very high confidence (pLDDT>90) are shown in dark blue, those with high confidence (90>pLDDT>70) appear in light blue, residues with low confidence (70>pLDDT>50) are shown in yellow, and residues with very low confidence (pLDDT<50) are shown in orange [51,86−87,89].

The main reasons for the low confidence in AlphaFold predictions include the following: (1) Supporting data are insufficient, as the AlphaFold-based prediction relies on the quality of the multiple

188 sequence alignment (MSA). If few homologous sequences are available in a certain region of the MSA,
189 the model will lack sufficient evolutionary information to infer the structure, resulting in low confidence.
190 (2) Some protein regions are inherently flexible under physiological conditions, such as the activation
191 domains of transcription factors, which do not have a fixed 3D structure, leading to low confidence in
192 the predicted structure assigned by AlphaFold. (3) In terms of special structural regions, such as small-
193 molecule binding sites and artificial linkers in fused proteins, the AlphaFold system may have limited
194 predictive power, leading to insufficient confidence in the predictions of complex structures. Thus, the
195 low-confidence regions in AlphaFold predictions are informative flags for highlighting the challenges of
196 prediction and should not be interpreted with excessive confidence.

197 2.5 Correlations of the primary, secondary, and tertiary structures of the DNA-
198 binding domains of the paired MAT1-1-1 and MAT1-2-1 proteins

199 Among diverse AlphaFold 3D structural heteromorphs, the changes in the tertiary structure around
200 the mutation sites within the MATα_HMGbox domains of MAT1-1-1 proteins or the HMG-box_ROX1-
201 like domains of MAT1-2-1 proteins were locally magnified to visualize the subtle 3D variations. Primary
202 sequence variations in the DNA-binding domains of the mating proteins, such as peptide chain
203 truncations and amino acid replacements, were correlated with topological structural and waveform
204 changes in hydrophobicity, α-helices, β-sheets, β-turns, and coils, as presented in the ExPASy ProtScale
205 plots, and with the locally magnified 3D structures around the variation sites. The variant MAT1-1-1 and
206 MAT1-2-1 proteins produced by the *O. sinensis* strains were paired to explore their diverse fungal origins.

207 3. Results

208 3.1 Primary structures of the truncated MAT1-1-1 proteins in *O. sinensis* strains

209 In the alignment with the sequence of the representative authentic full-length MAT1-1-1 protein
210 AGW27560 derived from the *H. sinensis* strain CS68-2-1229 [14], the 20 MAT1-1-1 proteins were
211 differentially truncated at both the N- and C-termini (Figure 1). These truncated proteins of varying
212 lengths were encoded by the cDNAs amplified using the same pair of primers (the forward primer *m1F3*
213 and the reverse complementary primer *m1R3* shown in Figure S1) from the *MAT1-1-1* genes of *O.*
214 *sinensis* strains. The MATα_HMGbox domains of the authentic full-length MAT1-1-1 proteins
215 represented by the protein AGW27560 are located at amino acids 51→225 (shown in pink in Figures 1
216 and S1). The MATα_HMGbox domains of the 20 MAT1-1-1 proteins are truncated at the N-termini and
217 correspond to 9 distinct AlphaFold 3D structural morphs (Figure 2, Table 1).

```
AGW27560 1 MTTRNEVMQRLSSVRADVLLNFLTDDAIFQLASRYHESTTEADVLTPVSTAAASRATRQTKE  62
AGW27528
AGW27535
AGW27530
AGW27534
AGW27522
AGW27525
AGW27526
AGW27527
AGW27536

AGW27560 63 ASCDRAKRPLNAFMAFRSYYLKLFPDVQQKTASGFLTTLWHKDPFRNKWALIAKVYSFVRD  123
AGW27528 1   ------------------------------------------------------------  60
AGW27535 1                                     --------------------------  26
AGW27530 1                                   V--------------------------  27
AGW27534 1                                                -------------  13
AGW27522 1   ------------------------------------------------------------  60
AGW27525 1   ------------------------------------------------------------  60
AGW27526 1   -SSFT-------------------------------------------------------  60
AGW27527 1                 ----------------------------------------------  46
AGW27536 1                                E-- -------------------------  28

AGW27560 124 QIGKDKVSLSYFMSLACPTMTIIEPAAYLNALGWCVQDDDAGSQKLFQDESSANLDQSSL  183
AGW27528 61  ------------------------------------------------------------  120
AGW27535 27  ------------------------------------------------------------  86
AGW27530 28  ------------------------------------------------------------  87
AGW27534 14  ------------------------------------------------------------  73
AGW27522 61  ------------------------------------------------------------  120
AGW27525 61  ------------------------------------------------------------  120
AGW27526 61  ------------------------------------------------------------  120
AGW27527 47  ------------------------------------------------------------  106
AGW27536 29  ------------------------------------------------------------  88

AGW27560 184 LSAEYPSTEIELLSALVNIGYFPDHGADLVERMGSSHSGIMAPRAANCTPPVSYTKEKID  243
AGW27528 121 ------------------------------------------------------------  180
AGW27535 87  ------------------------------------------------------------  146
AGW27530 88  ------------------------------------------------------------  147
AGW27534 74  ------------------------------------------------------------  133
AGW27522 121 ------------------------------------------------------------  180
AGW27525 121 ------------------------------------------------------------  180
AGW27526 121 ------------------------------------------------------------  180
AGW27527 107 ------------------------------------------------------------  166
AGW27536 69  ------------------------------------------------------------  148

AGW27560 244 FINTIRSDPVQATKEILGDCYDETTIKLLGVKSHNVESVDSITHLSMQREYQAPRFFYDY  304
AGW27528 181 ------------------------------------------------------------  240
AGW27535 147 ------------------------------------------------------------  206
AGW27530 148 ------------------------------------------------------------  207
AGW27534 134 ------------------------------------------------------------  193
AGW27522 181 ------------------------------------------------------------  240
AGW27525 181 ------------------------------------------------------------  240
AGW27526 181 ------------------------------------------------------------  240
AGW27527 167 ------------------------------------------------------------  226
AGW27536 149 ------------------------------------------------------------  208

AGW27560 305 SVSYAGMDFGGSNEPVMNLNNLPENETFDIDSPFDLDKILGQSQSEGERTSHLPPSPPHN  364
AGW27528 241 ------------------------------------------------------------  300
AGW27535 207 ------------------------------------------------------------  266
AGW27530 208 ------------------------------------------------------------  267
AGW27534 194 ------------------------------------------------------------  254
AGW27522 241 ----------------------------------------------------------L--  300
AGW27525 241 ------------------------------------------------------------  299
AGW27526 241 ---------------------------------------------------------     296
AGW27527 227 ---------------------------------------------------          277
AGW27536 209 ------------------------------------------------------------  268

AGW27560 365 PLDFYFAF                                                      372
AGW27528 301 -                                                             301
AGW27535 267 -                                                             267
AGW27530 268 -                                                             268
AGW27534 254
AGW27522 301 -                                                             301
AGW27525 299
AGW27526 296
AGW27527 277
AGW27536 269 -                                                             269
```

218

Figure 1. Alignment of the sequences of the query MAT1-1-1 protein AGW27560 derived from *O. sinensis* strain CS68-2-1229 [14] and the 9 truncated MAT1-1-1 proteins (AGW27528, AGW27522, AGW27525, AGW27526, AGW27527, AGW27535, AGW27530, AGW27536, and AGW27534 [14]) that are truncated at both the N- and C-termini. These truncated proteins represent the 20 MAT1-1-1 proteins under 9 AlphaFold 3D structural models (U3N9T9, U3N6U0, U3N919, U3N7G5, U3N6U4, U3N6U8, U3NE79, U3N7H7, and U3NE87, respectively). The MATα_HMGbox domain (amino acids 51→225 in the AGW27560 sequence) is shown in pink, and those outside the domain are shown in blue. The amino acid substitutions are shown in green. The hyphens indicate identical amino acids, and the spaces denote unmatched sequence gaps.

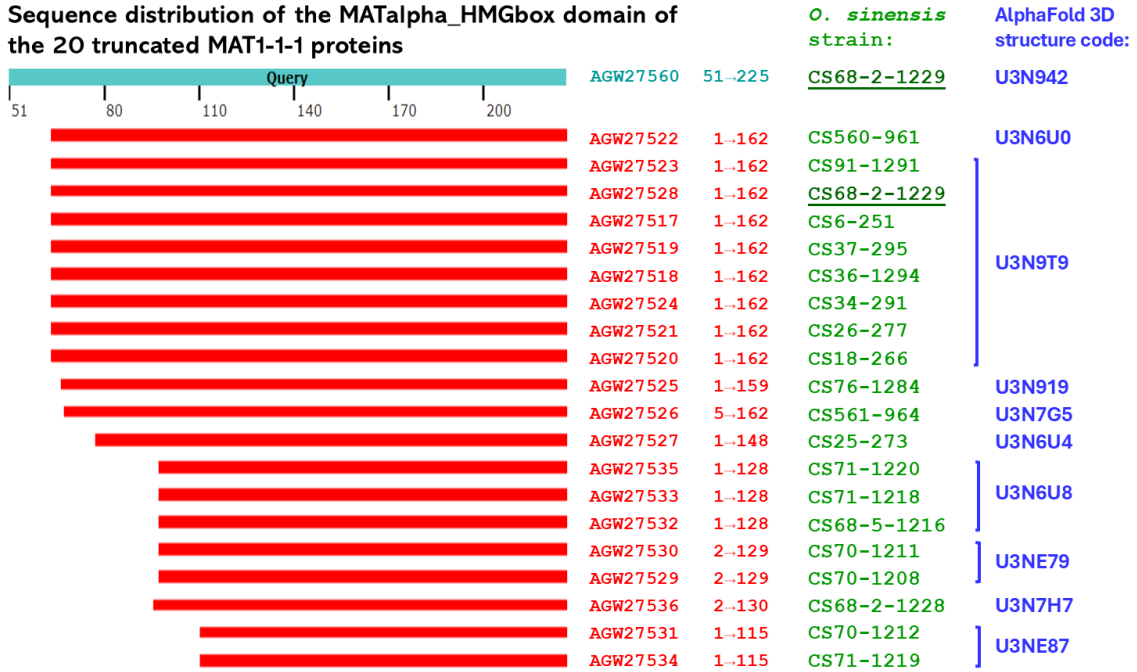

Figure 2. Sequence distribution of the N-terminally truncated MATα_HMGbox domains of 20 MAT1-1-1 proteins derived from *O. sinensis* strains (Table 1). The sequences are aligned with that of the full-length MATα_HMGbox domain (51→225) of the query MAT1-1-1 protein AGW27560 derived from the *H. sinensis* strain CS68-2-1229.

3.2 Primary structures of the truncated MAT1-2-1 proteins in *O. sinensis* strains

The AlphaFold database lists 5 MAT1-2-1 proteins produced by *O. sinensis* strains and are differentially truncated at their C-termini (Figure 3). These truncated MAT1-2-1 proteins of varying lengths are encoded by the *MAT1-2-1* cDNAs amplified using the same pair of primers (the forward primer *Mat1-2F* and the reverse complementary primer *Mat1-2R* shown in Figure S2 [14,70]) from the total RNA extracted from various *O. sinensis* strains. The full-length authentic MAT1-2-1 protein AEH27625 [70], under AlphaFold code U3N942 derived from the *H. sinensis* strain CS2, is used as an alignment reference; it contains an HMG-box_ROX1-like domain at amino acids 127→197, as shown in pink in Figures 3 and S2. In alignment with the HMG-box_ROX1-like domain sequence of the reference protein AEH27625, the domain sequences of the MAT1-2-1 proteins derived from the 5 *O. sinensis* strains are truncated differentially at the C-termini and each contains a tyrosine-to-histidine (Y-

to-H) substitution, contributing to diverse 3D structures under 4 AlphaFold codes (Figure 4). Additionally, the truncated MAT1-2-1 protein AGW27554 contains an additional glutamine-to-threonine (Q-to-T) substitution, as shown in Figure 3.

```
AEH27625 1   MANPINMIPNPQWNATDYEAIWKGLEAQVNPFSQILCLEGDFFRQLDDAAKLFIARKLME  60
AGW27543 1   ------------------------------------------------------------  60
AGW27554 1   ------------------------------------------------------------  60
AGW27555 1   ------------------------------------------------------------  60
AGW27548 1   ------------------------------------------------------------  60
AGW27552 1   ------------------------------------------------------------  60

AEH27625 61  HVQESVLYVNDGNGPDRVYLGAPRHFVVGGGMILQISGYAPYWIRRSVSKVVTATVLAPP  120
AGW27543 61  ------------------------------------------------------------  120
AGW27554 61  ------------------------------------------------------------  120
AGW27555 61  ------------------------------------------------------------  120
AGW27548 61  ------------------------------------------------------------  120
AGW27552 61  ------------------------------------------------------------  120

AEH27625 121 SPKDIKIPRPPNAYILYRKERHHYVKDANPGITNNEISQILGKAWNMESNDVRQKYKDMS  180
AGW27543 121 -----------------------H------------------------------------  180
AGW27554 121 -----------------------H------------------------------------  180
AGW27555 121 -----------------------H--------------------------------    175
AGW27548 121 -----------------------H-------------------------------     175
AGW27552 121 -----------------------H------------------------------      174

AEH27625 181 QQVKQALLEKHPDYQYKPRRPCERRRRRRASPNQNPKQSTSRNAATRDAAISSEDTSTAT  240
AGW27543 181 -----                                                        185
AGW27554 181 ----T                                                         185
AGW27555 175
AGW27548 175
AGW27552 174

AEH27625 241 GDTNTANGF                                                     249
AGW27543 185
AGW27554 185
AGW27555 175
AGW27548 175
AGW27552 174
```

Figure 3. Alignment of the sequences of 5 truncated AMT1-2-1 proteins derived from the *O. sinensis* strains and the reference query of the full-length MAT1-2-1 protein AEH27625 from the *H. sinensis* strain CS2 under AlphaFold code D7F2E9. The amino acids in the HMG-box_ROX1-like domain (amino acids 127→197 in the AEH27625 sequence) are shown in pink, and those outside the domain are shown in blue. The amino acid substitutions are shown in green. The hyphens indicate identical amino acids, and the spaces denote unmatched sequence gaps.

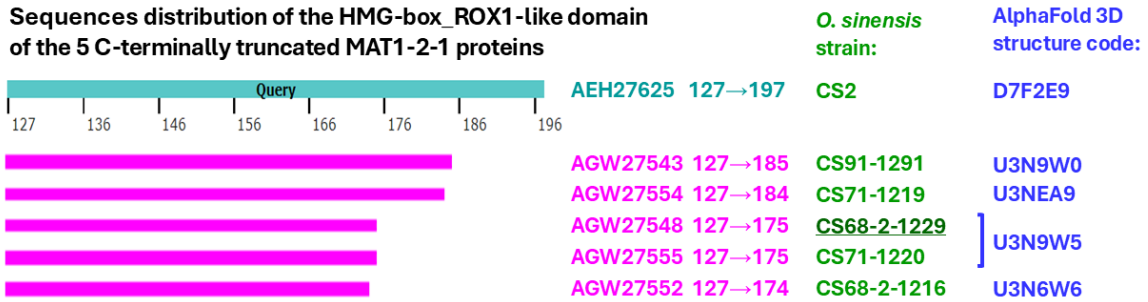

Figure 4. Sequence distribution of the C-terminally truncated HMG-box_ROX1-like domains of 5 MAT1-2-1 proteins derived from the *O. sinensis* strains (*cf.* Table 1). The sequences are aligned with the HMG-box_ROX1-like domain (127→197) of the full-length MAT1-2-1 protein AEH27625 from *H. sinensis* strain CS2.

3.3 Heteromorphic tertiary structures of the MATα_HMGbox domains of the truncated MAT1-1-1 proteins derived from *O. sinensis* strains

This section reports the results of the correlation analyses between changes in the hydrophobicity and structures of the MATα_HMGbox domains of truncated MAT1-1-1 proteins derived from various *O. sinensis* strains, which correspond to 9 AlphaFold codes (Table 1, Figures 1−2), compared to the reference MAT1-1-1 proteins. The reference protein, represented by AGW27560 (derived from the *O. sinensis* strain CS68-2-1229; Table S4), is associated with the AlphaFold code U3N942 [14]. The sequences of the MATα_HMGbox domain (amino acid residues 51→225) were extended by 9 amino acid residues both upstream and downstream of the domains and were used in the sequential ExPASy ProtScale plotting to analyze hydropathy, α-helices, β-sheets, β-turns, and coils with a window size of 9 amino acid residues (*cf*. Section 2.3).

Figure 5 compares the hydrophobicity and structural characteristics of the MATα_HMGbox domains between 2 groups of truncated MAT1-1-1 proteins: (1) the protein AGW27522 (under the AlphaFold code U3N6U0) derived from the *O. sinensis* strain CS560-961; and (2) 8 proteins, AGW27517, AGW27518, AGW27519, AGW27520, AGW27521, AGW27523, AGW27524, and AGW27528 (all under the AlphaFold code U3N9T9), derived from *O. sinensis* strains CS6-251, CS36-1294, CS37-295, CS18-266, CS26-277, CS91-1291, CS34-291, and CS68-2-1229, respectively (Table 1). The reference protein AGW27560 (under AlphaFold code U3N942) is derived from the *H. sinensis* strain CS68-2-1229 [14]. Panel (A) of Figure 5 shows that the MATα_HMGbox domains of both groups of subject proteins exhibit 13-residue truncations at N-termini of the DNA-binding domains. The truncations result in changes in the topological structure and waveform of the ExPASy ProtScale plots, as illustrated in Panels (B)–(F) for hydropathy, α-helices, β-sheets, β-turns, and coils, respectively. Panel (G) shows the 3D structure of the full-length reference protein AGW27560, where the 3 α-helices within the MATα_HMGbox domain form a core L-shaped stereostructure. Panels (H)–(I) illustrate that the N- and C-terminal truncations (*cf*. Figure 1) significantly alter the 3D structures of the proteins under the heteromorphic AlphaFold codes U3N6U0 and U3N9T9, respectively. The N-terminally truncated regions of these variant proteins are located upstream of the core structure of 3 α-helices and may exert a steric auxiliary effect on stabilizing the hydrophobic core structures of the MATα_HMGbox domains [90−91].

Panel (A): Alignment of amino acid sequences of the MATα_HMGbox domains

```
AGW27560  42   ADVLTPVSTAAASRATRQTKEASCDRAKRPLNAFMAFRSYYLKLFPDVQQKTASGFLTT  100
AGW27522  1    ------------------------------------------------------------  37
AGW27517  1    ------------------------------------------------------------  37
AGW27518  1    ------------------------------------------------------------  37
AGW27519  1    ------------------------------------------------------------  37
AGW27520  1    ------------------------------------------------------------  37
AGW27521  1    ------------------------------------------------------------  37
AGW27523  1    ------------------------------------------------------------  37
AGW27524  1    ------------------------------------------------------------  37
AGW27528  1    ------------------------------------------------------------  37

AGW27560  101  LWHKDPFRNKWALIAKVYSFVRDQIGKDKVSLSYFMSLACPTMTIIEPAAYLNALGWCVQ  160
AGW27522  38   ------------------------------------------------------------  97
AGW27517  38   ------------------------------------------------------------  97
AGW27518  38   ------------------------------------------------------------  97
AGW27519  38   ------------------------------------------------------------  97
AGW27520  38   ------------------------------------------------------------  97
AGW27521  38   ------------------------------------------------------------  97
AGW27523  38   ------------------------------------------------------------  97
AGW27524  38   ------------------------------------------------------------  97
AGW27528  38   ------------------------------------------------------------  97

AGW27560  161  DDDAGSQKLFQDESSANLDQSSLLSAEYPSTEIELLSALVNIGYFPDHGADLVERMGSSH  220
AGW27522  98   ------------------------------------------------------------  157
AGW27517  98   ------------------------------------------------------------  157
AGW27518  98   ------------------------------------------------------------  157
AGW27519  98   ------------------------------------------------------------  157
AGW27520  98   ------------------------------------------------------------  157
AGW27521  98   ------------------------------------------------------------  157
AGW27523  98   ------------------------------------------------------------  157
AGW27524  98   ------------------------------------------------------------  157
AGW27528  98   ------------------------------------------------------------  157

AGW27560  221  SGIMAPRAANCTPP                                               234
AGW27522  158  --------------                                               171
AGW27517  158  --------------                                               171
AGW27518  158  --------------                                               171
AGW27519  158  --------------                                               171
AGW27520  158  --------------                                               171
AGW27521  158  --------------                                               171
AGW27523  158  --------------                                               171
AGW27524  158  --------------                                               171
AGW27528  158  --------------                                               171
```

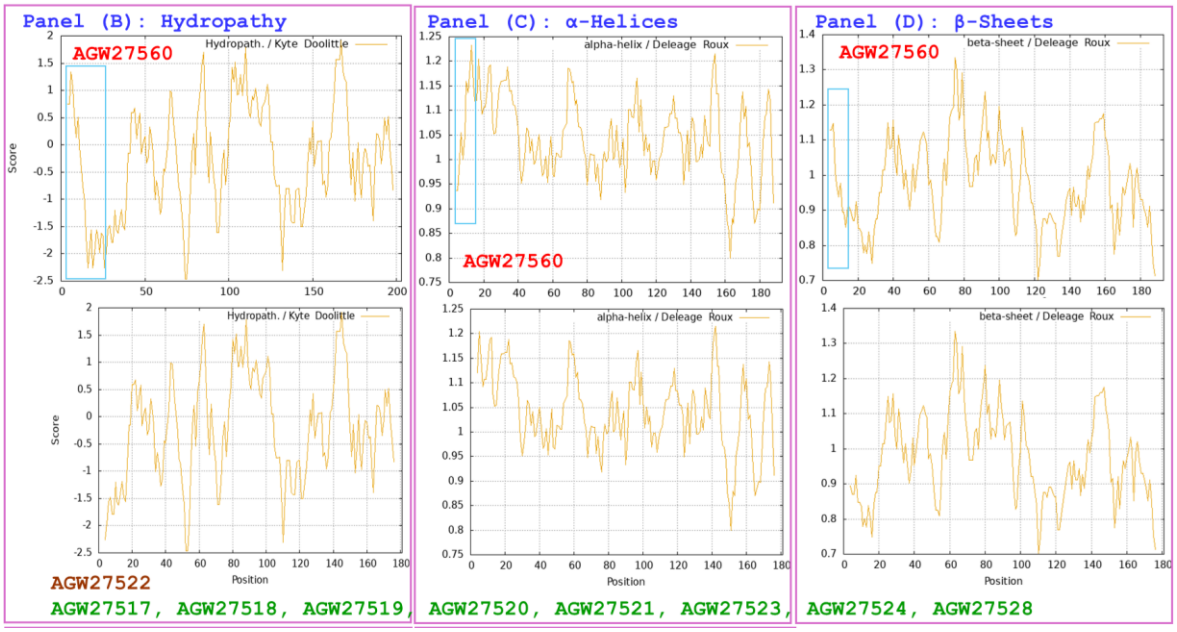

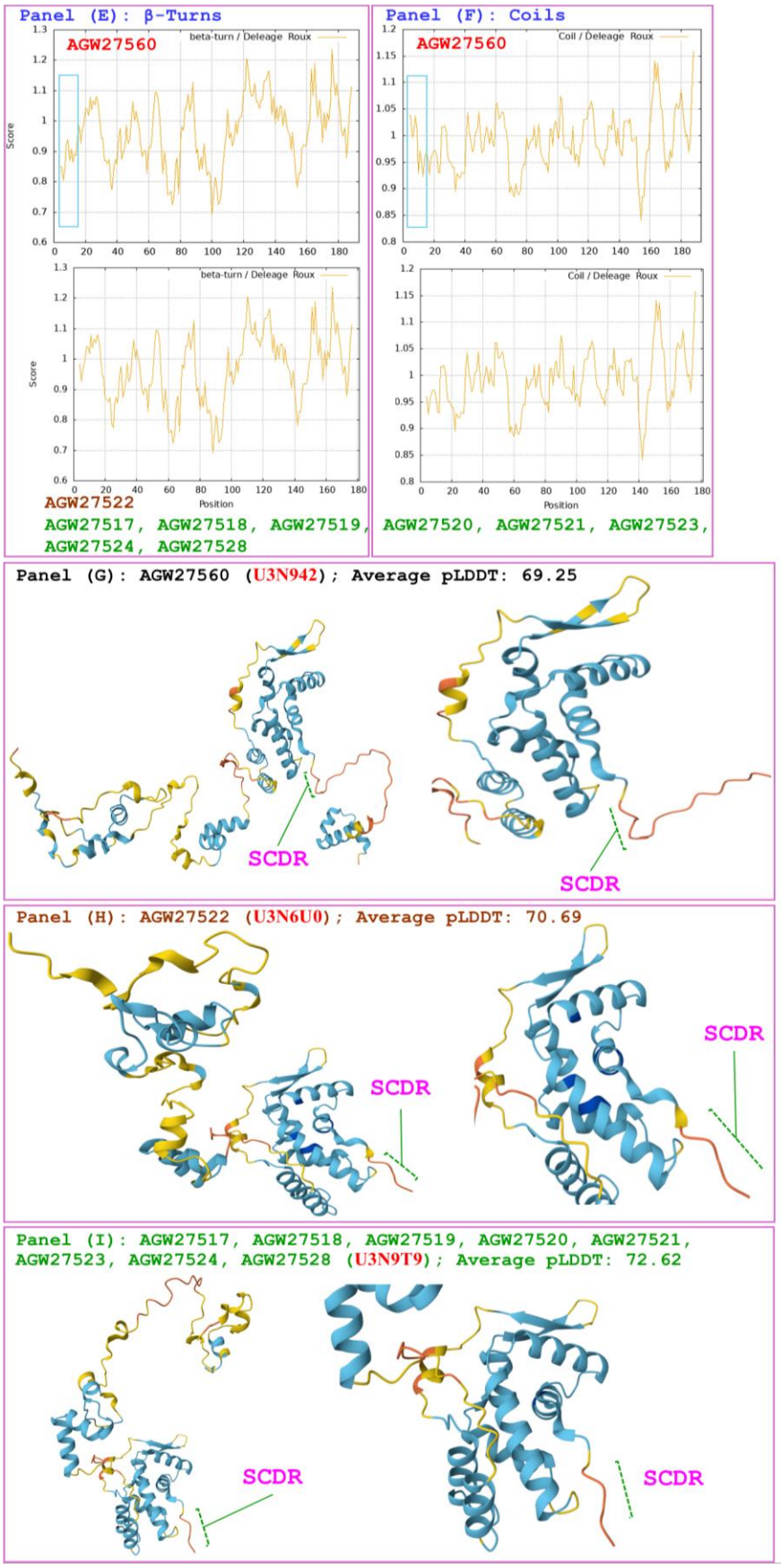
Panel (E): β-Turns
AGW27560
beta-turn / Deleage Roux
Score
Position
AGW27522
AGW27517, AGW27518, AGW27519, AGW27524, AGW27528
Panel (F): Coils
AGW27560
Coil / Deleage Roux
Score
Position
AGW27520, AGW27521, AGW27523,
Panel (G): AGW27560 (U3N942); Average pLDDT: 69.25
SCDR
SCDR
Panel (H): AGW27522 (U3N6U0); Average pLDDT: 70.69
SCDR
SCDR
Panel (I): AGW27517, AGW27518, AGW27519, AGW27520, AGW27521, AGW27523, AGW27524, AGW27528 (U3N9T9); Average pLDDT: 72.62
SCDR
SCDR

287

Figure 5. Correlations of the changes in the hydrophobicity and the primary, secondary, and tertiary structures of the MATα_HMGbox domains of MAT1-1-1 proteins: the reference protein AGW27560 (under the AlphaFold code U3N942) derived from *H. sinensis* strain CS68-2-1229 and the 2 groups of the truncated proteins: (1) AGW27522 shown in brown (under the AlphaFold code U3N6U0) derived from the *O. sinensis* strain CS560-961 and (2) the truncated proteins shown in green (under the AlphaFold code U3N9T9) derived from the *O. sinensis* strains CS6-251, CS36-1294, CS37-295, CS18-266, CS26-277, CS91-1291, CS34-291, and CS68-2-1229. Panel (A) shows an alignment of the amino acid sequences of the MATα_HMGbox domains of the MAT1-1-1 proteins; where the hyphens indicate identical amino acid residues and the spaces denote unmatched sequence gaps. The ExPASy ProtScale plots show the changes in hydrophobicity and the 2D structures in Panels (B)–(F) for hydropathy, α-helices, β-sheets, β-turns, and coils of the proteins, respectively; the open rectangles in blue highlight the N-terminally truncated region in the ExPASy plots. Panels (G)–(I) show the 3D structures of the full-length proteins on the left and the locally magnified structures surrounding the truncated region are shown on the right. The model confidence for the AlphaFold-predicted 3D structures is as follows: ■ very high (pLDDT>90); ■ high (90>pLDDT>70); ■ low (70>pLDDT>50); and ■ very low (pLDDT<50).

The hydrophobicity and structural characteristics of the MATα_HMGbox domain of the truncated MAT1-1-1 protein AGW27525 are compared with those of the reference full-length protein AGW27560 in Figure 6. The protein AGW27525 (under AlphaFold code U3N919) is derived from the *O. sinensis* strain CS76-1284 (Table 1), while the reference protein AGW27560 (under AlphaFold code U3N942) is derived from the *H. sinensis* strain CS68-2-1229 [14]. Panel (A) of Figure 6 shows a 16-residue truncation at the N-terminus of the MATα_HMGbox domain of the protein AGW27525. This truncation results in altered topological structures and waveforms in the ExPASy ProtScale plots, as illustrated in Panels (B)–(F) for hydropathy, α-helices, β-sheets, β-turns, and coils, respectively. Compared with the 3D structure of the reference protein AGW27560 shown in Panel (G), Panel (H) demonstrates that the truncated variant significantly alters the 3D structure of the protein AGW27525 under the AlphaFold code U3N919. Notably, the N-terminal amino acids 2–4 (AKR) shown in Panel (A) have hydropathy indices of 1.8, -3.9, and -4.5, respectively (Table S3) [73], and collectively exhibit hydrophilic characteristics. These amino acids initiate the formation of the β-sheet structure in the truncated protein AGW27525 shown in Panel (H); in contrast, the amino acids AKR in the full-length reference protein AGW27560 shown in Panel (G) are not part of the β-sheet structure or the hydrophobic core composed of the 3 critical α-helices within the MATα_HMGbox domain. The truncated region of the AGW27525 protein is located upstream of the 3 α-helix core within the MATα_HMGbox domain and may not directly participate in stabilizing the hydrophobic core of this domain [90−91].

Panel (A): Alignment of the amino acid sequences of the MATα_HMGbox domains

```
AGW27560  42   ADVLTPVSTAAASRATRQTKEASCDRAKRPLNAFMAFRSYYLKLFPDVQQKTASGFLTT  100
AGW27525  1                                ---------------------------------  34

AGW27560  101  LWHKDPFRNKWALIAKVYSFVRDQIGKDKVSLSYFMSLACPTMTIIEPAAYLNALGWCVQ  160
AGW27525  35   ------------------------------------------------------------  94

AGW27560  161  DDDAGSQKLFQDESSANLDQSSLLSAEYPSTEIELLSALVNIGYFPDHGADLVERMGSSH  220
AGW27525  95   ------------------------------------------------------------  154

AGW27560  221  SGIMAPRAANCTPP                                               234
AGW27525  155  --------------                                               168
```

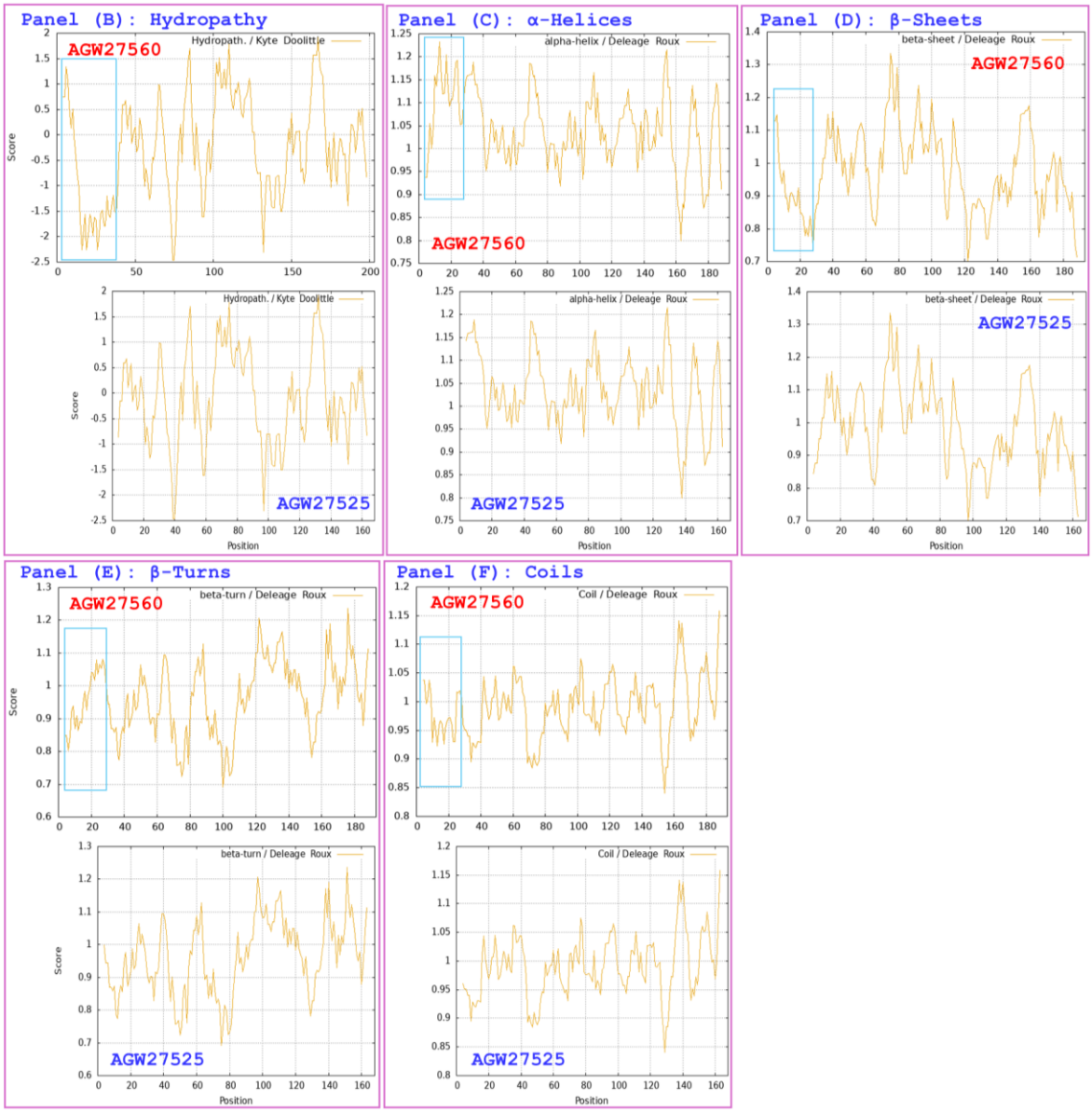

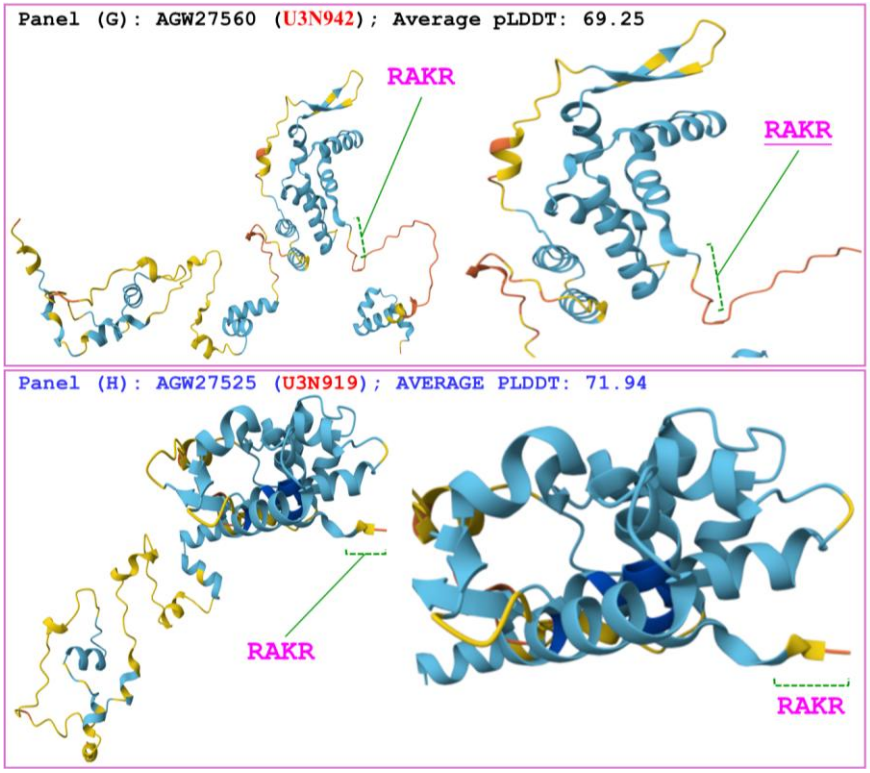

Figure 6. Correlations of the changes in hydrophobicity and the primary, secondary, and tertiary structures of the MATα_HMGbox domains of MAT1-1-1 proteins: the reference protein AGW27560 (under the AlphaFold code U3N942) derived from the *H. sinensis* strain CS68-2-1229 and the variant protein AGW27525 (under the AlphaFold code U3N919) derived from the *O. sinensis* strain CS76-1284. Panel (A) shows an alignment of the amino acid sequences of the MATα_HMGbox domains of the MAT1-1-1 proteins, where the hyphens indicate identical amino acid residues and the spaces denote unmatched sequence gaps. The ExPASy ProtScale plots show the changes in hydrophobicity and the 2D structure in Panels (B)–(F) for hydropathy, α-helices, β-sheets, β-turns, and coils of the protein, respectively; the open rectangles in blue highlight the N-terminally truncated region in the ExPASy plots. Panels (G)–(H) show the 3D structures of the full-length proteins on the left and the locally magnified structures surrounding the variation region are shown on the right. The model confidence for the AlphaFold-predicted 3D structures is as follows: ■ very high (pLDDT>90); ■ high (90>pLDDT>70); ■ low (70>pLDDT>50); and ■ very low (pLDDT<50).

The hydrophobicity and structural characteristics of the MATα_HMGbox domain of the variant MAT1-1-1 protein AGW27526 are compared with those of the full-length reference protein AGW27560 in Figure 7. The protein AGW27526 (under the AlphaFold code U3N7G5) is derived from the *O. sinensis* strain CS561-964 (Table 1), while the reference protein AGW27560 (under the AlphaFold code U3N942) is derived from the *H. sinensis* strain CS68-2-1229 [14]. Panel (A) of Figure 7 shows a 13-residue truncation at the N-terminus of the MATα_HMGbox domain of the protein AGW27526, along with 4 amino acid substitutions: C-to-S (cysteine to serine, both with polar neutral side chains; hydropathy indices changed from -3.5 to -0.8; *cf.* Table S3), D-to-S (acidic aspartic acid to serine with polar neutral side chains; hydropathy indices changed from 2.5 to -0.8), R-to-F (basic arginine to aromatic

phenylalanine; hydropathy indices changed from -4.5 to 2.8), and A-to-T (aliphatic alanine to threonine with polar neutral side chains; hydropathy indices changed from 1.8 to -0.7) (Table S3) [73]. The truncation and amino acid substitutions result in changes in the hydrophobicity and secondary structures of the variant protein, which are illustrated by the altered topological structure and waveform in the ExPASy ProtScale plots for hydropathy, α-helices, β-sheets, β-turns, and coils in Panels (B)–(F), respectively. Compared with the 3D structure of the reference protein AGW27560 shown in Panel (G), the truncation and replacement of amino acids in the variant protein AGW27526 shown in Panel (H) are located upstream of the 3 core α-helices of the MATα_HMGbox domain. These modifications caused apparent changes in the tertiary structure of the variant protein AGW27526 under the AlphaFold code U3N7G5.

Panel (A): Alignment of the amino acid sequences of the MATα_HMGbox domains

```
AGW27560  42   ADVLTPVSTAAASRATRQTKEASCDRAKRPLNAFMAFRSYYLKLFPDVQQKTASGFLTT  100
AGW27526  1                              -SSFT--------------------------------  37

AGW27560  101  LWHKDPFRNKWALIAKVYSFVRDQIGKDKVSLSYFMSLACPTMTIIEPAAYLNALGWCVQ  160
AGW27526  38   ------------------------------------------------------------  97

AGW27560  161  DDDAGSQKLFQDESSANLDQSSLLSAEYPSTEIELLSALVNIGYFPDHGADLVERMGSSH  220
AGW27526  98   ------------------------------------------------------------  157

AGW27560  221  SGIMAPRAANCTPP                                               234
AGW27526  158  --------------                                               171
```

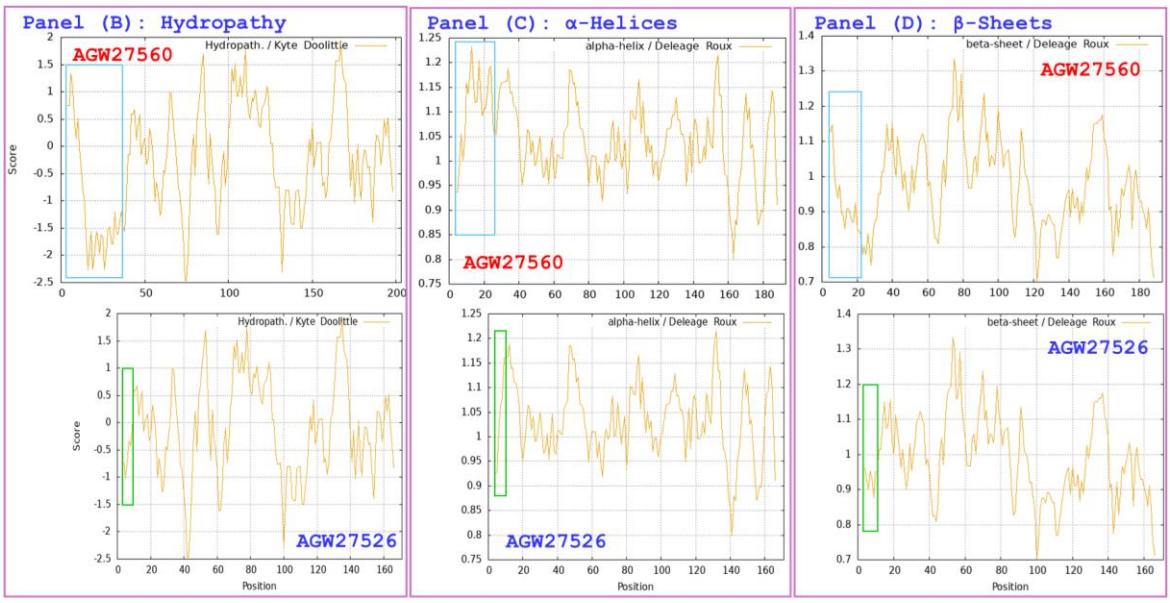

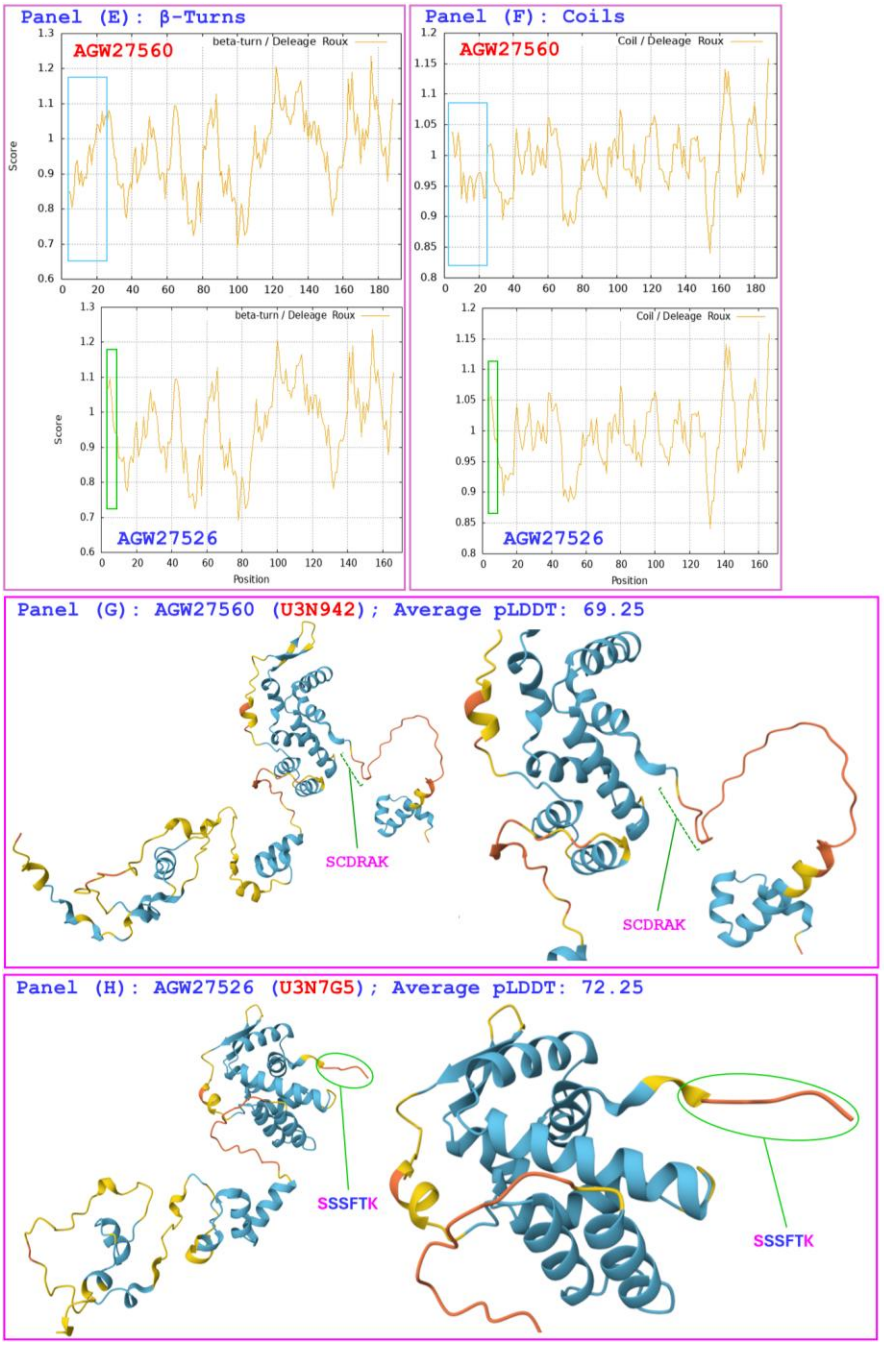

Figure 7. Correlations of the changes in the hydrophobicity and the primary, secondary, and tertiary structures of the MATα_HMGbox domains of MAT1-1-1 proteins: the reference protein AGW27560 (under the AlphaFold code U3N942) derived from the *H. sinensis* strain CS68-2-1229 and the variant protein AGW27526 (under the AlphaFold code U3N7G5) derived from the *O. sinensis* strain CS561-964. Panel (A) shows an alignment of the amino acid sequences of the MATα_HMGbox domains of the MAT1-1-1 proteins, where the hyphens indicate identical amino acid residues and the spaces denote unmatched sequence gaps. The ExPASy ProtScale plots show the changes in hydrophobicity and the 2D structure in Panels (B)–(F) for hydropathy, α-helices, β-sheets, β-turns, and coils of the protein, respectively; the open rectangles in blue highlight the N-terminally truncated regions, and those in green highlight the altered topological structure and waveform in the ExPASy plots. Panels (G)–(H) show the 3D structures of the full-length proteins on the left and the locally magnified structures surrounding the variation regions are shown on the right. The model confidence for the AlphaFold-predicted 3D structures is as

follows: very high (pLDDT>90); high (90>pLDDT>70); low (70>pLDDT>50); and very low (pLDDT<50).

The hydrophobicity and structural characteristics of the MATα_HMGbox domain of the variant MAT1-1-1 protein AGW27527 are compared with those of the reference protein AGW27560 in Figure 8. The protein AGW27527 (under the AlphaFold code U3N6U4) is derived from the *O. sinensis* strain CS25-273 (Table 1), while the reference protein AGW27560 (under the AlphaFold code U3N942) is derived from the *H. sinensis* strain CS68-2-1229 [14]. Panel (A) of Figure 8 shows a 27-residue truncation at the N-terminus of the MATα_HMGbox domain of the protein AGW27527. This truncation results in changes in the topological structure and waveform in the ExPASy ProtScale plots, which illustrate hydropathy, α-helices, β-sheets, β-turns, and coils in Panels (B)–(F), respectively. Compared with the 3D structure of the reference protein AGW27560 shown in Panel (G), Panel (H) shows that the truncation is located within the first of the 3 core α-helices of the MATα_HMGbox domain and the tertiary structure of the truncated protein AGW27527 under the AlphaFold code U3N6U4 is apparently altered.

Panel (A): Alignment of the amino acid sequences of the MATα_HMGbox domains

```
AGW27560  42   ADVLTPVSTAAASRATRQTKEASCDRAKRPLNAFMAFRSYYLKLFPDVQQKTASGFLTT  100
AGW27527  1                                   -----------------------  23

AGW27560  101  LWHKDPFRNKWALIAKVYSFVRDQIGKDKVSLSYFMSLACPTMTIIEPAAYLNALGWCVQ  160
AGW27527  24   ------------------------------------------------------------  83

AGW27560  161  DDDAGSQKLFQDESSANLDQSSLLSAEYPSTEIELLSALVNIGYFPDHGADLVERMGSSH  220
AGW27527  84   ------------------------------------------------------------  143

AGW27560  221  SGIMAPRAANCTPP                                               234
AGW27527  144  --------------                                               157
```

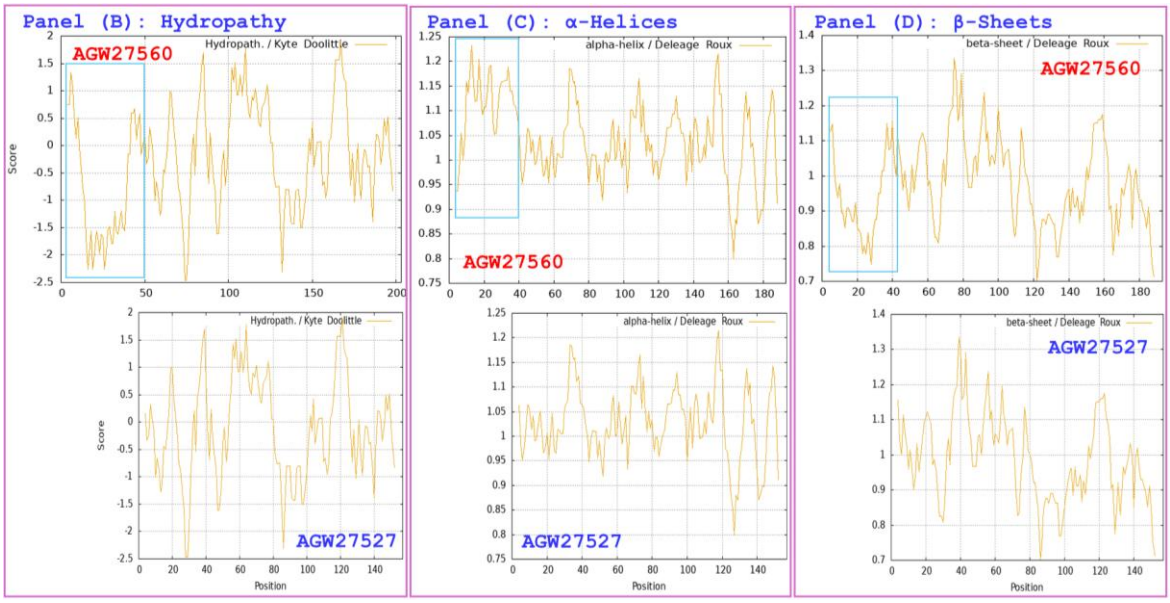

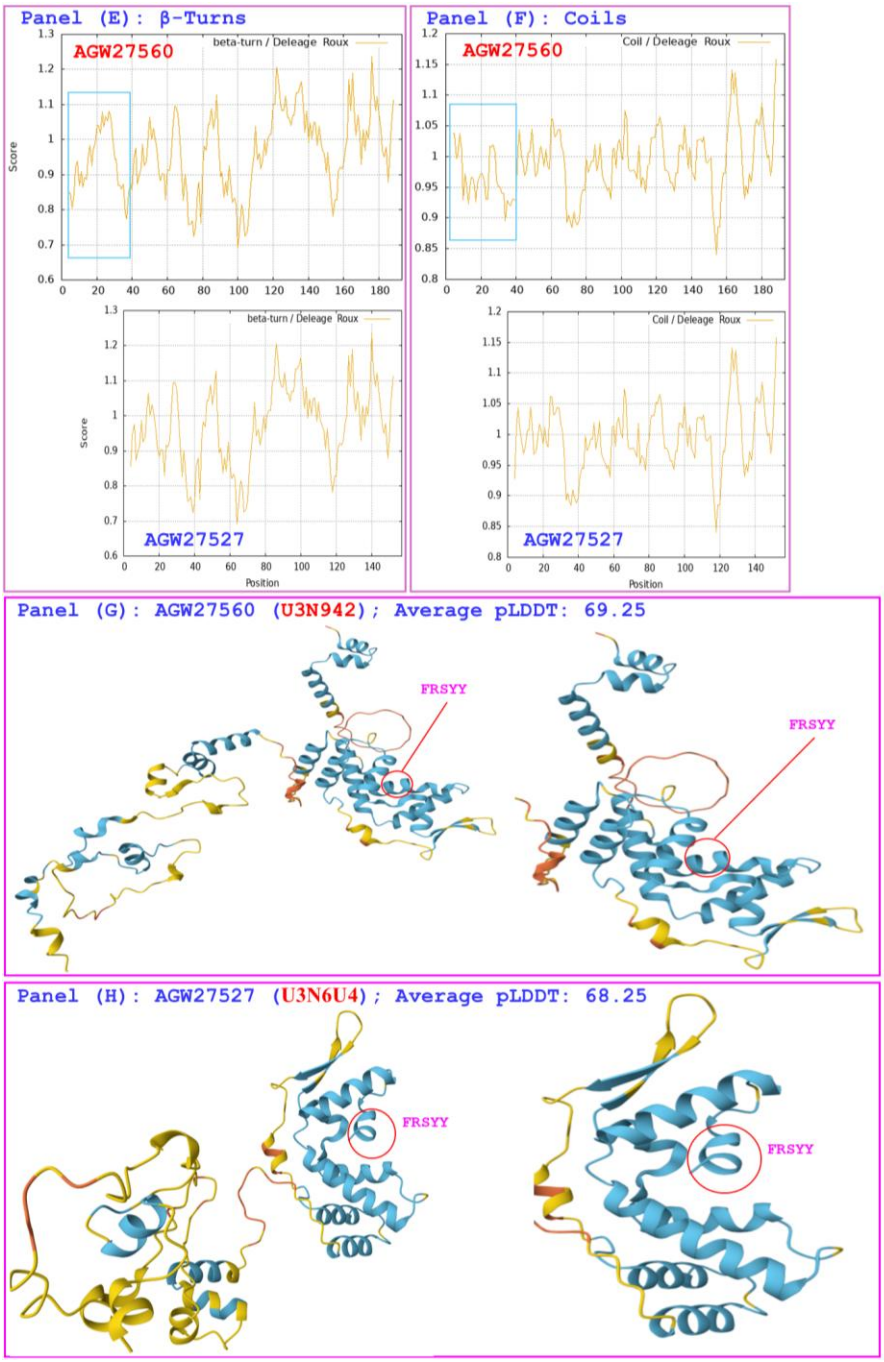

Figure 8. Correlations of the changes in the hydrophobicity and the primary, secondary, and tertiary structures of the MATα_HMGbox domains of MAT1-1-1 proteins: the reference protein AGW27560 (under the AlphaFold code U3N942) derived from the *H. sinensis* strain CS68-2-1229 and the variant protein AGW27527 (under the AlphaFold code U3N6U4) derived from the *O. sinensis* strain CS25-273. Panel (A) shows an alignment of the amino acid sequences of the MATα_HMGbox domains of the MAT1-1-1 proteins, where the hyphens indicate identical amino acid residues and the spaces denote unmatched sequence gaps. The ExPASy ProtScale plots) show the changes in hydrophobicity and the 2D structure in Panels (B)–(F for hydropathy, α-helices, β-sheets, β-turns, and coils of the protein, respectively; the open rectangles in blue highlight the N-terminal truncation regions in the ExPASy plots. Panels (G)–(H) show the 3D structures of the full-length proteins on the left and the locally magnified structures surrounding the truncated region are shown on the right. The model confidence for the

AlphaFold-predicted 3D structures is as follows: ■ very high (pLDDT>90); ■ high (90>pLDDT>70); ■ low (70>pLDDT>50); and ■ very low (pLDDT<50).

The hydrophobicity and structural characteristics of the MATα_HMGbox domain of the variant MAT1-1-1 proteins AGW27532, AGW27533, and AGW27535 are compared with those of the reference protein AGW27560 in Figure 9. These three variant proteins (all under the AlphaFold code U3N6U8) are derived from the *O. sinensis* strains CS68-5-1216, CS71-1218, and CS71-1220 (Table 1), whereas the reference protein AGW27560 (under the AlphaFold code U3N942) is derived from the *H. sinensis* strain CS68-2-1229 [14]. Panel (A) of Figure 9 shows 47-residue truncations at the N-termini of the MATα_HMGbox domains of the variant proteins. These truncations result in changes in the topological structure and waveform in the ExPASy ProtScale plots, which illustrate hydropathy, α-helices, β-sheets, β-turns, and coils in Panels (B)–(F), respectively. A comparison of the tertiary structures of the MAT1-1-1 proteins is illustrated in Panels (G)–(H). The truncations are located within the first of the 3 core α-helices of the MATα_HMGbox domains, which results in significant changes in the tertiary structures of the variant proteins AGW27532, AGW27533, and AGW27535 under the AlphaFold code U3N6U8.

Panel (A): Alignment of the amino acid sequences of the MATα_HMGbox domains

```
AGW27560  42   ADVLTPVSTAAASRATRQTKEASCDRAKRPLNAFMAFRSYYLKLFPDVQQKTASGFLTT  100
AGW27532  1                                                              3
AGW27533  1                                                              3
AGW27535  1                                                              3

AGW27560  101  LWHKDPFRNKWALIAKVYSFVRDQIGKDKVSLSYFMSLACPTMTIIEPAAYLNALGWCVQ  160
AGW27532  4    ------------------------------------------------------------  63
AGW27533  4    ------------------------------------------------------------  63
AGW27535  4    ------------------------------------------------------------  63

AGW27560  161  DDDAGSQKLFQDESSANLDQSSLLSAEYPSTEIELLSALVNIGYFPDHGADLVERMGSSH  220
AGW27532  64   ------------------------------------------------------------  123
AGW27533  64   ------------------------------------------------------------  123
AGW27535  64   ------------------------------------------------------------  123

AGW27560  221  SGIMAPRAANCTPP                                               234
AGW27532  124  --------------                                               137
AGW27533  124  --------------                                               137
AGW27535  124  --------------                                               137
```

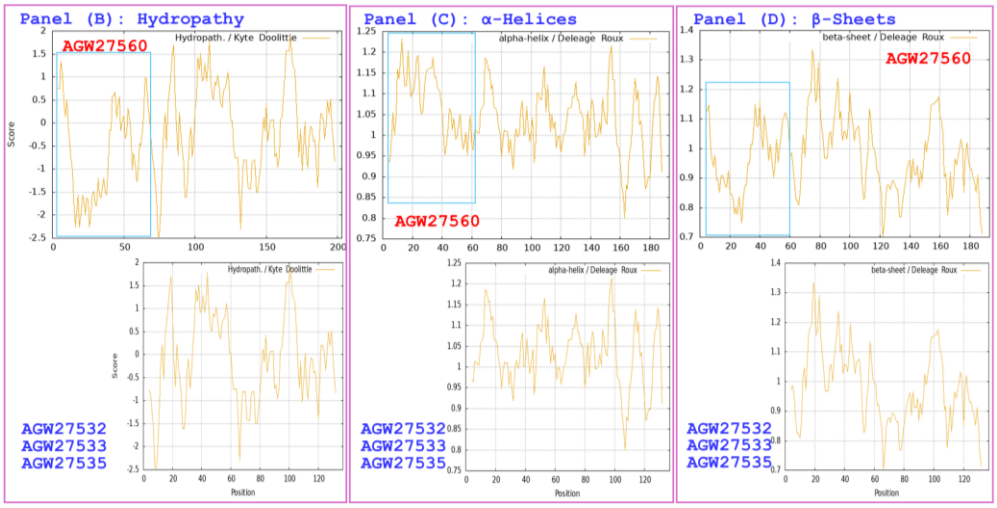

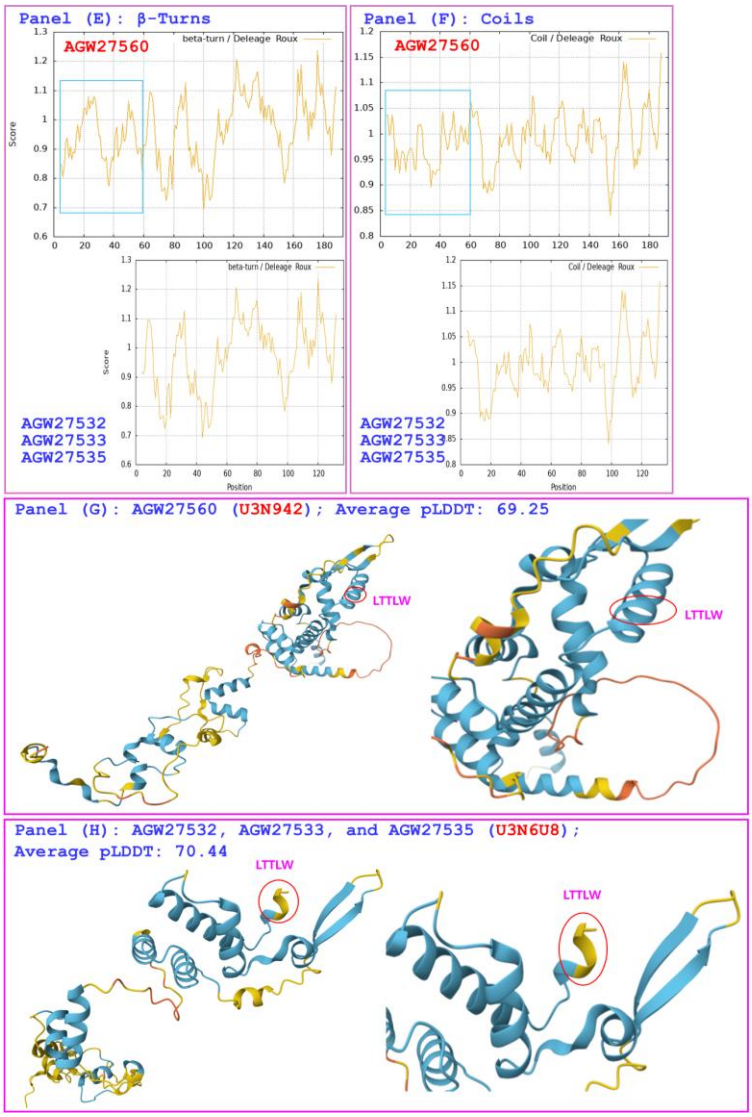

Figure 9. Correlations of the changes in the hydrophobicity and the primary, secondary, and tertiary structures of the MATα_HMGbox domains of MAT1-1-1 proteins: the reference protein AGW27560 (under the AlphaFold code U3N942) derived from the *H. sinensis* strain CS68-2-1229 and the variant proteins AGW27532, AGW27533, and AGW27535 (under the AlphaFold code U3N6U8) derived from the *O. sinensis* strains CS68-5-1216, CS71-1218, and CS71-1220, respectively. Panel (A) shows an alignment of the amino acid sequences of the MATα_HMGbox domains of the MAT1-1-1 proteins, where the hyphens indicate identical amino acid residues and the spaces denote unmatched sequence gaps. The ExPASy ProtScale plots show the changes in hydrophobicity and the 2D structure in Panels (B)–(F) for hydropathy, α-helices, β-sheets, β-turns, and coils of the protein, respectively; the open rectangles in blue highlight the N-terminally truncated regions in the ExPASy plots. Panels (G)–(I) show the 3D structures of the full-length proteins on the left and the locally magnified structures surrounding the truncation site on the right. The model confidence for the AlphaFold-predicted 3D structures is as follows: ■ very high (pLDDT>90); ■ high (90>pLDDT>70); ■ low (70>pLDDT>50); and ■ very low (pLDDT<50).

The hydrophobicity and structural characteristics of the MATα_HMGbox domains of the variant MAT1-1-1 proteins AGW27529 and AGW27530 are compared with those of the reference protein AGW27560 in Figure 10. The two variant proteins (under the AlphaFold code U3NE79) are derived

from the *O. sinensis* strains CS70-1208 and CS70-1211 (Table 1), whereas the reference protein AGW27560 (under the AlphaFold code U3N942) is derived from the *H. sinensis* strain CS68-2-1229 [14]. Panel (A) of Figure 10 shows 46-residue truncations at the N-termini of the MATα_HMGbox domains of the proteins AGW27529 and AGW27530, along with F-to-V substitutions (aromatic phenylalanine to aliphatic valine; hydropathy indices changed from 2.8 to 4.2 (Table S3) [73] within the MATα_HMGbox domains, indicating increased hydrophobicity. The truncation and increased hydrophobicity result in an altered secondary structure, as illustrated by the changes in topological structure and waveform in the ExPASy ProtScale plots for hydropathy, α-helices, β-sheets, β-turns, and coils shown in Panels (B)–(F), respectively. Compared the 3D structures of the MAT1-1-1 proteins illustrated in Panels (G)–(H), the truncation and replacement of amino acids in the proteins AGW27529 and AGW27530 are located within the first of the 3 core α-helices of the MATα_HMGbox domains. These modifications result in the significantly altered tertiary structures of the proteins AGW27529 and AGW27530 corresponding to the AlphaFold code U3NE79.

Panel (A): Alignment of the amino acid sequences of the MATα_HMGbox domains

```
AGW27560  42   ADVLTPVSTAAASRATRQTKEASCDRAKRPLNAFMAFRSYYLKLFPDVQQKTASGFLTT  100
AGW27529  1                                                        V---  4
AGW27530  1                                                        V---  4

AGW27560  101  LWHKDPFRNKWALIAKVYSFVRDQIGKDKVSLSYFMSLACPTMTIIEPAAYLNALGWCVQ  160
AGW27529  5    ------------------------------------------------------------  64
AGW27530  5    ------------------------------------------------------------  64

AGW27560  161  DDDAGSQKLFQDESSANLDQSSLLSAEYPSTEIELLSALVNIGYFPDHGADLVERMGSSH  220
AGW27529  65   ------------------------------------------------------------  124
AGW27530  65   ------------------------------------------------------------  124

AGW27560  221  SGIMAPRAANCTPP                                               234
AGW27529  125  --------------                                               138
AGW27530  125  --------------                                               138
```

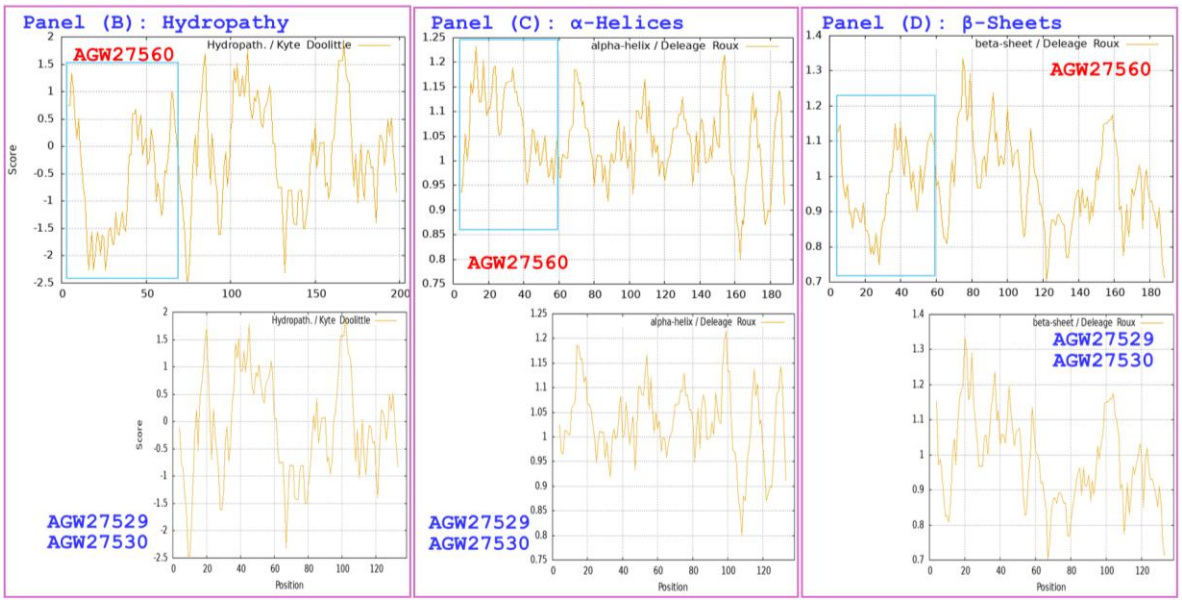

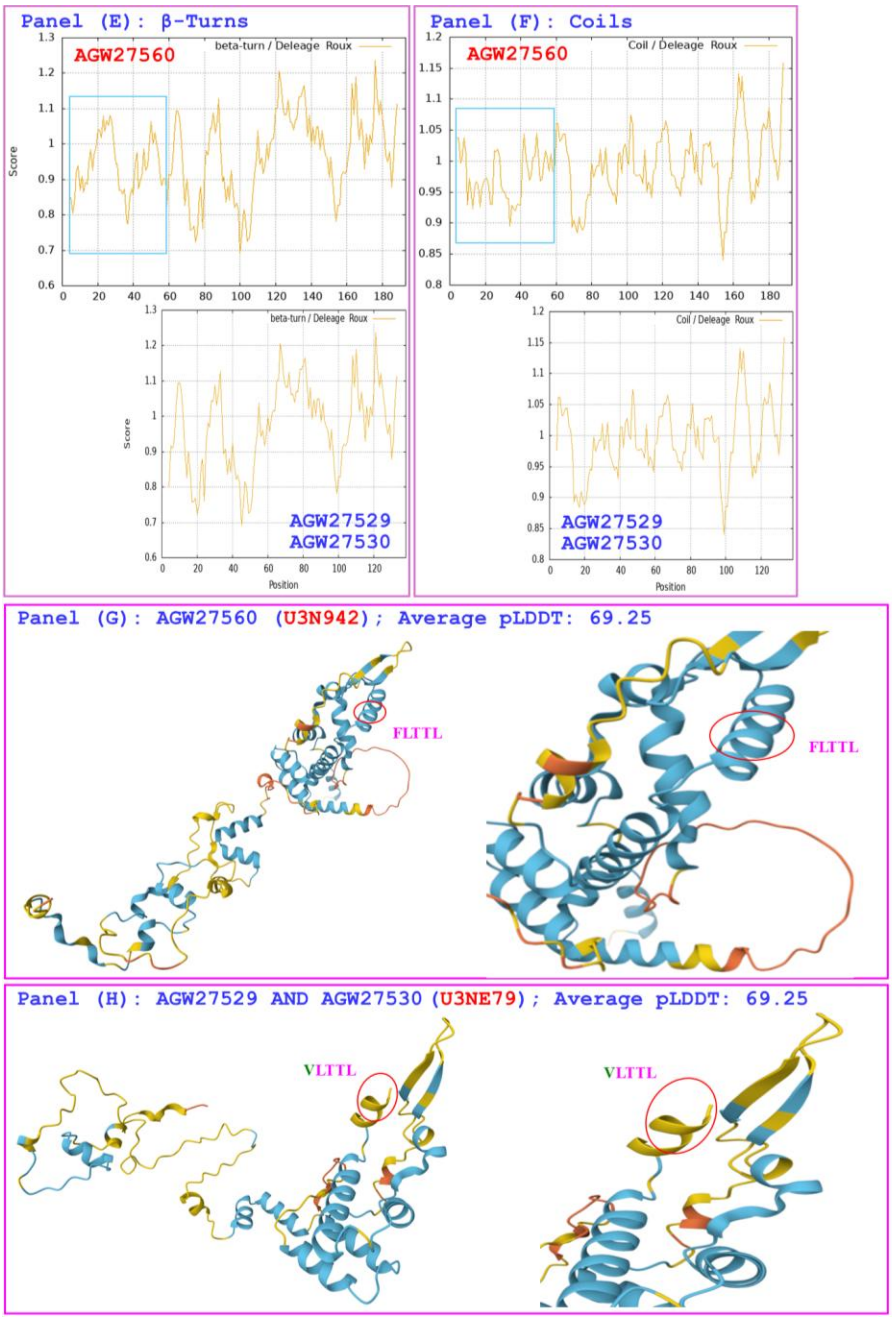

Figure 10. Correlations of the changes in the hydrophobicity and the primary, secondary, and tertiary structures of the MATα_HMGbox domains of MAT1-1-1 proteins: the reference protein AGW27560 (under the AlphaFold code U3N942) derived from the *H. sinensis* strain CS68-2-1229 and the variant proteins AGW27529 and AGW27530 (under the AlphaFold code U3NE79) derived from the *O. sinensis* strains CS70-1208 and CS70-1211. Panel (A) shows an alignment of the amino acid sequences of the MATα_HMGbox domains of the MAT1-1-1 proteins; amino acid substitutions are shown in green, the hyphens indicate identical amino acid residues, and the spaces denote unmatched sequence gaps. The ExPASy ProtScale plots show the changes in hydrophobicity and the 2D structure in Panels (B)–(F) for hydropathy, α-helices, β-sheets, β-turns, and coils of the protein, respectively; the open rectangles in blue highlight the N-terminally truncated regions in the ExPASy plots. Panels (G)–(I) show the 3D structures of the full-length proteins on the left and the locally magnified structures surrounding the variation site are shown on the right. The model confidence for the AlphaFold-predicted 3D structures is as follows:

455 very high (pLDDT>90); high (90>pLDDT>70); low (70>pLDDT>50); and very low (pLDDT<50).

456 The hydrophobicity and structural characteristics of the MATα_HMGbox domain of the variant
457 MAT1-1-1 protein AGW27536 are compared with those of the reference protein AGW27560 in Figure
458 11. The protein AGW27536 (under the AlphaFold code U3N7H7) is derived from the *O. sinensis* strain
459 CS68-2-1228 (Table 1), while the reference protein AGW27560 (under the AlphaFold code U3N942) is
460 derived from the *H. sinensis* strain CS68-2-1229 [14]. Panel (A) of Figure 11 shows a 44-residue
461 truncation at the N-terminus of the MATα_HMGbox domain of the protein AGW27536, along with an
462 S-to-E substitution and a deletion of leucine within the MATα_HMGbox domain. The S-to-E substitution
463 involves a change from serine (with polar neutral side chains) to acidic glutamic acid, with the
464 hydropathy index changing from -0.8 to -3.5 (Table S3) [73]; the deleted leucine has a hydropathy index
465 of 3.8. The truncation and replacement and deletion of amino acids lead to reduced hydrophobicity and
466 an altered secondary structure, as illustrated by the changes in topological structure and waveform in the
467 ExPASy ProtScale plots for hydropathy, α-helices, β-sheets, β-turns, and coils in Panels (B)–(F),
468 respectively. Compared the 3D structures of the MAT1-1-1 proteins illustrated in Panels (G)–(H), the
469 truncation and replaced and deleted amino acids in the protein AGW27536 are located within the first of
470 the 3 core α-helices of the MATα_HMGbox domain. These modifications result in significant changes
471 in the 3D structure of the protein AGW27536, corresponding to the AlphaFold code U3N7H7.

Panel (A): Alignment of the amino acid sequences of the MATα_HMGbox domains

```
AGW27560  42   ADVLTPVSTAAASRATRQTKEASCDRAKRPLNAFMAFRSYYLKLFPDVQQKTASGFLTT  100
AGW27536  1                                                E-- --  5

AGW27560  101  LWHKDPFRNKWALIAKVYSFVRDQIGKDKVSLSYFMSLACPTMTIIEPAAYLNALGWCVQ  160
AGW27536  6    ------------------------------------------------------------  65

AGW27560  161  DDDAGSQKLFQDESSANLDQSSLLSAEYPSTEIELLSALVNIGYFPDHGADLVERMGSSH  220
AGW27536  66   ------------------------------------------------------------  125

AGW27560  221  SGIMAPRAANCTPP                                               234
AGW27536  126  --------------                                               139
```

472

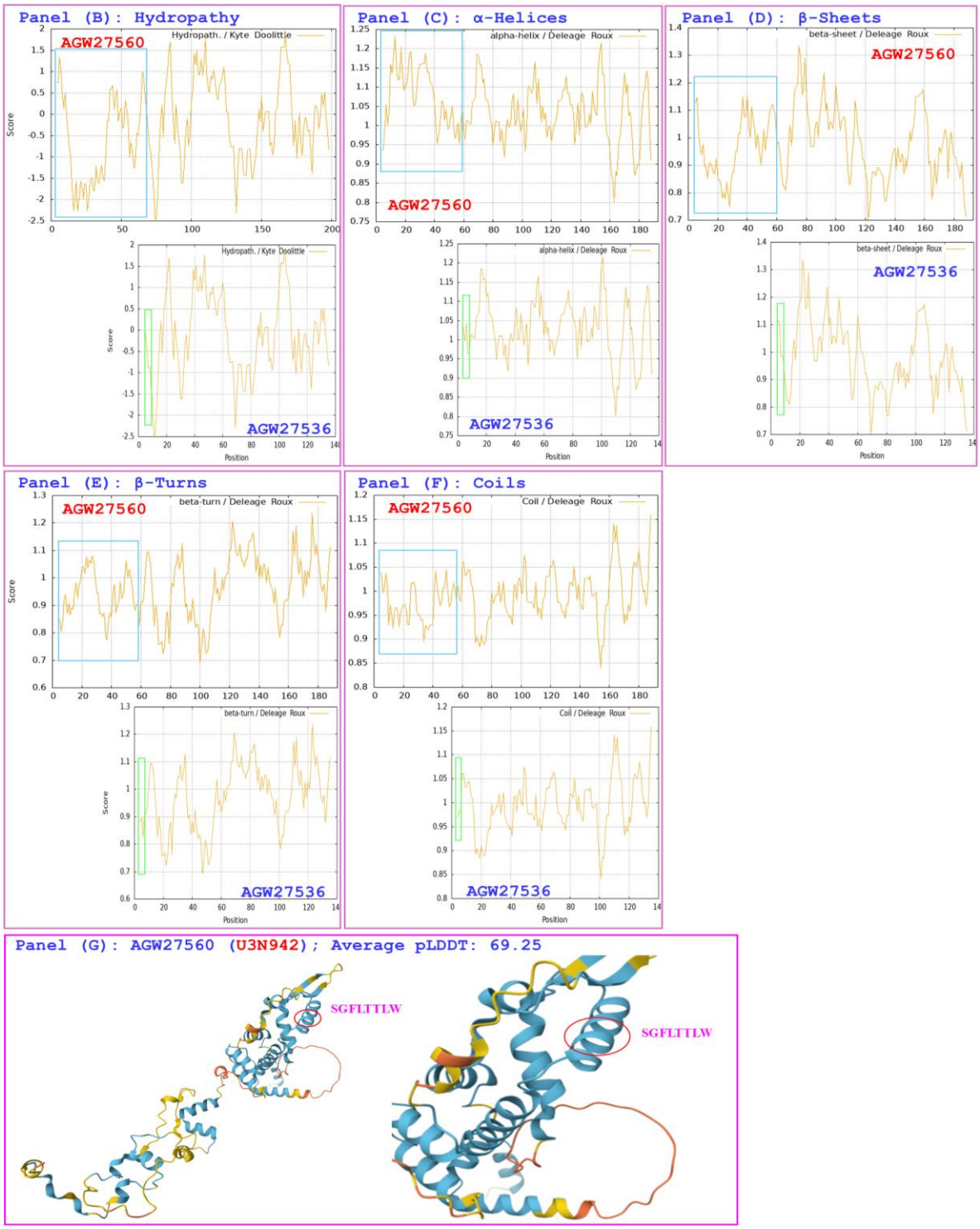
Panel (B): Hydropathy
AGW27560
Hydropath. / Kyte Doolittle
Score
AGW27536
Position
Panel (C): α-Helices
alpha-helix / Deleage Roux
AGW27560
AGW27536
Panel (D): β-Sheets
beta-sheet / Deleage Roux
AGW27560
AGW27536
Panel (E): β-Turns
beta-turn / Deleage Roux
AGW27560
AGW27536
Panel (F): Coils
Coil / Deleage Roux
AGW27560
AGW27536
Panel (G): AGW27560 (U3N942); Average pLDDT: 69.25
SGFLTTLW
SGFLTTLW

473

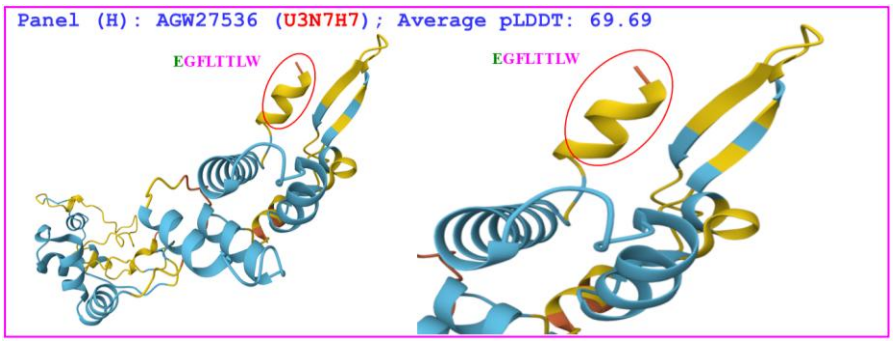

Figure 11. Correlations of the changes in the hydrophobicity and the primary, secondary, and tertiary structures of the MATα_HMGbox domains of MAT1-1-1 proteins: the reference protein AGW27560 (under the AlphaFold code U3N942) derived from the *H. sinensis* strain CS68-2-1229 and the variant protein AGW27536 (under the AlphaFold code U3N7H7) derived from the *O. sinensis* strain CS68-2-1228. Panel (A) shows an alignment of the amino acid sequences of the MATα_HMGbox domains of the MAT1-1-1 proteins, where the hyphens indicate identical amino acid residues and the spaces denote unmatched sequence gaps. The ExPASy ProtScale plots show the changes in hydrophobicity and the 2D structure in Panels (B)–(F) for hydropathy, α-helices, β-sheets, β-turns, and coils of the protein, respectively; the open rectangles in blue highlight the N-terminally truncated regions, and those in green highlight the altered topological structure and waveform in the ExPASy plots. Panels (G)–(H) show the 3D structures of the full-length proteins on the left and the locally magnified structures surrounding the variation site are shown on the right. The model confidence for the AlphaFold-predicted 3D structures is as follows: ■ very high (pLDDT>90); ■ high (90>pLDDT>70); ■ low (70>pLDDT>50); and ■ very low (pLDDT<50).

The hydrophobicity and structural characteristics of the MATα_HMGbox domains of the variant MAT1-1-1 proteins AGW27531 and AGW27534 are compared with those of the reference protein AGW27560 in Figure 12. These 2 variant proteins (both under the AlphaFold code U3NE87) are derived from the *O. sinensis* strains CS70-1212 and CS71-1219 (*cf.* Table 1), whereas the reference protein AGW27560 (under the AlphaFold code U3N942) is derived from the *H. sinensis* strain CS68-2-1229 [14]. Panel (A) of Figure 12 shows 60-residue truncations at the N-termini of the MATα_HMGbox domains of the proteins AGW27531 and AGW27534. The truncations result in altered hydrophobicity and secondary structures, as illustrated by the changes in topological structure and waveform in the ExPASy ProtScale plots for hydropathy, α-helices, β-sheets, β-turns, and coils in Panels (B)–(F), respectively. A comparison of the 3D structures of the MAT1-1-1 proteins, as illustrated in Panels (G)–(H), revealed that the truncations in the proteins AGW27531 and AGW27534 are located within the 3 core α-helices of the MATα_HMGbox domains and result in significantly altered tertiary structures of the variant proteins, both of which correspond to the same AlphaFold code U3NE87.

Panel (A): Alignment of the amino acid sequences of the MATα_HMGbox domains

```
AGW27560   42    ADVLTPVSTAAASRATRQTKEASCDRAKRPLNAFMAFRSYYLKLFPDVQQKTASGFLTT   100
AGW27531
AGW27534

AGW27560   101   LWHKDPFRNKWALIAKVYSFVRDQIGKDKVSLSYFMSLACPTMTIIEPAAYLNALGWCVQ   160
AGW27531   1                ---------------------------------------------------   50
AGW27534   1                ---------------------------------------------------   50

AGW27560   161   DDDAGSQKLFQDESSANLDQSSLLSAEYPSTEIELLSALVNIGYFPDHGADLVERMGSSH   220
AGW27531   51    ------------------------------------------------------------   110
AGW27534   51    ------------------------------------------------------------   110

AGW27560   221   SGIMAPRAANCTPP                                                234
AGW27531   111   --------------                                                124
AGW27534   111   --------------                                                124
```

500

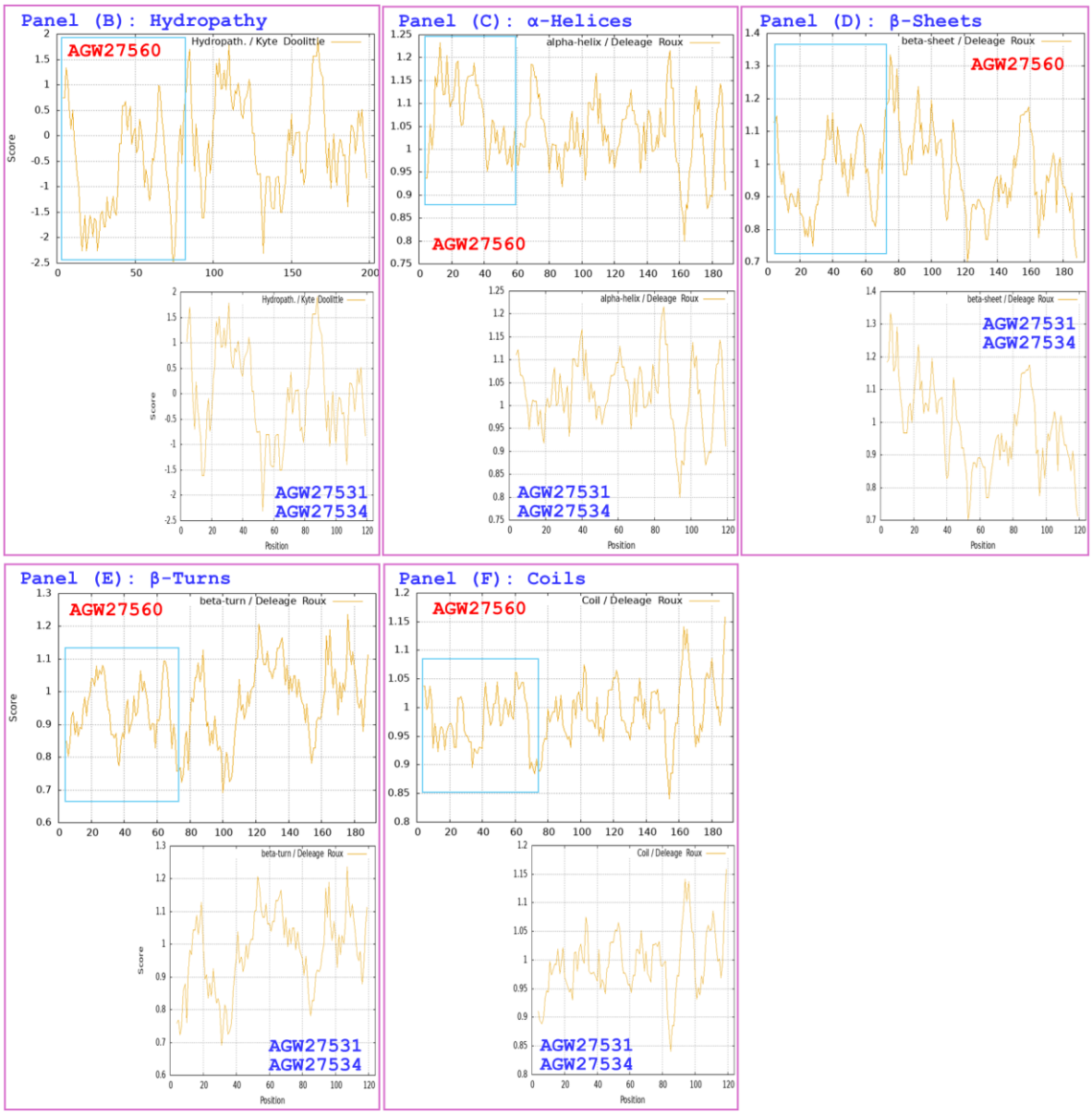

501

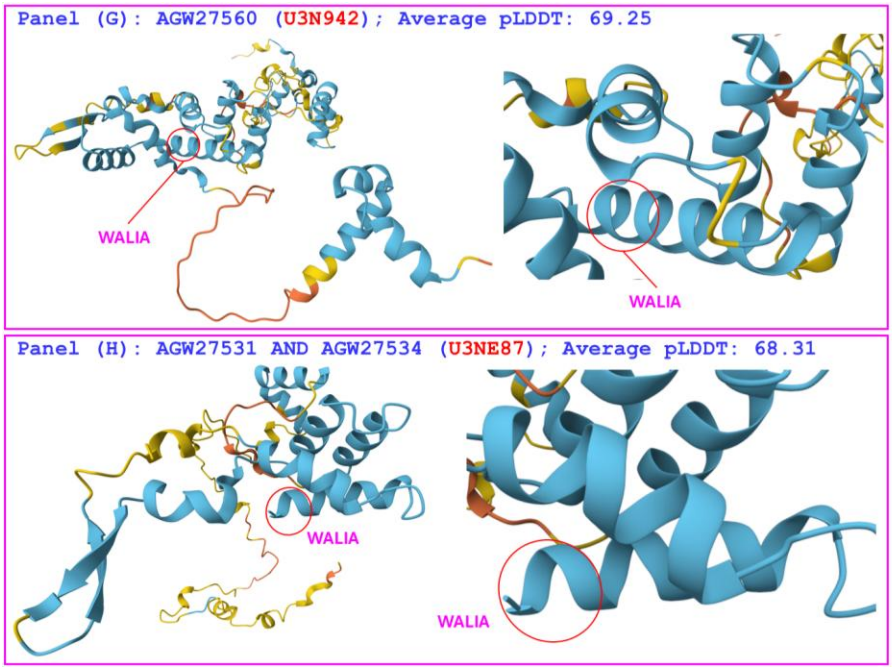

Figure 12. Correlations of the changes in the hydrophobicity and the primary, secondary, and tertiary structures of the MATα_HMGbox domains of MAT1-1-1 proteins: the reference protein AGW27560 (under the AlphaFold code U3N942) derived from the *H. sinensis strain* CS68-2-1229 and the variant proteins AGW27531 and AGW27534 (under the AlphaFold code U3NE87) derived from the *O. sinensis* strains CS70-1212 and CS71-1219, respectively. Panel (A) shows an alignment of the amino acid sequences of the MATα_HMGbox domains of the MAT1-1-1 proteins, where the hyphens indicate identical amino acid residues and the spaces denote unmatched sequence gaps. The ExPASy ProtScale plots show the changes in hydrophobicity and the 2D structure in Panels (B)–(F) for hydropathy, α-helices, β-sheets, β-turns, and coils of the protein; the open rectangles in blue highlight the N-terminally truncated regions in the ExPASy plots. Panels (G)–(H) show the 3D structures of the full-length proteins on the left and the locally magnified structures surrounding the truncation site are shown on the right. The model confidence for the AlphaFold-predicted 3D structures is as follows: ■ very high (pLDDT>90); ■ high (90>pLDDT>70); ■ low (70>pLDDT>50); and ■ very low (pLDDT<50).

Collectively, the data in Figures 5–12 in Section 3.3 demonstrate that the MAT1-1-1 protein variants derived from various *O. sinensis* strains exhibit N-terminal truncations (ranging from 13 to 60 residues) of their MATα_HMGbox domains, with different amino acid substitutions or deletions. These modifications significantly alter the hydrophobicity, secondary structures, and tertiary structures of the MATα_HMGbox domains, with truncation and substitution locations occurring either upstream of or within the three core α-helices of the domains. The variant MAT1-1-1 proteins correspond to one of nine distinct AlphaFold 3D structural conformations (*cf.* Table 1, Figure 2), highlighting the structural diversity of the MAT1-1-1 proteins.

3.4 Heteromorphic tertiary structures of the HMG-box_ROX1-like domains of the truncated MAT1-2-1 proteins derived from *O. sinensis* strains

This section presents the results of the correlation analyses between the changes in the hydrophobic properties and structures of the HMG-box_ROX1-like domains of variant MAT1-2-1 proteins derived from various *O. sinensis* strains under 4 AlphaFold codes (*cf.* Table 1) compared with the reference full-length MAT1-2-1 proteins. This reference protein, represented by AEH27625 derived from the *H. sinensis* strain CS2 (*cf.* Table S5), is associated with the AlphaFold 3D structural code D7F2E9 [70]. The HMG-box_ROX1-like domain sequences (amino acid residues 127→197 of the authentic protein AEH27625) were extended both upstream and downstream by 9 external amino acids, which was used in the sequential ExPASy ProtScale plotting for hydropathy, α-helices, β-sheets, β-turns, and coils with a window size of 9 amino acid residues (*cf.* Section 2.3).

The hydrophobicity and structural characteristics of the HMG-box_ROX1-like domain of the MAT1-2-1 protein AGW27543 are compared with those of the reference protein AEH27625 in Figure 13. The protein AGW27543 (under the AlphaFold code U3N9W0) is derived from the *O. sinensis* strain CS91-1291 (*cf.* Table 1) [14], while the reference protein AEH27625 (under the AlphaFold code D7F2E9) is derived from the *H. sinensis* strain CS2 [70]. Panel (A) of Figure 13 shows a 12-residue truncation at the C-terminus of the HMG-box_ROX1-like domain of the protein AGW27543, along with a Y-to-H substitution (tyrosine to histidine). This substitution changes the hydropathy index from -1.3 to -3.2 (Table S3) [73], resulting in reduced hydrophobicity. The C-terminal truncation and amino acid substitution, along with the accompanying reduction in hydrophobicity, resulted in altered secondary structures surrounding the variation sites within the HMG-box_ROX1-like domain of the protein AGW27543. This alteration is reflected by changes in the topological structure and waveform of the ExPASy ProtScale plots, which illustrate hydropathy, α-helices, β-sheets, β-turns, and coils in Panels (B)–(F), respectively. As shown in the 3D structures presented in Panels (G)–(H), the truncation and replaced amino acid residues are located in 2 of the 3 α-helices that form the core L-shaped stereostructure. These modifications result in an altered tertiary structure of the HMG-box_ROX1-like domain of the protein AGW27543 under the AlphaFold code U3N9W0.

Panel (A): Alignment of amino acid sequences the HMG-box_ROX1-like domains

```
AEH27625 118 APPSPKDIKIPRPPNAYILYRKERHHYVKDANPGITNNEISQILGKAWNMESNDVRQKYK  177
AGW27543 118 --------------------------H--------------------------------  177

AEH27625 178 DMSQQVKQALLEKHPDYQYKPRRPCERRR                                206
AGW27543 178 --------                                                     185
```

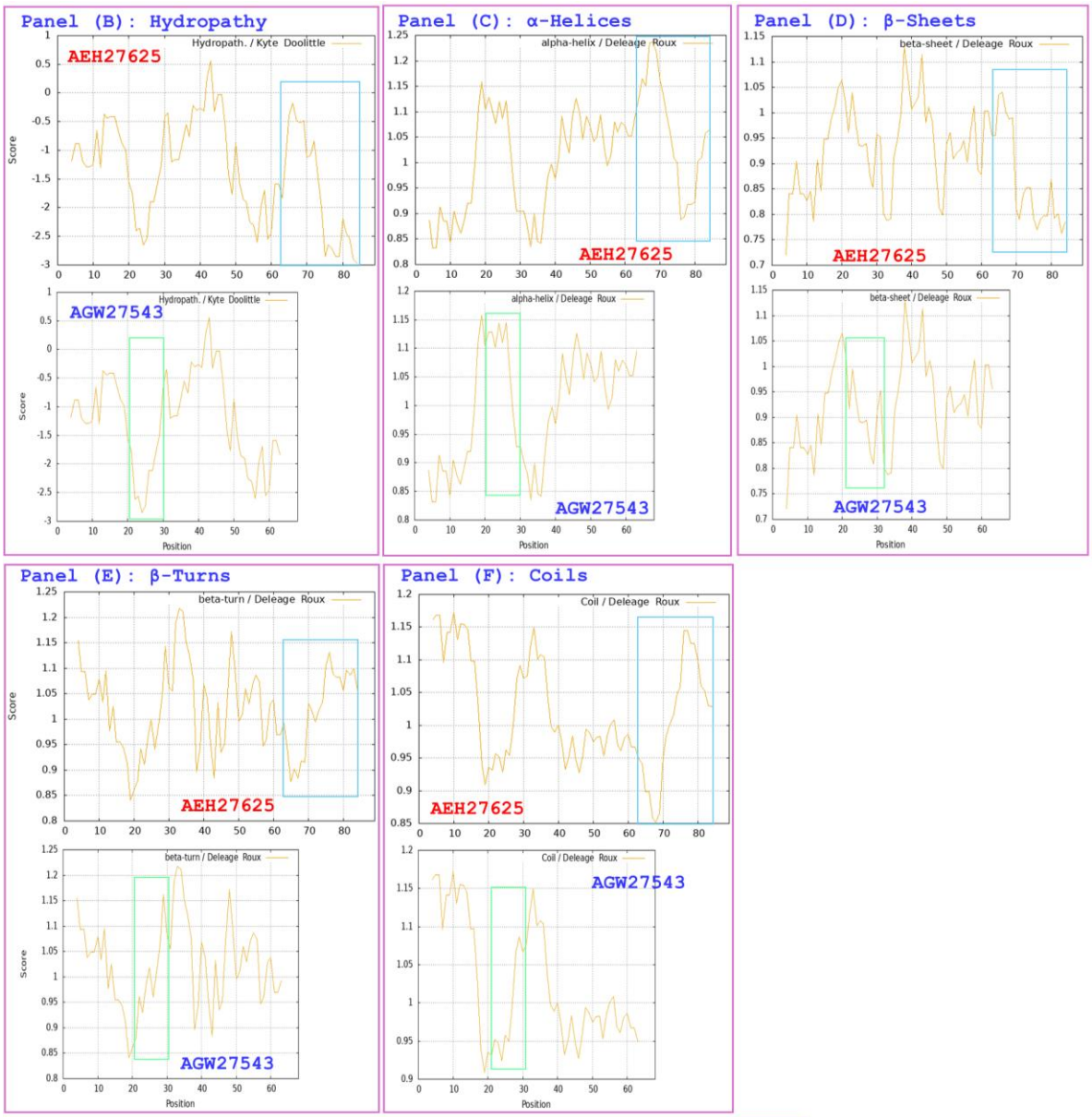
Panel (B): Hydropathy
Hydropath. / Kyte Doolittle
AEH27625
AGW27543
Score
Position
Panel (C): α-Helices
alpha-helix / Deleage Roux
AEH27625
AGW27543
Position
Panel (D): β-Sheets
beta-sheet / Deleage Roux
AEH27625
AGW27543
Position
Panel (E): β-Turns
beta-turn / Deleage Roux
AEH27625
AGW27543
Score
Position
Panel (F): Coils
Coil / Deleage Roux
AEH27625
AGW27543
Position

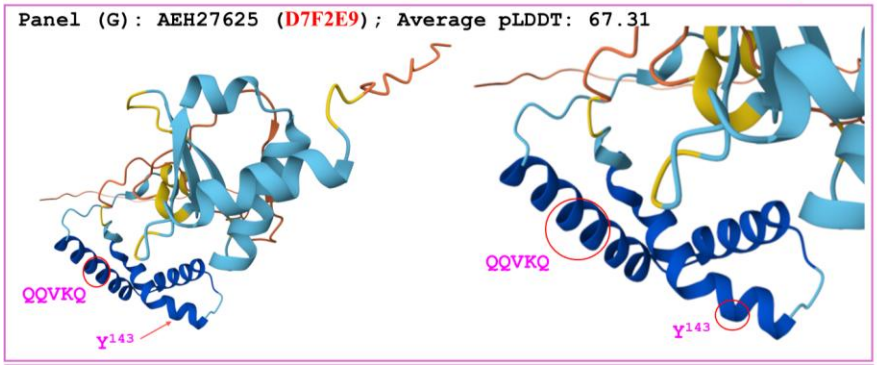
Panel (G): AEH27625 (D7F2E9); Average pLDDT: 67.31
QQVKQ
Y143
QQVKQ
Y143

551

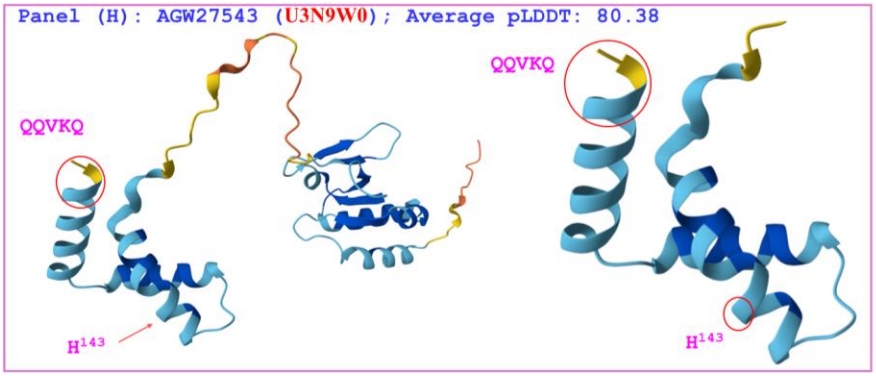

Figure 13. Correlations between the changes in hydrophobicity and the primary, secondary, and tertiary structures of the HMG-box_ROX1-like domains of MAT1-2-1 proteins. The reference protein AEH27625 (under the AlphaFold code D7F2E9) is derived from the *H. sinensis* strain CS2, and the variant MAT1-2-1 protein AGW27543 (under the AlphaFold code U3N9W0) is derived from the *O. sinensis* strain CS91-1291. Panel (A) shows an alignment of the amino acid sequences of the HMG-box_ROX1-like domains of the MAT1-2-1 proteins; the amino acid substitution is shown in green, the hyphens indicate identical amino acid residues, and the spaces denote unmatched sequence gaps. The ExPASy ProtScale plots show the changes in hydrophobicity and the 2D structure of the protein in Panels (B)–(F) for the hydropathy, α-helices, β-sheets, β-turns, and coils, respectively; the open rectangles in blue highlight the C-terminally truncated regions in the ExPASy plots, and those in green highlight the changes in topological structure and waveform observed in the plots. Panels (G)–(H) show representations of the 3D structures of the full-length proteins on the left; the locally magnified structures at the variation sites are shown on the right. The model confidence for the AlphaFold-predicted 3D structures is as follows: ■ very high (pLDDT>90); ■ high (90>pLDDT>70); ■ low (70>pLDDT>50); and ■ very low (pLDDT<50).

The hydrophobicity and structural characteristics of the HMG-box_ROX1-like domain of the MAT1-2-1 protein AGW27554 are compared with those of the reference protein AEH27625 in Figure 14. The protein AGW27554 (under the AlphaFold code U3NEA9) is derived from the *O. sinensis* strain CS71-1219 [14], whereas the reference protein AEH27625 (under the AlphaFold code D7F2E9) is derived from the *H. sinensis* strain CS2 [70]. Panel (A) of Figure 14 shows a 12-residue truncation at the C-terminus of the HMG-box_ROX1-like domain of the protein AGW27554, along with 2 amino acid substitutions: Y-to-H (tyrosine to histidine; hydropathy indices changed from -1.3 to -3.2) and Q-to-T (glutamine to threonine; hydropathy indices changed from -3.5 to -0.7 (Table S3) [73]. The C-terminal truncation and amino acid substitutions accompanied by altered hydrophobicity result in changes in the secondary structure surrounding the variation sites in the HMG-box_ROX1-like domain of the protein AGW27543. This alteration is reflected by the changes in the topological structure and waveform of the ExPASy ProtScale plots, which illustrate hydropathy, α-helices, β-sheets, β-turns, and coils, in Panels (B)–(F), respectively. As illustrated in the 3D structures in Panels (G)–(H), the truncated and replaced residues are located in 2 of the 3 core α-helices. These modifications result in an altered tertiary structure of the HMG-box_ROX1-like domain of the protein AGW27554 under the AlphaFold code U3NEA9.

Panel (A): Alignment of amino acid sequences the HMG-box_ROX1-like domains

```
AEH27625 118 APPSPKDIKIPRPPNAYILYRKERHHYVKDANPGITNNEISQILGKAWNMESNDVRQKYK  177
AGW27554 118 -------------------------H--------------------------------  177

AEH27625 178 DMSQQVKQALLEKHPDYQYKPRRPCERRR                                206
AGW27554 178 -------T                                                     185
```

582

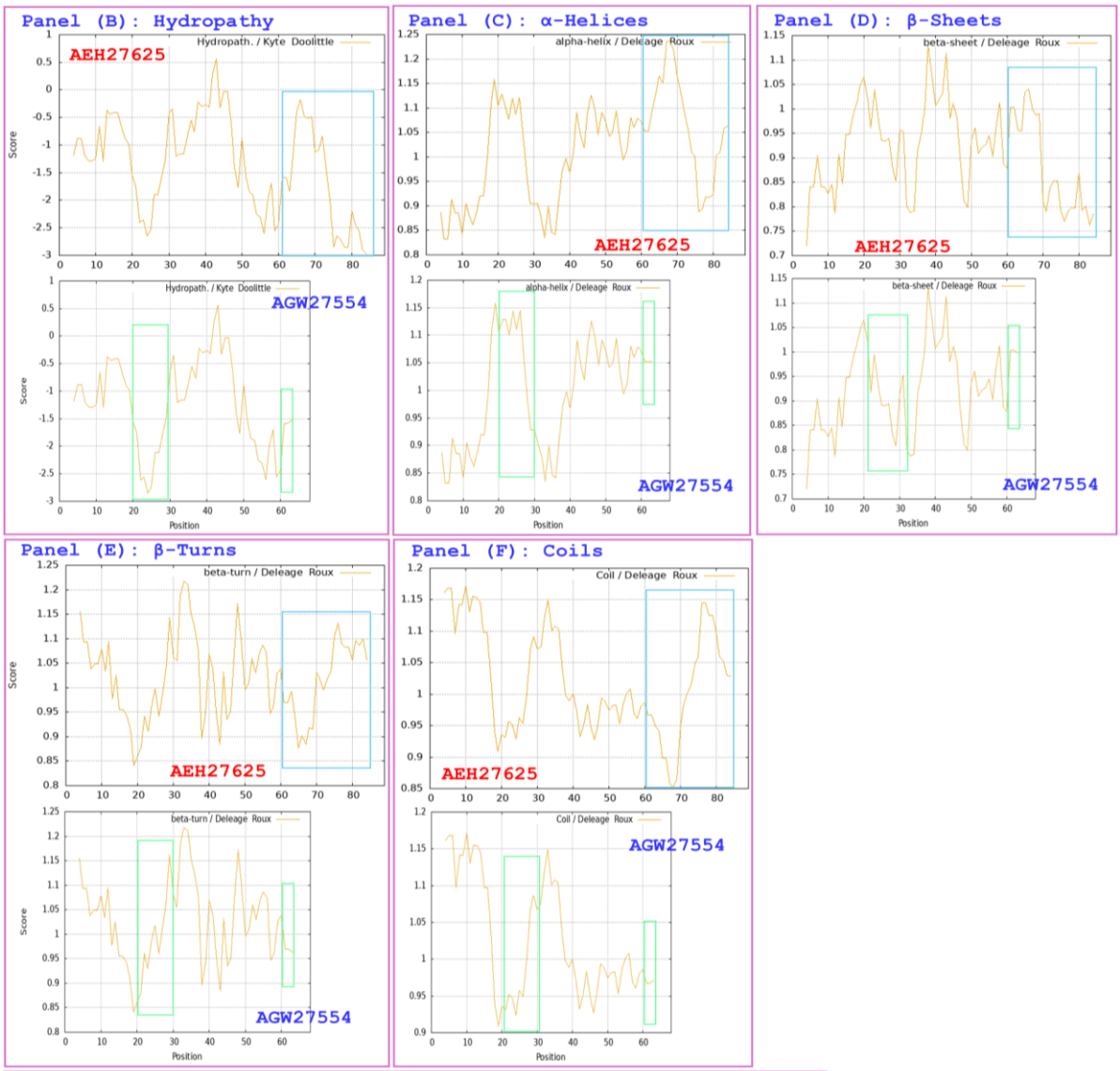

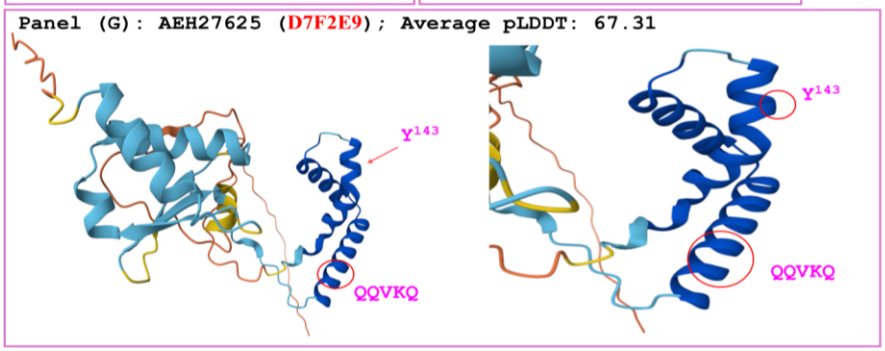

583

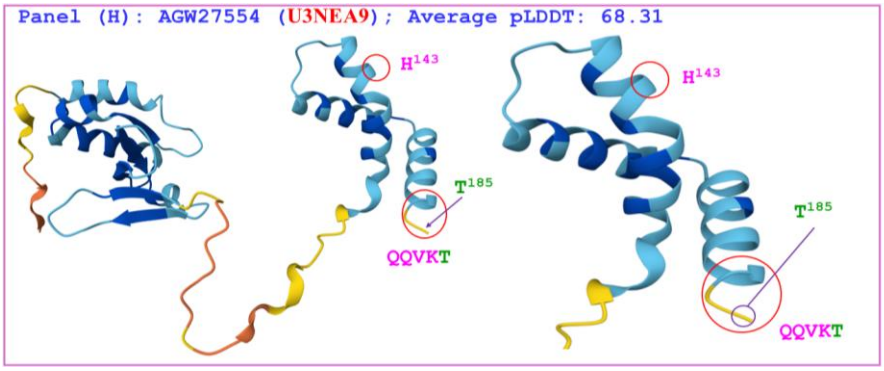

Figure 14. Correlations between changes in hydrophobicity and the primary, secondary, and tertiary structures of the HMG-box_ROX1-like domains of MAT1-2-1 proteins. The reference protein AEH27625 (under the AlphaFold code D7F2E9) is derived from the *H. sinensis* strain CS2, and the variant MAT1-2-1 protein AGW27554 (under the AlphaFold code U3NEA9) is derived from the *O. sinensis* strain CS71-1219. Panel (A) shows an alignment of the amino acid sequences of the HMG-box_ROX1-like domains of the MAT1-2-1 proteins; amino acid substitutions are shown in green, the hyphens indicate identical amino acid residues, and the spaces denote unmatched sequence gaps. The ExPASy ProtScale plots show the changes in hydrophobicity and the 2D structure of the protein in Panels (B)–(F) for hydropathy, α-helices, β-sheets, β-turns, and coils, respectively; the open rectangles in blue highlight the C-terminal truncation regions in the ExPASy plots and those in green highlight the changes in the topological structure and waveform. Panels (G)–(H) show representations of the 3D structures of the full-length proteins on the left; the locally magnified structures at the variation sites are shown on the right. The model confidence for the AlphaFold-predicted 3D structures is as follows: ■ very high (pLDDT>90); ■ high (90>pLDDT>70); ■ low (70>pLDDT>50); and ■ very low (pLDDT<50).

The hydrophobicity and structural characteristics of the HMG-box_ROX1-like domains of the MAT1-2-1 proteins AGW27548 and AGW27555 are compared with those of the reference protein AEH27625, as shown in Figure 15. These 2 variant proteins (both under the AlphaFold code U3N9W5) are derived from the *O. sinensis* strains CS68-2-1229 and CS71-1220, respectively (*cf*. Table 1) [14], while the reference protein AEH27625 (under the AlphaFold code D7F2E9) is derived from the *H. sinensis* strain CS2 [70]. Panel (A) of Figure 15 shows 22-residue truncations at the C-termini of the HMG-box_ROX1-like domains of the MAT1-2-1 proteins AGW27548 and AGW27555, along with a Y-to-H (tyrosine to histidine) amino acid substitution within the HMG-box_ROX1-like domains of both variant proteins. This substitution changes the hydropathy index from -1.3 to -3.2 (Table S3) [73]. The C-terminal truncations and amino acid substitutions caused decreased hydrophobicity and altered the secondary structures surrounding the variation sites in the HMG-box_ROX1-like domains of the MAT1-2-1 proteins AGW27548 and AGW27555. This alteration is reflected by changes in the topological structure and waveform of the ExPASy ProtScale plots, which illustrate hydropathy, α-helices, β-sheets, β-turns, and coils in Panels (B)–(F), respectively. As shown in the 3D structures in Panels (G)–(H), the truncations and replaced amino acid residues are located in 2 of the 3 core α-helices. These modifications result in altered tertiary structures of the HMG-box_ROX1-like domains of the MAT1-2-1 proteins

AGW27548 and AGW27555 under the AlphaFold code U3N9W5.

Panel (A): Alignment of amino acid sequences the HMG-box_ROX1-like domains

```
AEH27625 118 APPSPKDIKIPRPPNAYILYRKERHHYVKDANPGITNNEISQILGKAWNMESNDVRQKYK  177
AGW27548 118 --------------------------H------------------------------  175
AGW27555 118 --------------------------H------------------------------  175

AEH27625 178 DMSQQVKQALLEKHPDYQYKPRRPCERRR                               206
AGW27548 175
AGW27555 175
```

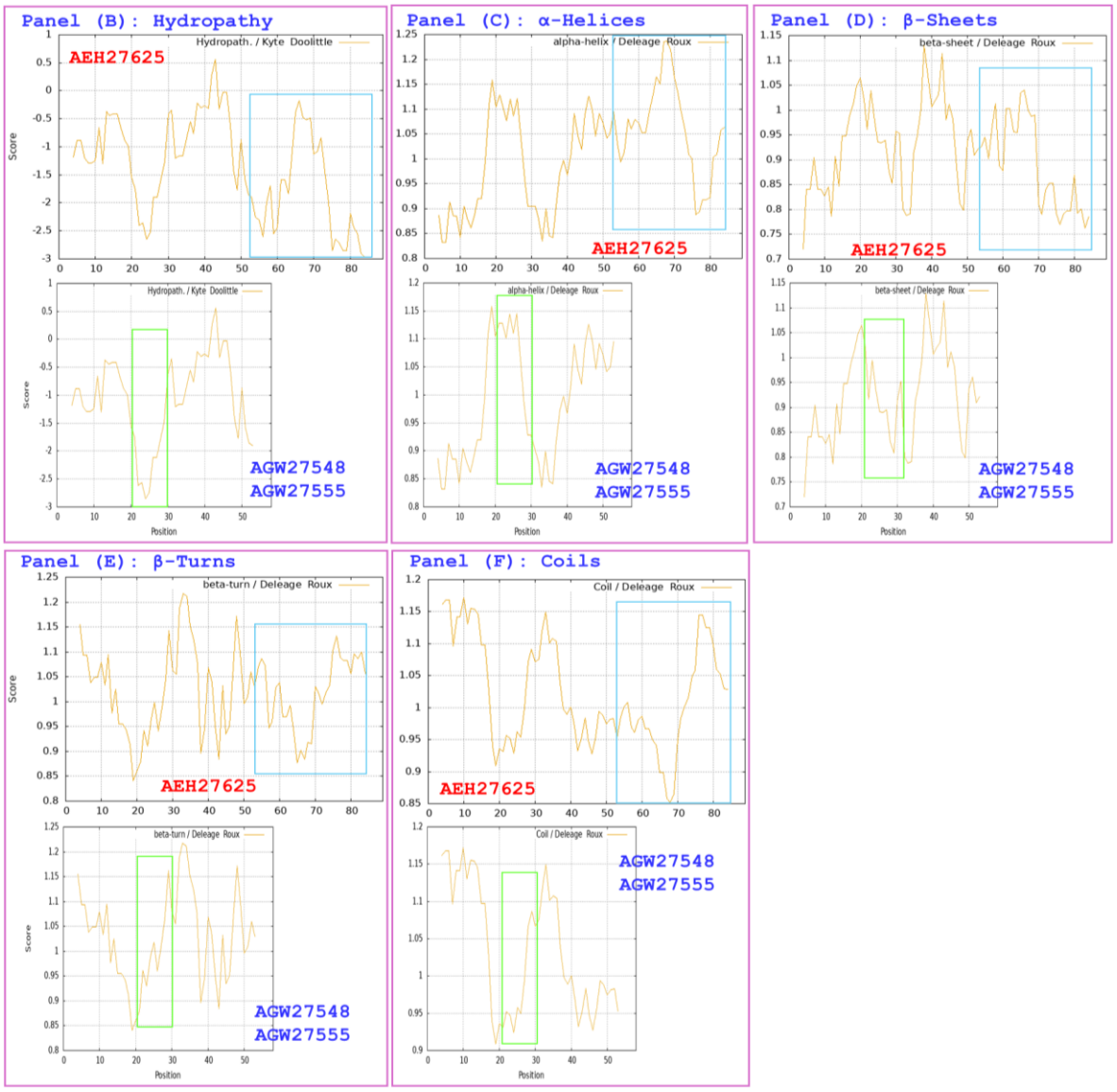

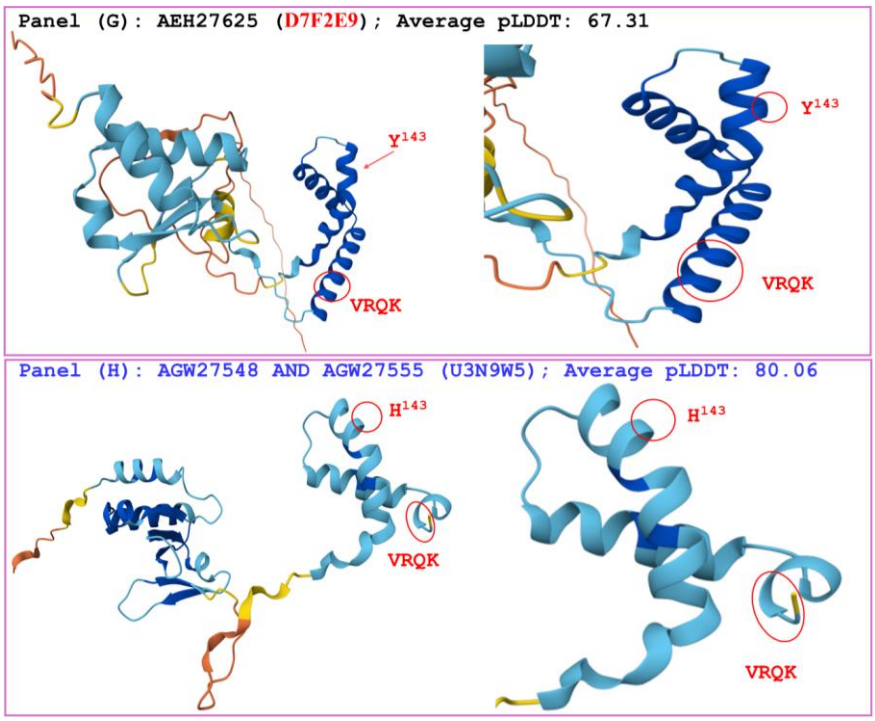

Figure 15. Correlations between changes in hydrophobicity and the primary, secondary, and tertiary structures of the HMG-box_ROX1-like domains of MAT1-2-1 proteins. The reference protein AEH27625 (under the AlphaFold code D7F2E9) is derived from the *H. sinensis* strain CS2, and the variant MAT1-2-1 proteins AGW27548 and AGW27555 (under the AlphaFold code U3N9W5) are derived from the *O. sinensis* strains CS68-2-1229 and CS71-1220, respectively. Panel (A) shows an alignment of the amino acid sequences of the HMG-box_ROX1-like domains of the MAT1-2-1 proteins; amino acid substitutions are shown in green, the hyphens indicate identical amino acid residues, and the spaces denote unmatched sequence gaps. The ExPASy ProtScale plots show the changes in hydrophobicity and the 2D structure in Panels (B)–(F) for the hydropathy, α-helices, β-sheets, β-turns, and coils of the proteins, respectively; the open rectangles in blue highlight the C-terminally truncated regions in the ExPASy plots, and the changes in topological structure and waveform observed in the plots are highlighted in red. Panels (G)–(H) show representations of the 3D structures of the full-length proteins on the left; the locally magnified structures at the variation sites are shown on the right. The model confidence for the AlphaFold-predicted 3D structures is as follows: ■ very high (pLDDT>90); ■ high (90>pLDDT>70); ■ low (70>pLDDT>50); and ■ very low (pLDDT<50).

The hydrophobicity and structural characteristics of the HMG-box_ROX1-like domain of the MAT1-2-1 protein AGW27552 are compared with those of the reference protein AEH27625, as shown in Figure 16. The variant protein (under the AlphaFold code U3N6W6) is derived from the *O. sinensis* strain CS68-5-1216 [14], while the reference protein AEH27625 (under the AlphaFold code D7F2E9) is derived from the *H. sinensis* strain CS2 [70]. Panel (A) of Figure 16 shows a 23-residue truncation at the C-terminus of the HMG-box_ROX1-like domain in the MAT1-2-1 protein AGW27552, along with a Y-to-H substitution (tyrosine to histidine; hydropathy indices changed from -1.3 to -3.2) (Table S3) [73]) within the HMG-box_ROX1-like domain. This amino acid substitution caused decreased hydrophobicity and modified the secondary structures surrounding the sites of variation within the HMG-box_ROX1-

like domain of the MAT1-2-1 protein AGW27552. Changes in the topological structure and waveform are reflected in the ExPASy ProtScale plots corresponding to hydropathy, α-helices, β-sheets, β-turns, and coils in Panels (B)–(F), respectively. As shown in the comparison of the 3D structures in Panels (G)–(H) for a comparison of 3D structures, the truncation and replaced residue occur within 2 of the 3 core α-helices and completely remodel the overall stereostructure of the HMG-box_ROX1-like domain of the MAT1-2-1 protein AGW27552 (under AlphaFold code U3N6W6).

Panel (A): Alignment of amino acid sequences the HMG-box_ROX1-like domains

```
AEH27625 118 APPSPKDIKIPRPPNAYILYRKERHHYVKDANPGITNNEISQILGKAWNMESNDVRQKYK  177
AGW27552 118 --------------------------H------------------------------  174

AEH27625 178 DMSQQVKQALLEKHPDYQYKPRRPCERRR                               206
AGW27552 174
```

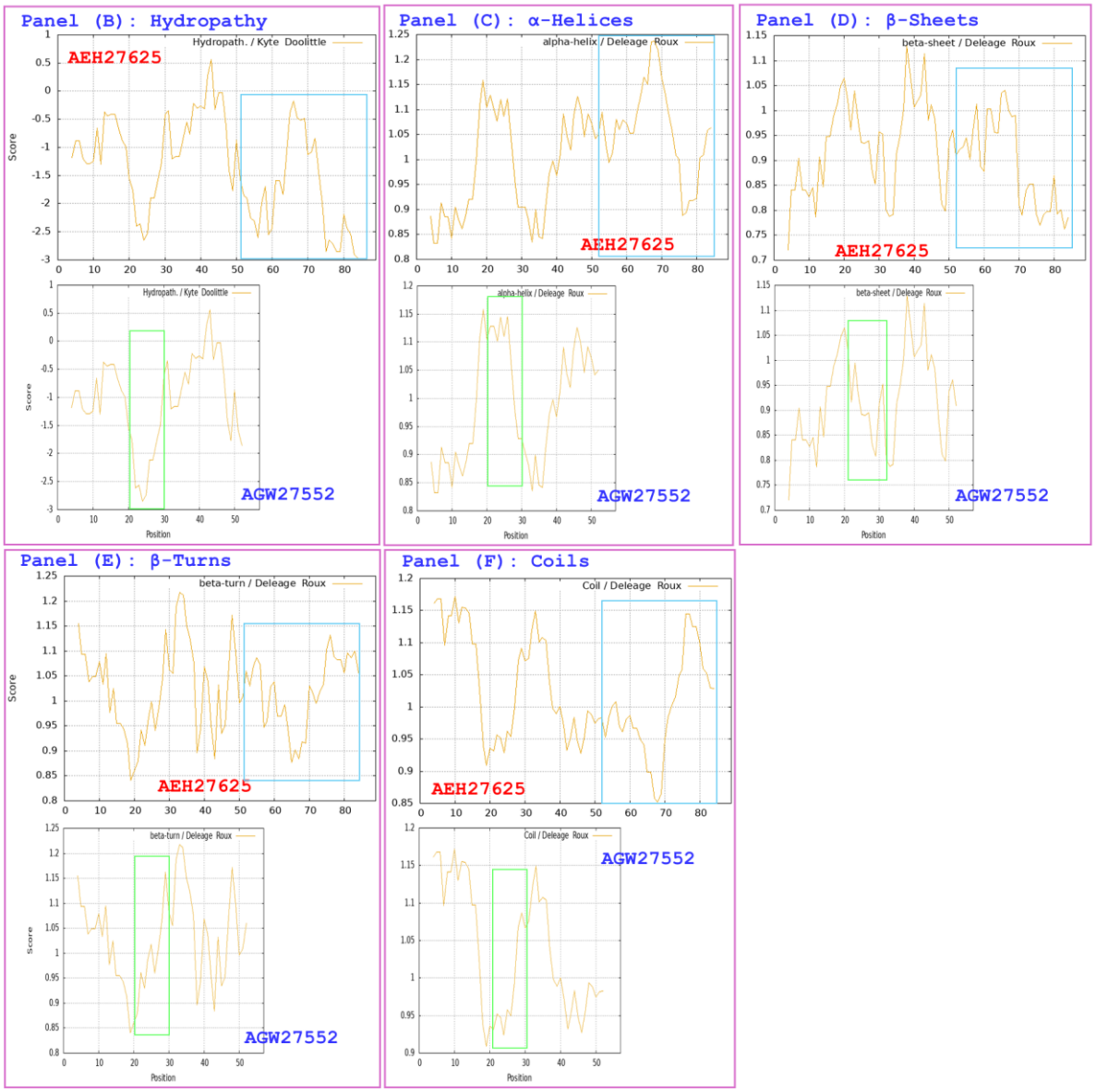

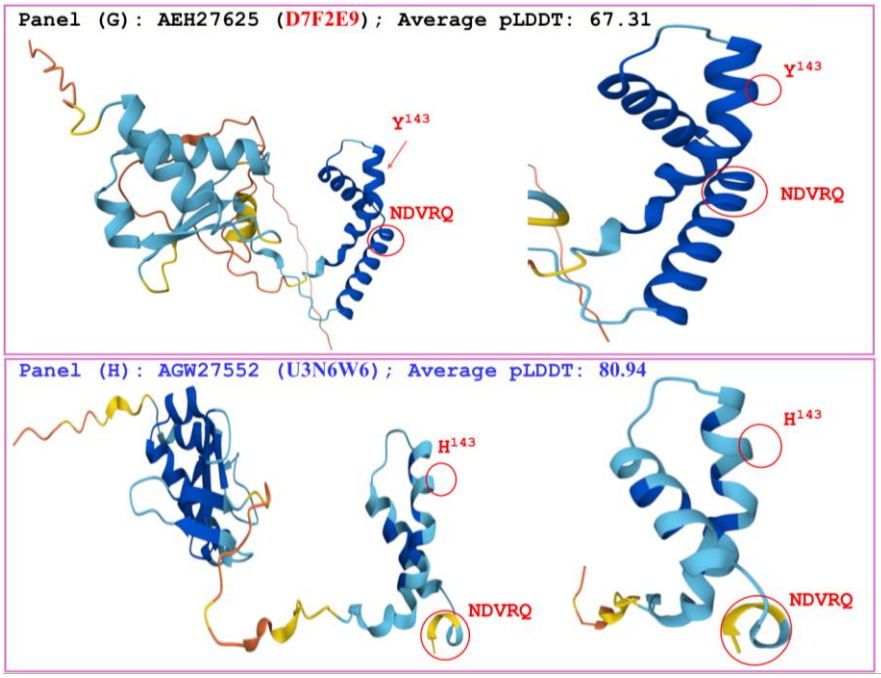

Figure 16. Correlations between changes in hydrophobicity and the primary, secondary, and tertiary structures of the HMG-box_ROX1-like domains of MAT1-2-1 proteins. The reference protein AEH27625 (under the AlphaFold code D7F2E9) is derived from the *H. sinensis* strain CS2, and the variant MAT1-2-1 protein AGW27552 (under the AlphaFold code U3N6W6) is derived from the *O. sinensis* strain CS68-5-1216. Panel (A) shows an alignment of the amino acid sequences of the HMG-box_ROX1-like domains of the MAT1-2-1 proteins; amino acid substitutions are shown in green, the hyphens indicate identical amino acid residues, and the spaces denote unmatched sequence gaps. The ExPASy ProtScale plots show the changes in hydrophobicity and the 2D structure of the protein in Panels (B)–(F) for the hydropathy, α-helices, β-sheets, β-turns, and coils, respectively; the open rectangles in blue highlight the C-terminally truncated regions in the ExPASy plots, and those in red highlight the changes in topological structure and waveform observed in the plots. Panels (G)–(H) show representations of the 3D structures of the full-length proteins on the left; the locally magnified structures at the sites of substitutions are shown on the right. The model confidence for the AlphaFold-predicted 3D structures is as follows: ■ very high (pLDDT>90); ■ high (90>pLDDT>70); ■ low (70>pLDDT>50); and ■ very low (pLDDT<50).

Collectively, the data in Figures 13–16 in Section 3.4 demonstrate that variant MAT1-2-1 proteins derived from various *O. sinensis* strains exhibit C-terminal truncations (ranging from 12 to 23 residues) within their HMG-box_ROX1-like domains, accompanied by tyrosine-to-histidine (Y-to-H) substitutions. These structural modifications alter the hydrophobicity, secondary structures, and tertiary structures of the HMG-box_ROX1-like domains. Both truncations and substitutions are localized within the 3 core α-helices of the domains. The variant MAT1-2-1 proteins correspond to one of four distinct AlphaFold 3D structural conformations (*cf.* Table 1, Figure 4), highlighting the structural diversity of this protein family among different *O. sinensis* strains.

3.5 Diverse fungal sources of the MAT1-1-1 and MAT1-2-1 protein variants

673 **produced simultaneously in pairs by the 20 *O. sinensis* strains**

674 **3.5a Complex genetic heterogeneity of the *O. sinensis* strains**

675 The ITS sequences used for phylogenetic analysis are available in GenBank for 15 of the 20 *O.*
676 *sinensis* strains obtained by Li *et al*. [36] but are lacking for the remaining 5 strains (*cf*. Table 1). The
677 design of the PCR experiment in that study included the use of a pair of fungal universal primers
678 (ITS5/ITS4 [92]) and 3 pairs of self-designed primers (GAF/GAR, GCF/GCR, and 5.8S-F/R) for ITS
679 sequence amplification and the annealing temperatures were set to 53°C for primers ITS5/ITS4, 55°C
680 for primers GAF/GAR specific for the GC-biased sequences of Group A (Genotype #1 of *O. sinensis*),
681 and 60°C for primers GCF/GCR specific for the AT-biased sequences of group C (Genotype #5 of *O.*
682 *sinensis*). Table S6 lists the percentage identities and sequence coverages between the sequences of the
683 primers and the representative GC- and AT-biased genotypes of *O. sinensis*. Some of the genotypes show
684 no or significantly low sequence identities and coverages in Table S6, indicating that they may not be
685 amplified if they truly co-occur in the test samples. Compared with other sequences, some genotypic
686 components of *O. sinensis* might be much more efficiently amplified, causing differential dominances
687 of the PCR amplicons. Furthermore, Li *et al*. [36] adopted a direct sequencing strategy for amplicons.
688 Obviously, this study did not employ rigorous amplicon cloning–sequencing techniques with the
689 selection of a sufficient number (30−50) of white colonies to achieve comprehensive, unbiased genetic
690 profiling, nor did it use the MassARRAY single-nucleotide polymorphism (SNP) MALDI-TOF mass
691 spectrum genotyping technique with multiple extension primers for comprehensive phylogenetic
692 examinations. Consequently, the molecular examination after 25 days of shaker incubation of *C. sinensis*
693 monoascospores and tissues of caterpillar bodies (sclerotium) would have inevitably overlooked
694 nonculturable fungal sequences, and some co-occurring amplicon sequences whose abundance in the
695 amplicon pools might have been low because of low amplification efficiency under the design used in
696 this study [36−37].

697 Under these experimental settings, Li *et al*. [36] reported that 10 of the 15 *O. sinensis* strains are
698 homogenous, harboring only GC-biased Genotype #1 *H. sinensis* (*cf*. Table 1); the remaining 5 strains
699 are heterogeneous, containing both GC-biased Genotype #1 (Group A) and AT-biased Genotype #17
700 (Group C) of *O. sinensis* strains (*cf*. Tables S1−S2) [9−10,12−13,36−37]. However, because of the
701 insufficiently refined research design adopted by Li *et al*. [36], a high level of vigilance is warranted
702 regarding the potential coexistence of additional fungal species or *O. sinensis* genotypes in previously
703 purportedly homogenous and heterogeneous strains. Given the complex genetic background of the *O.*

704 *sinensis* strains, the possibility cannot be excluded that the detected MAT1-1-1 and/or MAT1-2-1 protein
705 variants, which are characterized by differential truncations and various amino acid substitutions at
706 distinct variation sites, originate from other unnoticed coexisting fungi.

707 Notably, the remaining 5 *O. sinensis* strains (CS26-277, CS36-1294, CS68-5-1216, CS70-1211, and
708 CS70-1212, shown in black in Table 1) lack ITS sequence records in the GenBank database, and their
709 homo/heterogeneous characteristics remain unknown. Researchers who possess these strains [14,36] are
710 expected to upload the missing ITS sequences to GenBank, ensuring the comprehensive and impartial
711 molecular documentation of these strains.

712 **3.5b Differential pairing of the MAT1-1-1 and MAT1-2-1 proteins simultaneously produced by**
713 **the 20 *O. sinensis* strains**

714 Sections 3.1−3.4 present various AlphaFold tertiary structural models of the mating protein variants
715 derived from 20 *O. sinensis* strains. These strains simultaneously produced paired MAT1-1-1 and MAT1-
716 2-1 proteins that harbor differential truncations at the N- and/or C-termini and diverse amino acid
717 substitutions. As shown in Table 2, 10 of the 20 strains are "homogenous" strains shown in brown, 5 are
718 heterogeneous strains shown in red, and the remaining 5 strains have unknown homo/heterogeneous
719 characteristics and are indicated in black. Based on the pairing patterns of the 2 mating proteins, these
720 strains can be categorized into 2 groups (Table 2). **Group I** consists of 5 strains, which simultaneously
721 produce truncated MAT1-1-1 and MAT1-2-1 proteins in pairs; **Group II** is composed of the remaining
722 15 *O. sinensis* strains, which simultaneously produce in pairs the truncated MAT1-1-1 proteins and the
723 full-length MAT1-2-1 proteins (*cf*. Table S5). The MAT1-1-1 and MAT1-2-1 proteins that share the same
724 AlphaFold 3D structural morph are labeled with the same suffix symbol (⁋, †, *, ⁑, ‡, or ♦) in Table 2.

725 **Table 2**. The two groups of the 20 *O. sinensis* strains based on the differential co-occurrence of pairs of the MAT1-
726 1-1 and MAT1-2-1 proteins with different truncations and amino acid substitutions

Group	*O. sinensis* strains	MAT1-1-1 protein					MAT1-2-1 protein			
		GenBank accession #	Number of residues truncated at		Amino acid substitution	AlphaFold code	GenBank accession #	Number of residue(s) truncated at C-terminus	Amino acid substitution	AlphaFold code
			N-terminus	C-terminus						
I	CS71-1219	AGW27534	110	8		U3NE87 *	AGW27554	65	Y-to-H, Q-to-T	U3NEA9
	CS68-5-1216	AGW27532	97	8		U3N6U8 †	AGW27552	75	Y-to-H	U3N6W6
	CS71-1220	AGW27535	97	8		U3N6U8 †	AGW27555	74	Y-to-H	U3N9W5 ⁑
	CS68-2-1229	AGW27528	63	8		U3N9T9 ⁋	AGW27548	74	Y-to-H	U3N9W5 ⁑
	CS91-1291	AGW27523	63	8		U3N9T9 ⁋	AGW27543	64	Y-to-H	U3N9W0
II	CS37-295	AGW27519	63	8		U3N9T9 ⁋	AGW27539			D7F2E9 ♦
	CS36-1294	AGW27518	63	8		U3N9T9 ⁋	AGW27538			D7F2E9 ♦
	CS26-277	AGW27521	63	8		U3N9T9 ⁋	AGW27541			D7F2E9 ♦
	CS6-251	AGW27517	63	8		U3N9T9 ⁋	AGW27537		V-to-I, Y-to-H	U3N6V5
	CS18-266	AGW27520	63	8		U3N9T9 ⁋	AGW27540		Y-to-H	—
	CS34-291	AGW27524	63	8		U3N9T9 ⁋	AGW27544		Y-to-H	—
	CS71-1218	AGW27533	97	8		U3N6U8 †	AGW27553	1	Y-to-H, K-to-X	U3N9X0
	CS70-1211	AGW27530	97	8	F-to-V	U3NE79 ‡	AGW27550		Y-to-H	—
	CS70-1208	AGW27529	97	8	F-to-V	U3NE79 ‡	AGW27549		Y-to-H	—
	CS70-1212	AGW27531	110	8		U3NE87 *	AGW27551		Y-to-H	—
	CS560-961	AGW27522	63	8	P-to-L	U3N6U0	AGW27542		Y-to-H	D7F2E3
	CS76-1284	AGW27525	66	10		U3N919	AGW27545		Y-to-H	—
	CS561-964	AGW27526	63	13	CDRA-to-SSFT	U3N7G5	AGW27546		Y-to-H	—
	CS25-273	AGW27527	77	18		U3N6U4	AGW27547		Y-to-H	—
	CS68-2-1228	AGW27536	95	8	S-to-E, L-residue deletion	U3N7H7	AGW27556		Y-to-H	—

Note: The *O. sinensis* strains shown in brown are "homogenous" and were detected only GC-biased Genotype #1 of *O. sinensis*; those shown in red are heterogeneous and were detected both GC-biased Genotype #1 and AT-biased Genotype #17 of *O. sinensis*; and those shown in black have unknown homo/heterogeneous characteristics (*cf*. Tables 1 and S1−S2) [10,14,36]. The GenBank protein accession numbers in pink refer to truncated MAT1-1-1 and MAT1-2-1 proteins and those in green indicate full-length MAT1-2-1 proteins. **Group I** strains feature the production of paired truncated MAT1-1-1 and MAT1-2-1 proteins. **Group II** strains produce truncated MAT1-1-1 proteins that are paired with full-length MAT1-2-1 proteins. AlphaFold codes with the same suffix symbol (⁋, †, *, ⁑, ‡, or ♦) belong to the same AlphaFold-predicted 3D structural morphs. Those without a suffix symbol indicate unique 3D structural morphs.

The 15 **Group-II** *O. sinensis* strains produced the full-length MAT1-2-1 proteins shown in green in Table 2. Three (AGW27538, AGW27539, and AGW27541) of them are 100% identical to the authentic MAT1-2-1 proteins represented by protein AEH27625 and share the same tertiary structures under the AlphaFold code D7F2E9. The remaining 12 MAT1-2-1 proteins (AGW27537, AGW27540, AGW27542, AGW27544−AGW27547, AGW27549−AGW27551, AGW27553, and AGW27556) contain 1−2 amino acid substitutions (Figure S3, Tables 2 and S5), all of which contain Y-to-H substitutions in the HMG-box_ROX1-like domains. The MAT1-2-1 protein AGW27537 derived from the *O. sinensis* strain CS6-251 contains an additional V-to-I (valine-to-leucine) substitution located upstream of the HMG-box_ROX1-like domain. The protein AGW27553 derived from the *O. sinensis* strain CS71-1218 contains an additional K-to-X (lysine-to-an unidentified residue) substitution located within the HMG-box_ROX1-like domain. Six of the 12 MAT1-2-1 proteins exhibit diverse tertiary structures under distinct AlphaFold 3D structural codes, whereas the remaining 6 proteins have not been assigned AlphaFold-predicted 3D structural morphs (Tables 2 and S5).

3.5c *O. sinensis* strains simultaneously produced MAT1-1-1 proteins with the same tertiary structures and MAT1-2-1 proteins with various tertiary structures

The sequence distributions of the paired MAT1-1-1 and MAT1-2-1 proteins that were simultaneously produced by each of the 20 *O. sinensis* strains are shown in Figure 17. Panel (A) of Figure 17 includes 8 *O. sinensis* strains: 4 purportedly homogenous strains shown in brown in Table 2, two heterogeneous strains shown in red, and the remaining two strains shown in black with unknown homo/heterogeneous characteristics. All these strains produced MAT1-1-1 proteins truncated by 63- and 8-residues at the N- and C-termini, respectively, which exhibit the same tertiary structures under the AlphaFold 3D structural code U3N9T9 labeled with the suffix "⁋" in Table 2 and analyzed above in Figure 5. Two purportedly homogenous strains, CS68-2-1229 and CS91-1291, belong to **Group I**, as shown in blue in Figure 17; these strains simultaneously produce the MAT1-2-1 proteins AGW27548 and AGW27543, which are differentially truncated by 74- and 64-residues, respectively, at the C-termini

762 and contain Y-to-H (tyrosine-to-histidine) substitutions within the HMG-box_ROX1-like domains
763 (Table 2, Figures 13, 15, and 17), resulting in altered 3D structures under AlphaFold codes U3N9W5
764 and U3N9W0, respectively.

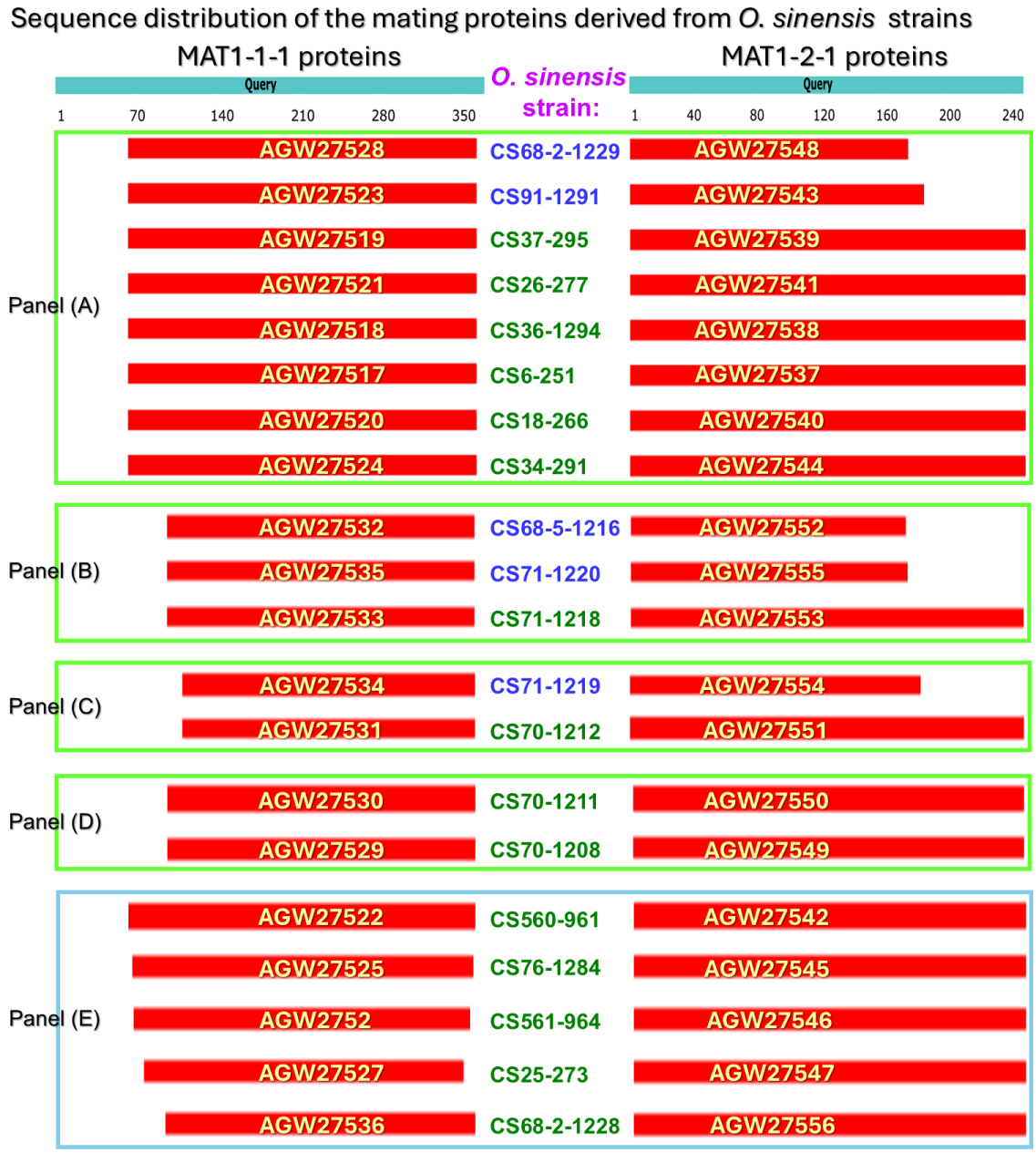

765
766 **Figure 17**. Alignment and sequence distributions of the paired MAT1-1-1 and MAT1-2-1 proteins derived from
767 the *O. sinensis* strains in **Group I** shown in blue and **Group II** shown in green (*cf.* Table 2). The MAT1-1-1 protein
768 AGW27560 (AlphaFold code U3N942) derived from the *H. sinensis* strain CS68-2-1229 was used as the query
769 MAT1-1-1 sequence, and the MAT1-2-1 protein AEH27625 (AlphaFold code D7F2E9) derived from the *H.*
770 *sinensis* strain CS2 was used as the query MAT1-2-1 sequence in the alignment. The panels outlined with open
771 rectangles in green and blue are arranged according to the AlphaFold 3D structural models for the MAT1-1-1 and
772 MAT1-2-1 proteins, respectively.

773 The remaining 6 *O. sinensis* strains in Panel (A) belong to **Group II**, as shown in green in Figure

774 17, including 2 purportedly homogenous strains, 2 heterogeneous strains, and 2 additional strains with
775 unknown homo/heterogeneous characteristics. In addition to producing the same truncated MAT1-1-1
776 proteins (under the AlphaFold code U3N9T9, labeled with the suffix "⁋" in Table 2), these 6 strains
777 simultaneously produced full-length MAT1-2-1 proteins with heteromorphic 3D structures, which
778 correspond to different AlphaFold codes or lack AlphaFold 3D structure codes and can be subgrouped
779 as described below (*cf*. Table 2 and Panel (A) of Figure 17):

780 (1) The coproduced full-length MAT1-2-1 proteins AGW27539, AGW27541, and AGW27538
781 exhibit the same 3D structure under the AlphaFold 3D structural code **D7F2E9**, which is marked
782 with a suffix symbol "♦" in Table 2. These proteins are 100% identical to the authentic MAT1-
783 2-1 protein AEH27625 (*cf*. Figure S3, Table S5) and were generated by the "homogenous" *O.*
784 *sinensis* strain CS37-295 and the strains CS26-277 and CS36-1294, which lack ITS sequence
785 records in GenBank (*cf*. Tables 1−2, Panel (A) of Figure 17).

786 (2) The coproduced full-length MAT1-2-1 protein AGW27537 has an altered tertiary structure
787 under the AlphaFold 3D structural code **U3N6V5** (*cf*. Figure 12 of [51] and Table S5) and was
788 produced by the heterogeneous *O. sinensis* strain CS6-251 (*cf*. Tables 1−2, Panel (A) of Figure
789 17). This protein is 99.2% similar to the authentic MAT1-2-1 protein AEH27625 and contains
790 V-to-I and Y-to-H substitutions, which are located upstream of and within the HMG-
791 box_ROX1-like domain, respectively (*cf*. Figures S3 and 17, Tables 2 and S3).

792 (3) The coproduced full-length MAT1-2-1 proteins AGW27540 and AGW27544 were produced by
793 the "homogenous" *O. sinensis* strain CS18-266 and the heterogeneous strain CS34-291.
794 Predicted 3D structures for these proteins are not available in the AlphaFold database (*cf*. Tables
795 1−2, Panel (A) of Figure 17). These proteins contain Y-to-H substitutions within the HMG-
796 box_ROX1-like domains and show 99.6% identity to the authentic MAT1-2-1 protein
797 AEH27625 (*cf*. Figure S3).

798 Panel (B) of Figure 17 includes 3 *O. sinensis* strains: CS68-5-1216 and CS71-1220 from **Group I**
799 and CS71-1218 from **Group II** (Table 2). Strain CS71-1218 is "homogenous", strain CS71-1220 is
800 heterogeneous, and strain CS68-5-1216 has unknown homo/heterogeneous characteristics [14,36] (*cf*.
801 Table 1). All 3 strains produced the MAT1-1-1 proteins (AGW27532, AGW27535, and AGW27533; *cf*.
802 Figures 9 and 17) with 97- and 8-residue truncations at the N- and C-termini, respectively, which
803 conform to the same AlphaFold 3D structural model (U3N6U8 marked with the suffix symbol "†" in
804 Table 2). Simultaneously, strains CS68-5-1216 and CS71-1220 produced the MAT1-2-1 proteins

805 AGW27552 and AGW27555 with 75- and 74-residue truncations at the C-termini, respectively, whereas
806 strain CS71-1218 produced the MAT1-2-1 protein AGW27553 with a single residue deletion at the C-
807 terminus (*cf*. Figures 3,15−17, and S3). These 3 MAT1-2-1 proteins contain Y-to-H substitutions within
808 the HMG-box_ROX1-like domains, whereas the full-length protein AGW27553 contains an additional
809 K-to-X (lysine-to-an unidentified residue) substitution in the HMG-box_ROX1-like domain. They show
810 99.6%, 99.6% and 99.2% similarity to the authentic MAT1-2-1 protein AEH27625 (*cf*. Figure S3) and
811 exhibit distinct 3D structures under the AlphaFold codes U3N6W6, U3N9W5, and U3N9X0,
812 respectively.

813 Panel (C) of Figure 17 lists the **Group-I** "homogenous" *O. sinensis* strain CS71-1219 and the
814 **Group-II** strain CS70-1212, which have unknown homo/heterogeneous characteristics (Tables 1−2).
815 These 2 strains produced the MAT1-1-1 proteins AGW27534 and AGW27531 with 110- and 8-residue
816 truncations at the N- and C-termini, respectively (*cf*. Figures 12 and 17), which conform to the same
817 AlphaFold 3D structural code U3NE87 (labeled with a suffix symbol "*" in Tables 1−2). Simultaneously,
818 strain CS71-1219 produced the MAT1-2-1 protein AGW27554, which is 65-residue truncated at the C-
819 terminus and contains Y-to-H and Q-to-T (glutamine-to-threonine) substitutions within the HMG-
820 box_ROX1-like domain. These variations resulted in an altered tertiary structure under the AlphaFold
821 3D structural code U3NEA9 (*cf*. Figures 14 and 17). In contrast, strain CS70-1212 produced the full-
822 length MAT1-2-1 protein AGW27551, which contains only a Y-to-H substitution within the HMG-
823 box_ROX1-like domain (*cf*. Figure S3, Table 2). No AlphaFold-predicted 3D structural model has been
824 assigned to the MAT1-2-1 protein AGW27551.

825 Panel (D) of Figure 17 lists 2 **Group-II** strains, CS70-1211 and CS70-1208; the former has
826 unknown homo/heterogeneous characteristics, and the latter is heterogeneous (Tables 1−2). These strains
827 produced the MAT1-1-1 proteins AGW27530 and AGW27529, whose N- and C-termini were truncated
828 by 97 and 8 residues, respectively. Both proteins contain F-to-V (phenylalanine-to-valine) substitutions
829 within the MATα_HMGbox domains, which conform to the same AlphaFold 3D model U3NE79 labeled
830 with a suffix symbol "‡" in Tables 1−2 (*cf*. Figures 10 and 17). Simultaneously, these strains produced
831 the full-length MAT1-2-1 proteins AGW27550 and AGW27549, which contain Y-to-H (tyrosine-to-
832 histidine) substitutions within the HMG-box_ROX1-like domains (*cf*. Tables 1−2; Figures 17 and S3)
833 and show 99.6% sequence identity to the authentic MAT1-2-1 protein AEH27625. No AlphaFold-
834 predicted 3D structural models have been assigned to the 2 MAT1-2-1 proteins.

835 **3.5e *O. sinensis* strains simultaneously produced MAT1-2-1 proteins with the same tertiary**
836 **structures and MAT1-1-1 proteins with various tertiary structures**

837 As shown in Table 2, the **Group-I** "homogenous" strain CS68-2-1229 and the heterogeneous strain
838 CS71-1220 produced the 74-residue truncated MAT1-2-1 proteins AGW27548 and AGW27555,
839 respectively, with Y-to-H substitutions within the HMG-box_ROX1-like domains (*cf*. Figures 15 and
840 17). These 2 proteins share the same tertiary structures under the AlphaFold code U3N9W5 labeled with
841 the suffix symbol "⁑" in Tables 1−2. Simultaneously, these strains produced the MAT1-1-1 proteins
842 AGW27528 and AGW27535, which have 63- and 8-residue truncations and 97- and 8-residue
843 truncations at the N- and C-termini of the proteins, respectively, and form distinct 3D structures under
844 AlphaFold codes U3N9T9 and U3N6U8 labeled with the suffix symbols "⁋" and "†" in Tables 1−2,
845 which were fall differently under Panels (A) and (B) of Figure 17, respectively (*cf*. Figures 5 and 9).

846 Panel (E) in Figure 17 (highlighted by the open rectangle in blue) includes 5 **Group-II** *O. sinensis*
847 strains (CS560-961, CS76-1284, CS561-964, CS25-273, and CS68-2-1228), which produced the full-
848 length MAT1-2-1 proteins (AGW27542, AGW27545, AGW27546, AGW27547, and AGW27556; *cf*.
849 Figure S3), respectively. These MAT1-2-1 proteins contain the same Y-to-H substitutions within the
850 HMG-box_ROX1-like domains. Unfortunately, only the protein AGW27542 was given an AlphaFold
851 3D structural code D7F2E3; the remaining 4 proteins exhibited the same structures as the protein
852 AGW27542 but were not assigned an AlphaFold 3D structural code. Simultaneously, these strains
853 generated truncated MAT1-1-1 protein variants (AGW27522, AGW27525, AGW27526, AGW27527,
854 and AGW27536; *cf*. Figures 9 and 17, Table 2) with different truncations (63-/8-residue, 66-/10-residue,
855 63-/13-residue, 77-/18-residue, and 95-/8-residue truncations) at the N-/C-termini, respectively, and
856 contain various amino acid substitutions, as shown in Table 2 and Figures 5−8, 11, and 17. The diverse
857 variations result in altered tertiary structures of the MAT1-1-1 proteins under distinct AlphaFold 3D
858 structural codes (U3N6U0, U3N919, U3N7G5, U3N6U4, and U3N7H7) (*cf*. Table 2, Figures 5−8 and
859 11).

860 **3.5f Distinct patterns of variation between the mating-type genes in the genome of pure *H.***
861 ***sinensis* and the mating proteins derived from the *O. sinensis* strains**

862 Table S7 summarizes the co-occurrence and differential occurrence of the MAT1-1-1 and MAT1-
863 2-1 proteins in *C. sinensis* insect–fungal complexes, wild-type *C. sinensis* isolates, and *O. sinensis* strains,
864 including various *O. sinensis* genotypes. Among the 183 total samples, the MAT1-1-1 and MAT1-2-1

865 proteins co-occur in 25.1% of the samples but differentially occur in 52.5% and 22.4% of the samples,
866 respectively.

867 Genomically, both the *MAT1-1-1* and *MAT1-2-1* genes are present in the genome assemblies
868 ANOV00000000 and LKHE00000000 of *H. sinensis* strains Co18 and 1229 (GC-biased Genotype #1 of
869 *O. sinensis*), respectively [65,93]. However, the *MAT1-1-1* gene is absent in the genome assemblies
870 LWBQ00000000 and NGJJ00000000 of *H. sinensis* strains ZJB12195 and CC1406-20395, respectively,
871 and the *MAT1-2-1* gene is absent in the genome assembly JAAVMX000000000 of *H. sinensis* strain
872 IOZ07 [94−96]. However, this differential pattern of the lack of *MAT1-1-1* and *MAT1-2-1* genes in the
873 genome of *H. sinensis* was not observed at the protein level. The 20 *O. sinensis* strains simultaneously
874 produced the MAT1-1-1 and MAT1-2-1 proteins in pairs without omissions.

875 Figure S1 of [51] revealed Y-to-M (tyrosine-to-methionine) substitutions in the MATα_HMGbox
876 domains of MAT1-1-1 proteins encoded by the genome assemblies LKHE00000000 and
877 JAAVMX000000000 of *H. sinensis* strains 1229 and IOZ07, respectively, but not by the genome
878 assembly ANOV00000000 of *H. sinensis* strain Co18 [51,65,93,96]. However, the Y-to-M substitution
879 was not detected in the MATα_HMGbox domains of variant MAT1-1-1 proteins derived from the 20 *O.*
880 *sinensis* strains.

881 Figure S2 of [51] revealed S-to-A (serine-to-alanine) substitutions in the HMG-box_ROX1-like
882 domains of MAT1-2-1 proteins encoded by the genome assemblies of ANOV00000000,
883 LKHE00000000, LWBQ00000000, and NGJJ00000000 of *H. sinensis* strains Co18, 1229, ZJB12195,
884 and CC1406-20395, respectively. However, the S-to-A substitution does not occur in the HMG-
885 box_ROX1-like domains of MAT1-2-1 proteins, regardless of whether they are truncated or full-length
886 proteins, derived from the 20 *O. sinensis* strains.

887 Aggregating the observations presented in Section 3.5, the 20 *O. sinensis* strains simultaneously
888 produced the MAT1-1-1 and MAT1-2-1 proteins in pairs, with differential truncations and diverse amino
889 acid substitutions. This finding highlights the genetic variations within the *MAT* loci in the fungal
890 genomes of impure *O. sinensis* strains, regardless of whether the strains were previously reported as
891 "homogenous" or heterogeneous by Li *et al.* [36]. The apparent differences in the presence/absence of
892 the *MAT1-1-1* and *MAT1-2-1* genes in the genome assemblies of the 5 *H. sinensis* strains were not
893 replicated at the protein level in the coproduction of MAT1-1-1 and MAT1-2-1 proteins in pairs from the
894 20 *O. sinensis* strains. Because repetitive copies of the *MAT1-1-1* or *MAT1-2-1* genes are not present in
895 the *H. sinensis* genome [69], these observations suggest that the paired MAT1-1-1 and MAT1-2-1

896 proteins are not necessarily the products of GC-biased Genotype #1 *H. sinensis* but are instead most
897 likely the products of different co-occurring heterospecific or genotypic fungi within the *O. sinensis*
898 strains.

899 4. Discussion

900 4.1 Altered tertiary structures of the critical DNA-binding domains of mating 901 proteins produced by various *O. sinensis* strains

902 Li *et al*. [67−68] previously reported the differential occurrence, differential transcription, and
903 alternative splicing of *MAT1-1-1* and *MAT1-2-1* and pheromone receptor genes in *H. sinensis*, wild-type
904 *C. sinensis* isolates, and the *C. sinensis* insect−fungal complex. The full-length MAT1-1-1 and MAT1-
905 2-1 proteins contribute to 15 and 17 heteromorphic stereostructures, belonging to 5 and 5 Bayesian
906 clusters, respectively [69], whereas the DNA-binding domains of the full-length mating proteins derived
907 from wild-type *C. sinensis* isolates clustered into 5 and 2 branched Bayesian clusters, respectively, as
908 summarized in Tables S6−S9 of [51]. Thus, the evidence at the genetic, transcriptional, and protein
909 structural levels supports that *O. sinensis* experiences self-sterility and employs a heterothallic, hybrid,
910 or even parasexual strategy to accomplish sexual reproduction during the lifecycle of the *C. sinensis*
911 insect–fungal complex [51,67−69]. The data analyzed in this paper extend the previous observations by
912 focusing on differential truncations and diverse amino acid substitutions within the MATα_HMGbox
913 and HMG-box_ROX1-like domains of MAT1-1-1 and MAT1-2-1 proteins, respectively, which are
914 coproduced in pairs by the 20 *O. sinensis* strains (Figure 17; Tables 1−2). The N- and/or C-terminal
915 truncations and 1−4 amino acid substitutions within the DNA-binding domains significantly influence
916 the hydrophobic properties and modify the secondary and tertiary structures of the functional domains
917 of mating proteins, particularly the tertiary structures of the hydrophobic cores formed by 3 α-helices
918 within the DNA-binding domains. These structural variations ultimately modulate the synergistic
919 interactions between the key functional domains of mating proteins during the sexual reproduction of *O.*
920 *sinensis*.

921 The HMGbox domains in mating proteins are multifunctional motifs that are central to the
922 transcriptional regulation of mating-related genes, *O. sinensis* sexual reproduction, and host adaptation
923 within the *C. sinensis* insect–fungal complex [51,59,67−69]. Researchers have inferred that the MATα-
924 HMGBox in the MAT1-1-1 protein has a conserved ancestral mating-type HMG lineage *via* conservative
925 continuation model, whereas the HMG-box_ROX1-like domain within the MAT1-2-1 protein represents

926 evolutionary cooperation of a different regulatory lineage (*e.g.*, ROX1-like) through functional
927 convergence, where it was repurposed to control mating-type specification [62−63,97−100].
928 The MATα_HMGbox and HMG-box_ROX1-like domains of the MAT1-1-1 and MAT1-2-1
929 proteins, respectively, are structurally defined DNA-binding domains characterized by a hydrophobic
930 core containing 3 asymmetrically arranged α-helices. The hydrophobic core, which is composed of
931 tightly packed amino acid residues, is the foundation of the structures and provides a precise
932 conformational stability and constraints that enable the 3 α-helices to form the characteristic L-shaped
933 fold [73,90−91]. These α-helices converge and create stable resistance to environmental perturbations
934 that might unfold or distort the domains. The unique tertiary structures of these sequence-specific DNA
935 binders preferentially ensure high-affinity, sequence-dependent binding to short, AT-rich DNA sequences
936 within the promoters of their target mating-type-specific genes [62,101−106]. The sequence-specific
937 binding of the HMG-box domains to AT-rich promoter motifs serves as the initial trigger, thereby playing
938 pivotal roles in controlling fungal mating identity and gene expression [63,97,107−108].
939 The disruption of this hydrophobic core, whether by 1–4 amino acid substitutions at distinct sites
940 that introduce incompatible residues or by differential peptide chain truncations that remove parts of it,
941 as identified in this study, directly impairs structural integrity and abolishes the crucial functions of the
942 domains in DNA binding specificity in recognizing the target DNA segments and the transcriptional
943 regulation of mating-type-specific genes. These variations have significant consequences for the
944 regulation of *O. sinensis* sexual reproduction during the sexual life of the *C. sinensis* insect−fungal
945 complex. Compared with the authentic MAT1-1-1 and MAT1-2-1 proteins of *O. sinensis* analyzed
946 previously by Li *et al*. [51,69], the differentially altered DNA-binding domains clustered into diverse
947 clades/branches in the Bayesian clustering trees [51,69].
948 Although the MATα_HMGbox domain within the MAT1-1-1 protein and the HMG-box_ROX1-like
949 domain within the MAT1-2-1 protein both belong structurally to the HMG-box superfamily and share a
950 conserved L-shaped fold that enables DNA binding and bending, they are functionally distinct in the
951 context of mating-type regulation in *O. sinensis* because they regulate different gene sets, resulting in
952 opposite regulatory outcomes. The MATα_HMGbox domain of the MAT1-1-1 protein activates the
953 transcription of genes encoding MAT1-1-specific receptors or other regulators. Although the HMG-
954 box_ROX1-like domain of the MAT1-2-1 protein binds to specific DNA sequences in the *MAT1-2*-
955 specific gene promoter encoding the *MAT1-2*-specific pheromone receptor, it may overlap differently
956 with the MATα_HMGbox targets and act through an opposite pathway to counterbalance the activity of

957 the MAT1-1-1 protein [109−111]. Functionally, the MATα_HMGbox domain primarily functions as an
958 activator of its cognate mating-type genes (*i.e., MAT1-1* genes). In contrast, the HMG-box_ROX1-like
959 domain acts as a repressor of genes specific to the opposite mating type (*MAT1-1* or "a-specific" genes)
960 and may also serve as an activator for *MAT1*-2-specific genes. This repressive capacity represents a key
961 functional hallmark derived from its homology to ROX1 [112]. Thus, despite their structural similarity
962 as DNA-binding and DNA-bending HMG-box domains, the MATα_HMGbox and HMG-box_ROX1-
963 like domains are functionally specialized to control distinct, complementary sets of target genes, thereby
964 defining the two different mating types. Their divergent regulatory outputs (activation *vs*. repression of
965 key target gene sets) constitute the molecular and protein structural basis of mating-type specification
966 during the sexual reproduction of *O. sinensis* during the lifecycle of the *C. sinensis* insect–fugal complex.
967 The putative heterodimerization between the MATα_HMGbox domain of the MAT1-1-1 protein and
968 the HMG-box_ROX1-like domain of the MAT1-2-1 protein has been proposed as a potential regulatory
969 mechanism to enforce outbreeding and initiate the sexual cycle in heterothallic fungi [113−115].
970 However, because of the lack of direct evidence in *O. sinensis*, it remains a compelling hypothesis and
971 future research must confirm the occurrence of this heterodimerization, characterize the interaction
972 interface, and define its precise regulatory targets and functional effects on mating and fruiting body
973 development in this economically and ecologically important insect–fungal complex. Nevertheless, the
974 MATα_HMGbox and HMG-box_ROX1-like domains may interact electrostatically and
975 complementarily, providing a plausible physicochemical basis for cooperative synergy in DNA binding.
976 This interaction could coordinate the transition from asexual growth to sexual development, distorting
977 target DNA to repress haploid programming and activating the mating/meiosis genes of *O. sinensis*
978 during the sexual life of the *C. sinensis* insect–fungal complex [116]. Nevertheless, direct experimental
979 validation using protein biochemistry and reproductive physiological approaches is warranted to confirm
980 this hypothetical model, clarify its species-specific characteristics, and determine the effects of protein-
981 level variations on the complementary interactions and alterations in the mating function of *O. sinensis*
982 [51,67−69], even as the genome-independent, multifungal, and multigenotypic nature of *O. sinensis*
983 remains to be fully elucidated [9−10,12−13,19,24,27,30,35,37−38,55,117]. Such protein-level variations
984 may provide critical evidence to support or refute the hypotheses of the anamorph–teleomorph linkage
985 and sexual reproduction strategy of *O. sinensis* [14,20,36,45,51,65,67−69,72].

986 **4.2 Heterogenous fungal sources of the MAT1-1-1 and MAT1-2-1 proteins**
987 **simultaneously produced in pairs by the impure *O. sinensis* strains**

988 **4.2a Phylogenetic heterogeneity of *O. sinensis* strains**

989 By employing a dual-fluorescence microscopy technique, Bushley *et al*. [14] characterized the
990 multicellular heterokaryotic microstructures of *C. sinensis* ascospores and hyphae, which contain mono-,
991 bi-, tri-, and tetra-nucleate cellular structures. Zhang & Zhang [72] subsequently commented on these
992 heterokaryotic microstructures and expressed doubts regarding whether binucleate (as well as tri- and
993 tetra-nucleate) cells might inconsistently harbor homogenous or heterogeneous hereditary substances.
994 Molecular biological observations reported by Li *et al*. [12−13,36−38] revealed multiple fungal
995 components in the ascospores and ascocarps of *C. sinensis* insect–fungal complex and in purportedly
996 "pure" *H. sinensis* strains. These findings provide indisputable evidence supporting the hypothesis
997 proposed by Zhang & Zhang [72] that multicellular heterokaryotic cells indeed contain heterogeneous
998 hereditary substances.

999 Evidence of culture dependence was reported by Li *et al*. [36], who deposited the ITS sequences of
1000 15 of the 20 *O. sinensis* strains in GenBank. Among the 15 *O. sinensis* strains, 10 were reported as
1001 "homogenous" strains, purportedly harboring only the GC-biased Genotype #1. The remaining 5 strains
1002 were characterized as heterogeneous, containing both GC-biased Genotype #1 (Group A) and AT-biased
1003 Genotype #17 (Group C). Li *et al*. [36,118−119] hypothesized that AT-biased genotypic sequences are
1004 nonfunctional repetitive copies within the single genome of GC-biased *H. sinensis* and are referred to as
1005 "ITS pseudogenes" and "rRNA pseudogenes", which are generated through repeat-induced point (RIP)
1006 mutation. However, subsequent studies have demonstrated that the sequences of Genotypes #2−17 of *O.*
1007 *sinensis*, including both GC- and AT-biased genotypes, do not reside in the genomic assemblies of 5 pure
1008 *H. sinensis* strains [9−10,12−13,38,120]. Thus, the 17 *O. sinensis* genotypes are actually genomically
1009 independent and belong to distinct fungal lineages, although they may share a common ancestral heredity
1010 [24]. These findings directly invalidate the hypotheses that the "RIP" mutation induced the nonfunctional
1011 AT-biased "ITS pseudogene" and "rRNA pseudogenes" in the genome of GC-biased Genotype #1 *H.*
1012 *sinensis*.

1013 In Section 3.5a, the less sophisticated research methodology employed by Li *et al*. [36] was
1014 analyzed. This technical limitation led to an imbalance in the amplification efficiency of coexisting
1015 fungal sequences. Consequently, the results of this study revealed that only the sequence(s) exhibiting
1016 the highest PCR amplification efficiency likely precluded the comprehensive detection of all the
1017 coexisting fungal taxa in the samples. Notably, the different abundances (high *vs*. low) of amplicons
1018 primarily reflect the level of PCR amplification efficiency and velocity under specific research settings

1019 and, obviously, should not be equated with the natural ratio of coexisting fungi in the tested samples.
1020 The natural ratio of coexisting fungal taxa can be quantified using other specialized non-PCR techniques,
1021 such as Southern blotting with the use of specific probes [27]. Notably, naturally occurring, less abundant
1022 fungal taxa may still play synergistic roles in the lifecycle of the *C. sinensis* insect–fungal complex.

1023 Furthermore, Li *et al*. [12−13,37] adopted an exhaustive culture-independent approach, including
1024 multiple primers, "touch-down" PCR protocols and the selection and sequencing of multiple (>30) white
1025 colonies, as well as MALDI-TOF SNP mass spectrum genotyping approaches using multiple extension
1026 primers, to exhaustively investigate the comprehensive fungal composition within *C. sinensis* ascospores
1027 and the "pure" *H. sinensis* strains Hs-Ma-4, Hs7.7, Hs7.8, and Hs-Qing2 (gifts from renowned
1028 mycologist Prof. Gou YL). These studies demonstrated that *C. sinensis* ascospores and "pure" *H. sinensis*
1029 strains co-occur with genomically independent fungal taxa, including the psychrophilic GC-biased
1030 Genotypes #1 and #14 and AT-biased Genotypes #5−6 and #16 of *O. sinensis*, as well as the mesophilic
1031 *Paecilomyces hepiali* (recently reclassified as *Samsoniella hepiali* [121]). These findings clearly indicate
1032 that the study by Li *et al*. [36] overlooked coexisting fungal sequences with low PCR amplification
1033 efficiency and nonculturable fungal components under particular experimental conditions. Thus, the
1034 origins of paired MAT1-1-1 and MAT1-2-1 proteins with differential truncations and various amino acid
1035 substitutions at distinct sites require further clarification using rigorously designed mycological and
1036 molecular protocols by the custodian(s) of the original *O. sinensis* strains.

1037 The paired heteromorphic MAT1-1-1 and MAT1-2-1 proteins are likely to have distinct fungal
1038 origins and were possibly derived from the co-occurring GC-biased Genotypes #1 and #3 and AT-biased
1039 Genotype #17 of *O. sinensis* in wild-type *C. sinensis* isolates [51] and the *O. sinensis* strains analyzed in
1040 this study. Given the limited available information on the diverse coexisting genotypes of *O. sinensis*,
1041 the different pairings of the MAT1-1-1 and MAT1-2-1 protein variants that exhibit differential
1042 truncations and diverse amino acid substitutions at distinct sites were coproduced by the differentially
1043 coexisting genomically independent fungi in *O. sinensis* strains [6,9−13,15−44].

1044 **4.2b Differential pairings of the MAT1-1-1 and MAT1-2-1 proteins simultaneously produced by**
1045 ***O. sinensis* strains**

1046 Table S7 summarizes the differential occurrence or co-occurrence of both authentic and variant
1047 MAT1-1-1 and MAT1-2-1 proteins in *C. sinensis* insect–fungal complexes, wild-type *C. sinensis* isolates,
1048 and various *O. sinensis* strains (including GC-biased Genotype #1 *H. sinensis* strains). The 20 *O. sinensis*
1049 strains analyzed in this study are categorized into 2 distinct groups based on the coproduction of the

1050 paired mating proteins: the Group-I strains produce the truncated MAT1-1-1 and MAT1-2-1 proteins in
1051 pairs, whereas the Group-II strains harbor truncated MAT1-1-1 proteins paired with full-length MAT1-
1052 2-1 proteins (*cf*. Tables 2 and S5, Figures 5−17 and S3) [14,36,69]. Many full-length or truncated MAT1-
1053 1-1 and MAT1-2-1 proteins contain diverse amino acid substitutions (*cf*. Figures 1−17 and S3, Table 2).

1054 When addressing the issue of overlooked co-occurring fungal taxa due to the unsophisticated study
1055 designed by Li *et al*. [36], namely, the nonculturable fungal taxa and low-abundance coexisting fungal
1056 sequences that likely arise from inefficient amplification and sequencing bias associated with the
1057 suboptimal experimental design, the 20 *O. sinensis* strains presumably exhibit a much greater diversity
1058 of uncharacterized fungal sequences than the "homogenous" and heterogeneous cultures of *C. sinensis*
1059 monoascospores and tissues of caterpillar bodies reported by Li *et al*. [36]. As analyzed in Sections 3.5
1060 and 4.2, the distinct pairings of the highly divergent MAT1-1-1 and MAT1-2-1 protein variants that were
1061 simultaneously and differentially produced by the 20 *O. sinensis* strains present a complex, nonuniform
1062 pairing pattern. These findings indicate diverse fungal origins of the mating proteins from co-occurring
1063 fungal taxa in the samples. Further investigations are therefore warranted, employing unbiased and
1064 rigorous culture-independent methods to comprehensively profile coexisting genomically independent
1065 genotypes of *O. sinensis* and heterospecific fungal taxa [12−13,37].

1066 **4.2c Paradoxical dilemmas regarding the high possible heterogeneity of previously reported**
1067 **"pure" *O. sinensis* strains**

1068 The first dilemma concerns the purportedly homogenous strain CS68-2-1229 of **Group I**
1069 (highlighted in dark green and underlined in Figures 2 and 4). Only the GC-biased Genotype #1 was
1070 detected in this purportedly "pure" culture of *C. sinensis* monoascospores under the settings adopted by
1071 Li *et al*. [36], which was incapable of completely covering all co-occurring fungal taxa (*cf*. Section 3.5a).
1072 Two MAT1-1-1 protein sequences from this strain have been deposited in GenBank: a full-length MAT1-
1073 1-1 protein, AGW27560, containing 372 amino acids, and a truncated MAT1-1-1 protein, AGW27528,
1074 containing 301 amino acids (*cf*. Figure 5). The 2 MAT1-1-1 proteins share 100% sequence identity, yet
1075 AGW27528 exhibits only 81% query coverage with 63- and 8-residue truncations at the N- and C-
1076 termini, respectively (*cf*. Figure 17, Table 2). This truncated pattern was likely attributable to the use of
1077 different primers for amplifying the *MAT1-1-1* gene or its transcript from the total RNA pool in the
1078 experiments. This strain also produced the truncated MAT1-2-1 protein AGW27548 (175 amino acids;
1079 *cf*. Figure 15), which shares 99.4% sequence identity with the authentic full-length MAT1-2-1 protein
1080 and has a Y-to-H substitution within the HMG-box_ROX1-like domain; notably, it shows only 70%

1081 sequence coverage because of a 74-residue truncation at the C-terminus relative to that of the authentic
1082 full-length MAT1-2-1 proteins, which contain 249 amino acids. All 3 mating protein sequences derived
1083 from strain CS68-2-1229 were released in GenBank on the same date (28-SEP-2013). The truncated
1084 MAT1-1-1 AGW27528 and MAT1-2-1 protein AGW27548 were derived from cDNAs that were
1085 amplified using the primer pair *m1F3*/*m1R3* to amplify *MAT1-1-1* cDNA and the primer pair Mat1-
1086 2F/Mat1-2R to amplify *MAT1-2-1* cDNA from the same batch of total RNA pool extracted from the
1087 strain CS68-2-1229 (*cf*. Figures S1−S2) [14,36,70]. Figure 2 shows that the MATα_HMGbox domain
1088 (162 amino acids) of the MAT1-1-1 protein AGW27528 is among the longest domains of all 9 truncated
1089 MAT1-1-1 proteins. In contrast, Figure 4 shows that the HMG-box_ROX1-like domain (49 amino acids)
1090 of the MAT1-2-1 protein AGW27548 (*cf*. Figures 4 and 15) is 10 residues shorter than the longest
1091 truncated HMG-box_ROX1-like domain (59 amino acids) of the MAT1-2-1 protein AGW27543 and 22
1092 residues shorter than the HMG-box_ROX1-like domain (71 amino acids) of the authentic MAT1-2-1
1093 protein AEH27625 [51,70]. The truncated MAT1-2-1 protein AGW27548, which harbors a Y-to-H
1094 substitution, exhibits altered secondary and tertiary structures under the AlphaFold 3D structural code
1095 U3N9W5 (*cf*. Figure 15, Table 2). Li *et al*. [69] reported no repetitive copies of the *MAT1-1-1* and *MAT1-*
1096 *2-1* genes in the genome of the *H. sinensis* strain. These findings suggest that the MAT1-1-1 protein
1097 AGW27528 is most likely encoded by the authentic *MAT1-1-1* gene in the *H. sinensis* genome. However,
1098 the MAT1-2-1 protein AGW27548 is presumably encoded by a variant *MAT1-2-1* gene within the *H.*
1099 *sinensis* genome or by an independent co-occurring fungal taxon in the actually "impure" *O. sinensis*
1100 strain CS68-2-1229. Thus, the true genetic identity of strain CS68-2-1229 requires re-evaluation:
1101 whether this strain is genuinely homogenous, containing only Genotype #1 *H. sinensis*, or it is indeed
1102 heterogeneous, harboring 2 or more fungal taxa similar to the other heterogeneous strains, as shown in
1103 Tables 1–2 and S1–S2, remains to be determined.

1104 Another paradoxical "homogenous" *O. sinensis* strain, CS561-964 (**Group II**), was also reported
1105 to harbor only GC-biased Genotype #1 *H. sinensis* [14,36]. This strain produced the MAT1-1-1 protein
1106 AGW27526, featuring 63- and 13-residue truncations at the N- and C-termini, respectively, along with
1107 4 amino acid substitutions (CDRA-to-SSEF) within the MATα_HMGbox domains (*cf*. Figures 7 and 17,
1108 Tables 1−2). Clearly, the altered protein AGW27526 is encoded by a variant *MAT1-1-1* gene, plausibly
1109 from a genome-independent, co-occurring fungal taxon. This fungal taxon was likely overlooked in the
1110 study by Li *et al*. [36] because of the use of suboptimal culture-dependent experimental protocols (*cf*.
1111 Section 3.5a),

1112 Analyses of the purportedly homogenous *O. sinensis* strains raise fundamental questions regarding
1113 fungal purification, *in vitro* culture characteristics, and the comprehensive detection of all co-occurring
1114 fungal taxa in such cultures. Two key questions remain unresolved: First, do the purportedly homogenous
1115 strains listed in Tables 1−2 and S1−S2 truly harbor only GC-biased Genotype #1, or are they indeed
1116 heterogeneous and contain a few or multiple fungi? Second, do the characterized heterogeneous strains
1117 contain only the GC-biased Genotype #1 and AT-biased Genotype #17 or an even greater number of
1118 undetected coexisting fungal taxa? A reasonable hypothesis is that the differentially paired truncated and
1119 full-length MAT1-1-1 and MAT1-2-1 protein variants, which exhibit diverse amino acid substitutions at
1120 distinct variation sites, are not necessarily produced by GC-biased Genotype #1 *H. sinensis*. Instead,
1121 these protein variants likely originate from AT-biased Genotype #17 (*cf*. Tables S1−S2) or from other
1122 uncharacterized co-occurring fungal taxa that were not detected in the culture-dependent study by Li *et*
1123 *al*. [36].

1124 4.3 The self-sterility of *O. sinensis* and the requirement for sexual partners to 1125 accomplish heterothallic or hybrid reproduction

1126 Wei *et al*. [45] proposed that *H. sinensis* (GC-biased Genotype #1 of *O. sinensis*) represents the sole
1127 anamorph of *O. sinensis* teleomorph. Zhang *et al*. [52] proposed the implementation of the "One
1128 Fungus=One Name" nomenclature principle established by the International Mycological Association
1129 [53−54] and replaced the anamorphic name *H. sinensis* with the teleomorphic name *O. sinensis* [45].
1130 This renaming implementation, however, was not only applied to the GC-biased Genotype #1 *H. sinensis*
1131 but also uniformly applied to all 17 genomically independent genotypes of *O. sinensis*, although they
1132 may share a common hereditary ancestor [9−10,24,55]. Eleven of the 17 genotypes are GC biased,
1133 whereas the remaining 6 genotypes are AT biased. The genotypes coexist in different combinations of
1134 different compartments of the *C. sinensis* insect–fungal complex, and their natural abundance changes
1135 dynamically during *C. sinensis* maturation [9−10,12−13,27,35,37]. In support of the sole anamorph
1136 hypothesis for *H. sinensis* [45], Bushley *et al*. [14] and Hu *et al*. [65] studied the mating-type genes in
1137 the genome of GC-biased Genotype #1 *H. sinensis* and proposed the self-fertilization hypothesis for *O.*
1138 *sinensis* to accomplish homothallic or pseudohomothallic reproduction. However, several research
1139 groups [65,122−123] have reported unsuccessful attempts to artificially cultivate the fruiting bodies and
1140 ascospores of *C. sinensis* insect–fungal complexes using pure fungal cultures. Zhang *et al*. [52] then
1141 summarized the 40-year history of failed attempts to cultivate the insect–fungal complex in academic
1142 research-oriented settings. Qin *et al*. [124] elaborated on the key obstacles hindering the artificial

1143 cultivation of *C. sinensis* fruiting bodies and ascospores. Li *et al*. [125] further attributed the decades-
1144 long history of failures in the cultivation of the *C. sinensis* insect–fungal complex to "the low rate of the
1145 fungal invasion to host insects and primordium induction after infection". Compared with the nearly
1146 noninfectious characteristics of pure *H. sinensis*, Li *et al*. [37] advanced the inoculation technique using
1147 cocultures of natural fungal clusters with a natural abundance ratio of multiple genotypic and
1148 heterospecific fungal taxa isolated from the *C. sinensis* insect–fungal complex. This advanced technique
1149 resulted in up to 39-fold greater infectivity in the larvae of *Hepialus armoricanus* and significantly
1150 shortened the latency (from 35−50 days to 5−8 days) from inoculation to mummification/death.
1151 Evidently, the hypotheses of contentious sole anamorph and concomitant self-fertilization have not yet
1152 been scientifically validated in academia to meet all 4 criteria of Koch's postulations.

1153 In contrast to the hypothesis that *H. sinensis* represents the sole anamorph of *O. sinensis* [45],
1154 molecular studies have revealed complex genetic diversity of *O. sinensis,* and this Latin name
1155 encompasses at least 17 distinct genotypes [9−10,12−13,27,30,35,55,94]. The sequences of Genotypes
1156 #2−17 of *O. sinensis* are not present in the genome of Genotype #1 *H. sinensis*, indicating that they
1157 represent diverse genome-independent fungal taxa [9−10,24,30]. A medicinal mycology group led by
1158 Prof. S.P. Wasser reported that *H. sinensis* and *Tolypocladium sinensis* serve as conjoint anamorphs of
1159 *O. sinensis* [34], supporting the prior detection of *T. sinensis* and *T. sinense* from natural *C. sinensis*
1160 insect–fungal complexes [15,20−21,25]. Quandt *et al*. [126] subsequently proposed taxonomic revisions
1161 within the genus *Tolypocladium*, reassigning several species to the family Ophiocordycipitaceae. To date,
1162 the taxonomic positions of 17 evolutionarily related genotypes as independent fungi, as well as the
1163 precise anamorph–teleomorph relationship of *O. sinensis*, remain unresolved. With respect to
1164 reproductive modes, although early hypotheses propose homothallic or pseudohomothallic reproduction
1165 for *O. sinensis*, Zhang and Zhang [72] reported the differential presence of *MAT1-1-1* and *MAT1-2-1*
1166 genes across numerous wild-type *C. sinensis* isolates and proposed a facultative hybridization hypothesis
1167 for *O. sinensis*. Li *et al*. [67−68] further documented the differential occurrence, alternative splicing, and
1168 differential translation of the *MAT1-1-1* and *MAT1-2-1* genes and the pheromone receptor genes. More
1169 recently, the studies by Li *et al*. [51,69] and the present study revealed heteromorphic tertiary structures
1170 of the MAT1-1-1 and MAT1-2-1 protein variants, particularly variations within the DNA-binding
1171 domains of the mating proteins. These structural observations provide protein-level evidence for
1172 heterogeneous fungal origins of mating-type loci in numerous wild-type *C. sinensis* isolates and *O.*
1173 *sinensis* strains. Notably, Li *et al*. [69] reported that both the *MAT1-1-1* and *MAT1-2-1* genes exist as

1174 single copies in the *H. sinensis* genome with no repetitive genomic copies. Collectively, the evidence
1175 from genetics, transcription, and protein structure is inconsistent with the self-fertilization hypothesis for
1176 *O. sinensis* and instead supports self-sterility, implying that *O. sinensis* relies on heterothallic mating,
1177 hybridization, or even parasexual outcrossing to accomplish sexual reproduction [13,51,67−69,
1178 127−136]. Similar self-sterile reproductive strategies have been documented in many other
1179 *Ophiocordyceps* species, which require compatible mating partners to undergo sexual reproduction
1180 [104,137−141].

1181 Wei *et al*. [46] reported the successful industrial cultivation of *C. sinensis* insect–fungal complexes.
1182 However, this study revealed a puzzling species paradox between the input and output of the artificial
1183 cultivation project: 3 GC-biased *H. sinensis* strains were used as inoculants, yet only the teleomorph of
1184 AT-biased Genotype #4 was detected in the fruiting bodies of the cultivated *C. sinensis* insect–fungal
1185 complexes. Hence, the sole teleomorphic AT-biased Genotype #4 identified in the cultivated fruiting
1186 bodies had replaced the inoculant GC-biased Genotype #1 strains, resulting in a species contradiction.
1187 The sequences of Genotypes #2−17 of *O. sinensis* are not present in the genome assemblies
1188 ANOV00000000, JAAVMX000000000, LKHE00000000, LWBQ00000000, or NGJJ00000000 of the
1189 pure *H. sinensis* strains Co18, IOZ07, 1229, ZJB12195, and CC1406-20395, respectively
1190 [9−10,12−13,24,30,35−36,38,65,93−96,117,120]. Instead, these genotypes belong to distinct genome-
1191 independent fungal taxa. These results invalidate the unfounded assumptions proposed by Li *et al*.
1192 [36,118−119] that AT-biased genotypes are nonfunctional "ITS pseudogenes" or "rRNA pseudogenes"
1193 that were generated through "RIP" mutation in the genome of *H. sinensis*. Supporting genomic or
1194 transcriptomic evidence has not been available to support these unfounded speculations [38,120]. In
1195 contrast to the significantly variable maturation-related dynamics of AT-biased genotypes of *O. sinensis*,
1196 GC-biased *O. sinensis* genotypes maintain a relatively constant low abundance in the stromata
1197 throughout the entire maturation course of the *C. sinensis* insect–fungal complex [27,35]. These
1198 observations suggest that the 17 genome-independent genotypes of *O. sinensis*, regardless of whether
1199 they are GC or AT biased, represent distinct fungal species [10,12−13,30], further reinforcing the
1200 invalidation of the RIP mutation/pseudogene hypotheses proposed by Li *et al*. [36,118−119]. The
1201 successful industrial cultivation of *C. sinensis* insect–fungal complexes, coupled with the apparent
1202 species paradox, indicates that the sole anamorph hypothesis for *H. sinensis* proposed by Wei *et al*. [46]
1203 failed to satisfy all 4 criteria of Koch's postulates.

1204 Li *et al*. [125] subsequently clarified that the inoculant used in the industrial cultivation project was

1205 an *O. sinensis* conidial suspension obtained after 3 months of culture of *C. sinensis* ascospores, rather
1206 than the 3 pure *H. sinensis* strains initially described by Wei *et al*. [46]. However, Li *et al*. [125] did not
1207 disclose the molecular components of the inoculant to the public or redress the previously reported
1208 teleomorphic AT-biased Genotype #4 of *O. sinensis* in the fruiting bodies of cultivated *C. sinensis* insect–
1209 fungal complexes. On the other hand, several other studies reported that AT-biased Genotype #4 was
1210 detected in the stromata throughout all maturation stages of the *C. sinensis* insect–fungal complex
1211 [10,27,35−36,38]. The abundance of Genotype #4 exhibited markedly altered ontogenetic dynamics, *i.e.*,
1212 it was highly abundant in immature stromata during the asexual growth phase and was substantially
1213 reduced in the mature stromata and the stroma-fertile portion of the *C. sinensis* insect–fungal complex
1214 during the sexual reproduction stage or the transition from asexual growth to sexual reproduction
1215 [9−10,12−13,35,38]. Regrettably, several studies [12−13,36−37] failed to detect AT-biased Genotype #4
1216 from *C. sinensis* ascospores using both culture-dependent and culture-independent approaches. Thus, the
1217 dynamic maturation pattern for AT-biased Genotype #4 of *O. sinensis* and its absence in *C. sinensis*
1218 ascospores suggest that Genotype #4 may not participate in the sexual reproduction of *O. sinensis*.
1219 Consequently, the puzzling species paradox between the inoculant and the sole teleomorphic AT-biased
1220 Genotype #4 of *O. sinensis* detected in the fruiting body of the cultivated *C. sinensis* insect–fungal
1221 complex [46] remains an unresolved mycological enigma. Unfortunately, Li *et al*. [125] did not address
1222 the genetic complexity of the ascospores of cultivated insect–fungal complexes.

1223 Li *et al*. [51] discussed the evidence related to the industrial success of cultivating the insect–fungal
1224 complex and postulated that the design for the cultivation project may adopt a "mycological impurity"
1225 strategy, facilitating the synergistic interplay of coexisting fungi that is the potential key to success. The
1226 supporting evidence includes the following: (1) Li *et al*. [125] reported that the inoculant was a culture
1227 of *C. sinensis* ascospores to address the weak infectivity of GC-biased Genotype #1 *H. sinensis*. Li *et al*.
1228 [12−13,36] revealed that *C. sinensis* ascospores harbor multiple genotypic and heterospecific fungi. (2)
1229 *C. sinensis* ascospores do not contain AT-biased Genotype #4 of *O. sinensis* [10, 12−13,36,38].
1230 Therefore, the origin of teleomorphic Genotype #4 detected in the fruiting body of the cultivated *C.*
1231 *sinensis* insect–fungal complex by Wei *et al*. [46] might be derived from cocultures of *C. sinensis*
1232 ascospores with the stroma and/or stromal fertile portion of the *C. sinensis* insect–fungal complex that
1233 indeed contain AT-biased Genotype #4 of *O. sinensis*, along with other genotypic and heterospecific
1234 fungi. Li *et al*. [37] demonstrated that cocultures of multiple genotypic and heterospecific fungal taxa in
1235 wild-type *C. sinensis* isolates exhibit up to 39-fold greater infectivity in the larvae of *Hepialus*

1236 *armoricanus* than on those of pure *H. sinensis*. (3) The industrial cultivation system was supplemented
1237 with soil collected from the natural *C. sinensis* production areas on the Qinghai–Tibet Plateau [46].

1238 To date, the purification and genomic analysis of GC- and AT-biased Genotypes #2–17 of *O. sinensis*
1239 have not been reported. Thus, genomic and transcriptomic information for the divergent *MAT1-1-1* and
1240 *MAT1-2-1* genes in Genotypes #2–17 of *O. sinensis* is lacking, especially concerning the critical DNA-
1241 binding domains of the MAT1-1-1 and MAT1-2-1 proteins. Regardless of the precise biophysical details
1242 of their interaction, whether the paired MAT1-1-1 and MAT1-2-1 proteins form heterodimers or interact
1243 *via* complementary electrostatic surfaces, the synergy of paired mating proteins serves as the central and
1244 indispensable molecular trigger for mating compatibility and the initiation of sexual reproduction in *O.*
1245 *sinensis* [57−61]. Molecular evidence regarding the differential occurrence, alternative splicing, and
1246 differential transcription of mating-type and pheromone receptor genes in *H. sinensis* unequivocally
1247 indicates that *O. sinensis* is self-sterile and relies on heterothallism or hybrid outcrossing to complete
1248 sexual reproduction, thereby ruling out homothallism (self-fertilization) as a viable mechanism in this
1249 species [14,45,64,66−69,142]. Furthermore, the discovery of heteromorphic tertiary structures of variant
1250 MATα_HMGbox domains (in MAT1-1-1 proteins) and HMG-box_ROX1-like domains (in MAT1-2-1
1251 proteins) provides protein-level validation that (1) self-fertilization is biochemically unfeasible and (2)
1252 coordinated heterothallic or hybrid reproduction (even parasexuality) is enforced through structural
1253 complementarity between the paired mating proteins, which are likely generated by divergent
1254 heterogeneous *O. sinensis* strains. This self-sterility hypothesis resolves the longstanding uncertainty in
1255 the cultivation of the *C. sinensis* insect–fungal complex, namely, the failure of single-species cultures to
1256 produce fruit, and underscores the role of the synergistic effect of multiple fungal symbionts on its
1257 ecological success throughout the lifecycle of the naturally occurring or artificially cultivated *C. sinensis*
1258 insect–fungal complex.

1259 # Conclusions

1260 This study presents evidence at the protein structure level for self-sterile *O. sinensis* and further
1261 verifies the heterothallic or hybrid reproduction of *O. sinensis*. The diverse pairings of MAT1-1-1 and
1262 MAT1-2-1 protein variants coproduced simultaneously by the 20 *O. sinensis* strains examined in this
1263 study exhibit differential truncations and 1−4 amino acid substitutions in their DNA-binding domains.
1264 The primary structural variations caused dramatic changes in the hydrophobic properties and secondary
1265 and tertiary structures of the MATα_HMGbox and HMG-box_ROX1-like domains of the differentially

paired MAT1-1-1 and MAT1-2-1 proteins, respectively. The structural heterogeneity of differentially paired mating proteins not only indicates the co-occurrence of heterogeneous fungal origins in impure *O. sinensis* strains but also invalidates the hypothesis of homothallic or pseudohomothallic self-fertilization in *O. sinensis*. Complementing the evidence of differential occurrence, differential transcription, and alternative splicing of the *MAT1-1-1* and *MAT1-2-1* genes and pheromone receptor genes, the variations in the protein structures of these DNA-binding domains of the mating proteins impair the homologous interaction required for homothallic or pseudohomothallic self-fertilization. Collectively, our findings of differential pairings of the mating protein variants in *O. sinensis* strains clarify the sexual reproduction mechanism of *O. sinensis* and confirm that the selection of suitable heterologous mating partners is an essential natural strategy for self-sterile *O. sinensis* to complete sexual reproduction during the lifecycle of *Cordyceps sinensis* insect–fungal complexes on the Qinghai–Tibet Plateau.

Acknowledgments

The authors are grateful to Prof. Mu Zang, Prof. Ru-Qin Dai, and Prof. Zong-Qi Liang for their consultation.

Supplementary Materials: The following supporting information can be downloaded at www.xxxxxx.

Figure S1. Alignment of the DNA sequence of the *MAT1-1-1* gene KC437356 (6530→7748) and the encoded sequence of the MAT1-1-1 protein AGW27560 (1→ 372) derived from *Ophiocordyceps sinensis* strain CS68-2-1229 [Bushley *et al*. 2013]. Residues in pink indicate the MATα_HMGbox domain of the *MAT1-1-1* gene and MAT1-1-1 protein; those in green indicate Introns I and II. The underlined residues in red indicate the forward primer m1F3/*MAT1-1-1* (CCACTAGGCAGACCAAAGAAG) and the reverse complementary primer m1R3/*MAT1-1-1* (CGCAAAGTAAAAGTCGTCCAGA) reported by [Bushley *et al*. 2013]. The triplet residues (TAG) in red represent the stop codon.

Figure S2. Alignment of the *MAT1-2-1* gene HM212637 (3241→4097) and the encoded sequence of MAT1-2-1 protein AEH27625 (1→249) by derived from *Ophiocordyceps sinensis* strain CS2 [Zhang *et al*. 2009]. Residues in pink indicate the HMG-box_ROX1-like domain of the *MAT1-2-1* gene and MAT1-2-1 proteins; those in green indicate Introns I and II. The underlined residues in red indicate the forward primer Mat1-2F/*MAT1-2-1* (TGGAATGCGACTGACTACGA) and the reverse complementary primer Mat1-2R/*MAT1-2-1* (CCAGGAGAGCTTGCTTGACT) reported by [Zhang *et al*. 2009; Bushley *et al*. 2013]. The triplet residues (TAA) in red represent the stop codon.

Figure S3. Alignment of the sequences of full-length MAT1-2-1 proteins derived from **Group II** *O. sinensis* strains listed in Table 2 with that of the authentic MAT1-2-1 protein AEH27625 (under the AlphaFold code D7F2E9) derived from the *H. sinensis* strain CS2. The residues in pink indicate the HMG-box_ROX1-like domains of the proteins, those in green indicate the variant amino acids; the hyphens indicate identical amino acid residues; and the space denotes the unmatched sequence gap.

Table S1. The *O. sinensis* strains, GenBank accession numbers for the ITS nucleic acid sequences corresponding to the GenBank accession numbers for the MAT1-1-1 and MAT1-2-1 proteins, and percent similarities *vs*. GC-biased Genotypes #1–3, #7–10, and #12 of *O. sinensis*.

Table S2. The *O. sinensis* strains, GenBank accession numbers for the ITS nucleic acid sequences corresponding to the GenBank accession numbers for the MAT1-1-1 and MAT1-2-1 proteins, and percent similarities *vs*. AT-biased Genotypes #4–6 and #15–17 of *O. sinensis*.

Table S3. Amino acid scales based on the general chemical characteristics of their side chains for ProtScale analysis (https://web.expasy.org/protscale/) to predict hydrophobicity and secondary structures (α-helices, β-sheets, β-turns, and coils) of proteins.

Table S4. GenBank accession numbers (in red in parentheses) for the full-length MAT1-1-1 proteins in the AlphaFold database under the corresponding AlphaFold UniProt codes [Li *et al*. 2025].

Table S5. GenBank accession numbers (in red) for the full-length MAT1-2-1 proteins of 69 *H. sinensis* strains or wild-type *C. sinensis* isolates under the corresponding AlphaFold UniProt codes [Li *et al*. 2025].

Table S6. Similarity of the 3 pairs of primers that were used by Li *et al*. [2013] to amplify the ITS sequences of the *O. sinensis* strains listed in Table 1 that were isolated either from the caterpillar body specimens that were collected from various production areas on Qinghai-Tibet Plateau or from the cultures of mono-ascospores that were collected from mature *C. sinensis* insect–fungal complexes obtained from a single production region (Maqên, Guoluo, Qinghai Provence of China).

Table S7. Cooccurrence or differential occurrence of the MAT1-1-1 and MAT1-2-1 proteins in the O. sinensis strains, wild-type C. sinensis isolates, and C. sinensis insect–fungal complex that are listed in the GenBank database.

Author Contributions: Conceptualization, XZL, YLL, and JSZ; methodology, JSZ; formal analysis, JSZ; investigation, XZL and JSZ; data curation, XZL and JSZ; writing–original draft preparation, JSZ; writing—review and editing, XZL, YLL, and JSZ; project administration, YLL; funding acquisition, YLL. All authors have read and agreed to the published version of the manuscript.

Funding: This research was funded by (1) the Chinese Academy of Sciences−People's Government of Qinghai Province on Sanjiangyuan National Park (#LHZX-2022-01); (2) Forestry and Grassland Bureau of Qinghai Province: "Wild *Ophiocordyceps sinensis* Identification and Application Project" (QHRD-2025-004); (3) Department of Science and Technology of Qinghai Province: "Process Optimization and Application of Antioxidant Performance of Yushu *Cordyceps sinensis* Extract" (2025-NK-P45); and (4) the Shaanxi Key Laboratory of Natural Product & Chemical Biology Open Foundation (SXNPCB 2024003).

Institutional Review Board Statement: Not applicable because this paper is an *in silico* reanalysis of public data.

Informed Consent Statement: Not applicable because this paper is a public bioinformatic data reanalysis.

Data Availability Statement: All sequence and 3D structure data are available in the GenBank and AlphaFold databases.

Conflicts of Interest: The authors declare no conflicts of interest.

[REFERENCES]

1. Zhu, J.-S.; Halpern, G.M.; Jones, K. The scientific rediscovery of a precious ancient Chinese herbal regimen: *Cordyceps sinensis*: Part I. *J. Altern. Complem. Med.* **1998a**, *4*, 289–303. https://doi.org/10.1089/acm.1998.4.3-289.
2. Zhu, J.-S.; Halpern, G.M.; Jones, K. The scientific rediscovery of an ancient Chinese herbal medicine: *Cordyceps sinensis*: Part II. *J. Altern. Complem. Med.* **1998b**, *4*, 429–457. https://doi.org/10.1089/acm.1998.4.429.
3. Zhu, J.-S.; Li, C.-L.; Tan, N.-Z.; Berger, J.L.; Prolla, T.A. Combined use of whole-gene expression profiling technology and mouse lifespan test in anti-aging herbal product study. In Proceedings of the 2011 New TCM Products Innovation and Industrial Development Summit, Hangzhou, China, 27 November 2011; pp. 443–448. Available online:

https://xueshu.baidu.com/usercenter/paper/show?paperid=08341c17fa58c8f85584b92572b90f75&site=xueshu_se (accessed on 30 January 2025).

4. Song, L.-R.; Hong, X.; Ding, X.-L.; Zang, Z.-Y. A comprehensive dictionary of modern pharmacy of Chinese traditional medicine. People's Medical Press, Beijing. 2001; pp 733-737.
5. China Ministry of Agriculture and Rural Affairs. Announcement (No. 15 of 2021) of National Forestry and Grassland Administration: List of National Key Protected Wild Plants. 7 September 2021. Available online: https://m.163.com/dy/article/HHCVOJPU055360T7.html (accessed on 3 May 2025).
6. Ren, Y.; Wan, D.-G.; Lu, X.-M.; Guo, J.-L. The study of scientific name discussion for TCM Cordyceps. *LisShenzhen Med. Mater. Medica Res.* **2013**, *24*, 2211–2212.
7. Zhang, Y.-J.; Zhang, S.; Li, Y.-L.; Ma, S.-L.; Wang, C.-S.; Xiang, M.-C.; Liu, X.; An, Z.-Q.; Xu, J.-P.; Liu, X.-Z. Phylogeography and evolution of a fungal–insect association on the Tibetan Plateau. *Mol. Ecol.* **2014**, *23*, 5337–5355. https://doi.org/10.1111/mec.12940.
8. Lu, H.-L.; St. Leger, R.J. Chapter Seven—Insect Immunity to Entomopathogenic Fungi. In *Advances in Genetics*; Lovett, B., St. Leger, R.J., Eds.; Academic Press: Cambridge, MA, USA, 2016; Volume 94, pp. 251–285.
9. Zhu, J.-S.; Li, Y.-L. A Precious Transitional Chinese Medicine, *Cordyceps sinensis*: Multiple heterogeneous *Ophiocordyceps sinensis* in the insect–fungi complex. Lambert Academic Publishing, Saarbrüchen. Germany, 2017.
10. Li, Y.-L.; Li, X.-Z.; Yao, Y.-S.; Xie, W.-D.; Zhu, J.-S. Molecular identification of *Ophiocordyceps sinensis* genotypes and the indiscriminate use of the Latin name for the multiple genotypes and the natural insect–fungi complex. *Am. J. BioMed. Sci.* **2022**, *14*, 115–135. https://doi.org/10.5099/aj220300115.
11. Li, M.-M.; Zhang, J.-H.; Qin, Q.-L.; Zhang, H.; Li, X.; Wang, H.-T.; Meng, Q. Transcriptome and Metabolome Analyses of Thitarodes xiaojinensis in Response to *Ophiocordyceps sinensis* Infection. *Microorganisms* **2023a**, *11*, 2361. https://doi.org/10.3390/microorganisms11092361.
12. Li, Y.-L.; Gao, L.; Yao, Y.-S.; Wu, Z.-M.; Lou, Z.-Q.; Xie, W.-D.; Wu, J.-Y.; Zhu, J.-S. Altered GC- and AT-biased genotypes of *Ophiocordyceps sinensis* in the stromal fertile portions and ascospores of natural *Cordyceps sinensis*. *PLoS ONE.* **2023d**, *18*, e0286865. https://doi.org/10.1371/journal.pone.0286865.
13. Li, Y.-L.; Li, X.-Z.; Yao, Y.-S.; Wu, Z.-M.; Gao, L.; Tan, N.-Z.; Lou, Z.-Q.; Xie, W.-D.; Wu, J.-Y.; Zhu, J.-S. Differential cooccurrence of multiple genotypes of *Ophiocordyceps sinensis* in the stromata, stromal fertile portion (ascocarps) and ascospores of natural *Cordyceps sinensis*. *PLoS ONE* **2023e**, *18*, e0270776. https://doi.org/10.1371/journal.pone.0270776.
14. Bushley, K.E.; Li, Y.; Wang, W.-J.; Wang, X.-L.; Jiao, L.; Spatafora, J.W.; Yao, Y.-J. Isolation of the MAT1-1 mating type idiomorph and evidence for selfing in the Chinese medicinal fungus *Ophiocordyceps sinensis*. *Fungal Biol.* **2013**, *117*, 599–610. https://doi.org/10.1016/j.funbio.2013.06.001.
15. Li, C.-L. A study of *Tolypocladium sinense* C.L. Li. sp. nov. and cyclosporin production. *Acta Mycol. Sin.* **1988**, *7*, 93–98.
16. Dai, R.-Q.; Lan, J.-L.; Chen, W.-H.; Li, X.-M.; Chen, Q.-T.; Shen, C.-Y. Discovery of a new fungus *Paecilomyces hepiali* Chen & Dai. *Acta Agricult. Univ. Pekin.* **1989**, *15*, 221–224.
17. Dai, R.-Q.; Li, X.-M.; Shao, A.-J.; Lin, S.-F.; Lan, J.-L.; Chen, W.-H.; Shen, C.-Y. Nomenclatural validation of *Paecilomyces hepiali*. *Mycosystema* **2008**, *27*, 641–644.
18. Liu, X.-J.; Guo, Y.-L.; Yu, Y.-X.; Zeng, W. Isolation and identification of the anamorph of *Cordyceps sinensis* fungus. *Acta Mycol. Sin.* **1989**, *8*, 35–40.
19. Kinjo, N.; Zang, M. Morphological and phylogenetic studies on *Cordyceps sinensis* distributed in southwestern China. *Mycoscience* **2001**, *42*, 567–574. https://doi.org/10.1007/BF02460956.
20. Jiang, Y.; Yao, Y.-J. A review for the debating studies on the anamorph of *Cordyceps sinensis*. *Mycosistema* **2003**, *22*, 161–176.
21. Chen, Y.-Q.; Hu, B.; Xu, F.; Zhang, W.; Zhou, H.; Qu, L.-H. Genetic variation of *Cordyceps sinensis*, a fruit-body-producing entomopathogenic species from different geographical regions in China. *FEMS Microbiol. Lett.* **2004**, *230*, 153–158. https://doi.org/10.1016/S0378-1097(03)00889-9.

1386 22. Chen, C.-S.; Hseu, R.-S.; Huang, C.-T. Quality Control of *Cordyceps sinensis* Teleomorph, Anamorph, and Its Products,
1387 Chapter 12. In *Quality Control of Herbal Medicines and Related Areas*; Shoyama, Y., Ed.; InTech: Rijeka, Croatia, **2011**; pp.
1388 223–238. Available online: www.intechopen.com (accessed on 3 May 2024).
1389 23. Stensrud, Ø.; Hywel-Jones, N.L.; Schumacher, T. Towards a phylogenetic classification of Cordyceps: ITS nrDNA
1390 sequence data confirm divergent lineages and paraphyly. *Mycol. Res.* **2005**, *109*, 41–56.
1391 https://doi.org/10.1017/s095375620400139x.
1392 24. Stensrud, Ø.; Schumacher, T.; Shalchian-Tabrizi, K.; Svegardenib, I.B.; Kauserud, H. Accelerated nrDNA evolution and
1393 profound AT bias in the medicinal fungus *Cordyceps sinensis*. *Mycol. Res.* **2007**, *111*, 409–415.
1394 https://doi.org/10.1016/j.mycres.2007.01.015.
1395 25. Leung, P.-H.; Zhang, Q.-X.; Wu, J.-Y. Mycelium cultivation, chemical composition and antitumour activity of a
1396 *Tolypocladium* sp. fungus isolated from wild *Cordyceps sinensis*. *J. Appl. Microbiol.* **2006**, *101*, 275–283.
1397 https://doi.org/10.1111/j.1365-2672.2006.02930.x.
1398 26. Zhu J-S, Guo Y-L, Yao Y-S, Zhou Y-J, Lu J-H, Qi Y, Chen W, Zheng T-Y, Zhang L, Wu Z-M, Zhang L-J, Liu X-J, Yin W-T.
1399 Maturation of *Cordyceps sinensis* associates with co-existence of *Hirsutella sinensis* and *Paecilomyces hepiali* DNA and
1400 dynamic changes in fungal competitive proliferation predominance and chemical profiles. *J. Fungal Res*. **2007**, 5(4), 214–
1401 224.
1402 27. Zhu, J.-S.; Gao, L.; Li, X.-H.; Yao, Y.-S.; Zhou, Y.-J.; Zhao, J.-Q.; Zhou, Y.-J. Maturational alterations of oppositely orientated
1403 rDNA and differential proliferations of CG:AT-biased genotypes of *Cordyceps sinensis* fungi and *Paecilomyces hepiali* in
1404 natural *C.* sinensis. *Am. J. Biomed. Sci.* **2010**, *2*, 217–238. https://doi.org/10.5099/aj100300217.
1405 28. Yang, J.-L.; Xiao, W.; He, H.-X.; Zhu, H.-X.; Wang, S.-F.; Cheng, K.-D.; Zhu, P. Molecular phylogenetic analysis of
1406 *Paecilomyces hepiali* and *Cordyceps sinensis*. *Acta Pharmaceut. Sinica.* **2008**, *43*, 421–426.
1407 29. Yang, J.-Y.; Tong, X.-X.; He, C.-Y.; Bai, J.; Wang, F.; Guo, J.-L. Comparison of endogenetic microbial community diversity
1408 between wild *Cordyceps sinensis*, artificial *C. sinensis* and habitat soil. *Chin. J. Chin. Mater. Medica* **2021**, *46*, 3106–3115.
1409 30. Xiao, W.; Yang, J.-P.; Zhu, P.; Cheng, K.-D.; He, H.-X.; Zhu, H.-X.; Wang, Q. Non-support of species complex hypothesis
1410 of *Cordyceps sinensis* by targeted rDNA-ITS sequence analysis. *Mycosystema* **2009**, *28*, 724–730.
1411 31. Zhang, Y.-J.; Sun, B.-D.; Zhang, S.; Wàngmǔ Liu, X.-Z.; Gong, W.-F. Mycobiotal investigation of natural *Ophiocordyceps*
1412 *sinensis* based on culture-dependent investigation. *Mycosistema* **2010a**, *29*, 518–527.
1413 32. Zhang, Y.-J.; Zhang, S.; Wàngmǔ; Bai, F.-Y.; Liu, X.-Z. High Diversity of the Fungal Community Structure in Naturally-
1414 Occurring *Ophiocordyceps sinensis*. *PLoS ONE* **2010b**, 5(12), e15570. doi:10.1371/journal.pone.0015570
1415 33. Zhang, S.-W.; Cen, K.; Liu, Y.; Zhou, X.-W.; Wang, C.-S. Metatranscriptomics analysis of the fruiting caterpillar fungus
1416 collected from the Qinghai-Tibetan plateau. *Sci. Sinica Vitae* **2018**, *48*, 562–570.
1417 34. Barseghyan, G.S.; Holliday, J.C.; Price, T.C.; Madison, L.M.; Wasser, S.P. Growth and cultural-morphological
1418 characteristics of vegetative mycelia of medicinal caterpillar fungus *Ophiocordyceps sinensis* G.H. Sung et al. (Ascomycetes)
1419 Isolates from Tibetan Plateau (P. R. China). *Intl. J. Med. Mushrooms* **2011**, *13*, 565–581.
1420 https://doi.org/10.1615/intjmedmushr.v13.i6.90.
1421 35. Gao, L., Li, X.-H., Zhao, J.-Q., Lu, J.-H., Zhao, J.-G., Zhu, J.-S. Maturation of *Cordyceps sinensis* associates with alterations
1422 of fungal expressions of multiple *Ophiocordyceps sinensis* mutants with transition and transversion point mutations in
1423 stroma of *Cordyceps sinensis*. *Beijing Da Xue Xue Bao*. **2012**, *44*, 454–463. doi: 10.3969/j.issn.1671-167X.2012.03.025
1424 36. Li, Y.; Jiao, L.; Yao, Y.-J. Non-concerted ITS evolution in fungi, as revealed from the important medicinal fungus
1425 *Ophiocordyceps sinensis*. *Mol. Phylogenet. Evol.* **2013**, *68*, 373–379. https://doi.org/10.1016/j.ympev.2013.04.010.
1426 37. Li, Y.-L.; Yao, Y.-S.; Zhang, Z.-H.; Xu, H.-F.; Liu, X.; Ma, S.-L.; Wu, Z.-M.; Zhu, J.-S. Synergy of fungal complexes isolated
1427 from the intestines of *Hepialus lagii* larvae in increasing infection potency. *J. Fungal Res.* **2016b**, *14*, 96–112.
1428 38. Li X-Z, Li Y-L, Yao Y-S, Xie W-D, Zhu J-S. Further discussion with Li *et al*. (2013, 2019) regarding the "ITS pseudogene
1429 hypothesis" for *Ophiocordyceps sinensis*. *Mol. Phylogenet. Evol*. **2020b**, *146*, 106728.
1430 https://doi.org/10.1016/j.ympev.2019.106728

1431 39. Meng, Q.; Yu, H.-Y.; Zhang, H.; Zhu, W.; Wang, M.-L.; Zhang, J.-H.; Zhou, G.-L.; Li, X.; Qin, Q.-L.; Hu, S.-N.; et al.
1432 Transcriptomic insight into the immune defenses in the ghost moth, Hepialus xiaojinensis, during an *Ophiocordyceps*
1433 *sinensis* fungal infection. Insect Biochem. *Mol. Biol.* **2015**, *64*, 1–15. https://doi.org/10.1016/j.ibmb.2015.06.014.
1434 40. Xia, F.; Liu, Y.; Shen, G.-L.; Guo, L.-X.; Zhou, X.-W. Investigation and analysis of microbiological communities in natural
1435 *Ophiocordyceps sinensis*. *Can. J. Microbiol.* **2015**, *61*, 104–111. https://doi.org/10.1139/cjm-2014-0610.
1436 41. Xia, F.; Liu, Y.; Guo, L.-X.; Shen, G.-L.; Lin, J.; Zhou, X.-W. Pyrosequencing analysis revealed complex endogenetic
1437 microorganism community from natural DongChong XiaCao and its microhabitat. *BMC Microbiol*. **2016**, *16*, 196. DOI
1438 10.1186/s12866-016-0813-5
1439 42. Guo, M.-Y.; Liu, Y.; Gao, Y.-H.; Jin, T.; Zhang, H.-B.; Zhou, X.-W. Identification and bioactive potential of endogenetic
1440 fungi isolated from medicinal caterpillar fungus *Ophiocordyceps sinensis* from Tibetan Plateau. *Int. J. Agric. Biol.* **2017**, *19*,
1441 307–313. https://doi.org/10.17957/IJAB/15.0281.
1442 43. Zhong, X.; Gu, L.; Wang, H.-Z.; Lian, D.-H.; Zheng, Y.-M.; Zhou, S.; Zhou, W.; Gu, J.; Zhang, G.; Liu, X. Profile of
1443 *Ophiocordyceps sinensis* transcriptome and differentially expressed genes in three different mycelia, sclerotium and fruiting
1444 body developmental stages. *Fungal Biol.* **2018**, *122*, 943–951. https://doi.org/10.1016/j.funbio.2018.05.011.
1445 44. Kang, Q.; Zhang, J.; Chen, F.; Dong, C.; Qin, Q.; Li, X.; Wang, H.; Zhang, H.; Meng, Q. Unveiling mycoviral diversity in
1446 *Ophiocordyceps sinensis* through transcriptome analyses. *Front. Microbiol.* **2024**, *15*, 1493365.
1447 https://doi.org/10.3389/fmicb.2024.1493365.
1448 45. Wei, X.-L.; Yin, X.-C.; Guo, Y.-L.; Shen, N.-Y.; Wei, J.-C. Analyses of molecular systematics on *Cordyceps sinensis* and its
1449 related taxa. *Mycosystema* **2006**, *25*, 192–202.
1450 46. Wei, J.-C.; Wei, X.-L.; Zheng, W.-F.; Guo, W.; Liu, R.-D. Species identification and component detection of *Ophiocordyceps*
1451 *sinensis* cultivated by modern industry. *Mycosystema* **2016**, *35*, 404–410.
1452 47. Lu, D. Western records and studies of the Chinese caterpillar fungus to the beginning of the 20th century. *J. Fungal. Res.*
1453 **2014**, *12*, 233–244. https://doi.org/10.13341/j.jfr.2014.0043.
1454 48. Sung, G.-H.; Hywel-Jones, N.L.; Sung, J.-M.; Luangsa-ard, J.J.; Shrestha, B.; Spatafora, J.W. Phylogenetic classification of
1455 *Cordyceps* and the clavicipitaceous fungi. *Stud. Mycol.* **2007**, *57*, 5–59. https://doi.org/10.3114/sim.2007.57.01.
1456 49. Zhang, Y.-J.; Li, E.-W.; Wang, C.-S.; Li, Y.-L.; Liu, X.-Z. *Ophiocordyceps sinensis*, the flagship fungus of China: Terminology,
1457 life strategy and ecology. *Mycology* **2012**, *3*, 2–10. https://doi.org/10.1080/21501203.2011.654354.
1458 50. Wang, Y.; Stata, M.; Wang, W.; Stajich, J.E.; White, M.M.; Moncalvo, J.M. Comparative genomics reveals the core gene
1459 toolbox for the fungus-insect symbiosis. *mBio* **2018**, *9*, e00636-e18. https://doi.org/10.1128/mBio.00636-18.
1460 51. Li, X.-Z.; Li, Y.-L.; Liu, W.; Zhu, J.-S. Altered stereostructures of the DNA-binding domains of variant mating proteins of
1461 *Ophiocordyceps sinensis* and the wild insect–fungal complex. *Biol. (Basel).* **2026**, *15(2)*, 186.
1462 https://doi.org/10.3390/biology15020186
1463 52. Zhang, S.; Zhang, Y.-J.; Shrestha, B.; Xu, J.-P.; Wang, C.-S.; Liu, X.-Z. *Ophiocordyceps sinensis* and *Cordyceps militaris*:
1464 Research advances, issues and perspectives. *Mycosystema* **2013**, *32*, 577–597.
1465 53. Hawksworth, D.L.; Crous, P.W.; Redhead, S.A.; Reynolds, D.R.; Samson, R.A.; Seifert, K.A.; Taylor, J.W.; Wingfield, M.J.;
1466 Abaci, Ö.; Aime, C.; et al. The Amsterdam declaration on fungal nomenclature. *IMA Fungus* **2011**, *2*, 105–112.
1467 https://doi.org/10.5598/imafungus.2011.02.01.14.
1468 54. Taylor JW. One Fungus = One Name: DNA and fungal nomenclature twenty years after PCR. *IMA Fungus*. **2011**, *2(2)*,
1469 113–120. doi:10.5598/imafungus.2011.02.02.01
1470 55. Yao, Y.-S.; Zhu, J.-S. Indiscriminate use of the Latin name for natural *Cordyceps sinensis* and *Ophiocordyceps sinensis* fungi.
1471 *Chin. J. Chin. Mater. Med*. **2016**, *41*(7), 1316–1366.
1472 56. Turgeon, B.G.; Yoder, O.C. Proposed nomenclature for mating type genes of filamentous ascomycetes. *Fungal Genet. Biol.*
1473 **2000**, *31*, 1–5. https://doi.org/10.1006/fgbi.2000.1227.
1474 57. Debuchy, R.; Turgeo, B.G. Mating-Type Structure, Evolution, and Function in Euascomycetes. In *Growth, Differentiation*
1475 *and Sexuality*; Kües, U., Fischer, R., Eds.; Springer: Berlin/Heidelberg, Germany, 2006; pp. 293–323.

58. Jones, S.K.; Bennett, R.J. Fungal mating pheromones: Choreographing the dating game. *Fungal Genet. Biol.* **2011**, *48*, 668–676. https://doi.org/10.1016/j.fgb.2011.04.001.
59. Zheng, P.; Wang, C.-S. Sexuality Control and Sex Evolution in Fungi. *Sci. Sin. Vitae* **2013**, *43*, 1090–1097.
60. Wilson, A.M.; Wilken, P.M.; van der Nest, M.A.; Steenkamp, E.T.; Wingfield, M.J.; Wingfield, B.D. Homothallism: An umbrella term for describing diverse sexual behaviours. *IMA Fungus* **2015**, *6*, 207–214. https://doi.org/10.5598/imafungus.2015.06.01.13.
61. Sun, S.; Coelho, M.A.; David-Palma, M.; Priest, S.J.; Heitman, J. The evolution of sexual reproduction and the mating-type locus: Links to pathogenesis of *Cryptococcus* human pathogenic fungi. *Annu. Rev. Genet.* **2019**, *53*, 417–444. https://doi.org/10.1146/annurev-genet-120116-024755.
62. Ramšak, B.; Kűck, U.; Hofmann, E. The mating type transcription factor MAT1-1-1 from the fungal human pathogen *Aspergillus fumigatus*: Synthesis, purification, and crystallization of the DNA binding domain. *bioRxiv* **2021**. https://doi.org/10.1101/2021.12.13.472399.
63. Ramšak, B.; Kück, U. The *Penicillium chrysogenum* tom1 gene a major target of transcription factor MAT1-1-1 encodes a nuclear protein involved in sporulation. *Front. Fungal Bio.* **2022**, *3*, 937023. https://doi.org/10.3389/ffunb.2022.937023.
64. Metin, B.; Findley, K.; Heitman, J. The mating type locus (MAT) and sexual reproduction of *Cryptococcus heveanensis*: Insights into the evolution of sex and sex-determining chromosomal regions in fungi. *PLoS Genet.* **2010**, *6*, e1000961. https://doi.org/10.1371/journal.pgen.1000961.
65. Hu, X.; Zhang, Y.-J.; Xiao, G.-H.; Zheng, P.; Xia, Y.-L.; Zhang, X.-Y.; St Leger, R.J.; Liu, X.-Z.; Wang, C.-S. Genome survey uncovers the secrets of sex and lifestyle in caterpillar fungus. *Chin. Sci. Bull.* **2013**, *58*, 2846–2854. https://doi.org/10.1007/s11434-013-5929-5.
66. Li, X.; Wang, F.; Liu, Q.; Li, Q.-P.; Qian, Z.-M.; Zhang, X.-L.; Li, K.; Li, W.-J.; Dong, C.-H. Developmental transcriptomics of Chinese cordyceps reveals gene regulatory network and expression profiles of sexual development-related genes. *BMC Genom.* **2019**, *20*, 337. https://doi.org/10.1186/s12864-019-5708-z.
67. Li, X.-Z.; Li, Y.-L.; Zhu, J.-S. Differential transcription of mating-type genes during sexual reproduction of natural *Cordyceps sinensis*. *Chin. J. Chin. Mater. Medica* **2023c**, *48*, 2829–2840. https://doi.org/10.19540/j.cnki.cjcmm.20230213.102.
68. Li, X.-Z.; Xiao, M.-J.; Li, Y.-L.; Gao, L.; Zhu, J.-S. Mutations and differential transcription of mating-type and pheromone receptor genes in *Hirsutella sinensis* and the natural *Cordyceps sinensis* insect–fungi complex. *Biology* **2024b**, *13*, 632. https://doi.org/10.3390/biology13080632.
69. Li, X.-Z.; Li, Y.-L.; Zhu, J.-S. Three-dimensional structural heteromorphs of mating-type proteins in *Hirsutella sinensis* and the natural *Cordyceps sinensis* insect–fungal complex. *J. Fungi.* **2025**, *11*, 244. https://doi.org/10.3390/jof11040244.
70. Zhang, Y.-J.; Xu, L.-L.; Zhang, S.; Liu, X.-Z.; An, Z.-Q.; Wàngmǔ Guo, Y.-L. Genetic diversity of *Ophiocordyceps sinensis*, a medicinal fungus endemic to the Tibetan Plateau: Implications for its evolution and conservation. *BMC Evol. Biol.* **2009**, *9*, 290. doi:10.1186/1471-2148-9-290
71. Zhang, S.; Zhang, Y.-J.; Liu, X.-Z.; Wen, H.-A.; Wang, M.; Liu, D.-S. Cloning and analysis of the MAT1-2-1 gene from the traditional Chinese medicinal fungus *Ophiocordyceps sinensis*. *Fungal Biol.* **2011**, *115*, 708–714.
72. Zhang, S.; Zhang, Y.-J. Molecular evolution of three protein-coding genes in the Chinese caterpillar fungus *Ophiocordyceps sinensis*. *Microbiol. China.* **2015**, *42*, 1549–1560.
73. Kyte, J.; Doolittle, R.F. A simple method for displaying the hydropathic character of a protein. *J. Mol. Biol.* **1982**, *157*, 105–132. https://doi.org/10.1016/0022-2836(82)90515-0.
74. Deleage, G.; Roux, B. An algorithm for protein secondary structure prediction based on class prediction. *Protein Eng. Des. Sel.* **1987**, *1*, 289–294. https://doi.org/10.1093/protein/1.4.289.
75. Gasteiger, E.; Hoogland, C.; Gattiker, A.; Duvaud, S.; Wilkins, M.R.; Appel, R.D.; Bairoch, A. Protein Identification and Analysis Tools on the ExPASy Server, Chapter 52. In *The Proteomics Protocols Handbook*; Walker, J.M., Ed.; Humana Press: Totowa, NJ, USA, **2005**; pp. 571–607.
76. Peters, C.; Elofsson, A. Why is the biological hydrophobicity scale more accurate than earlier experimental hydrophobicity scales? *Proteins* **2014**, *82*, 2190–2198. https://doi.org/10.1002/prot.24582.

1522 77. Simm, S.; Einloft, J.; Mirus, O.; Schleiff, E. 50 years of amino acid hydrophobicity scales, revisiting the capacity for peptide
1523 classification. *Biol. Res.* **2016**, *49*, 31. https://doi.org/10.1186/s40659-016-0092-5.
1524 78. Jumper, J.; Evans, R.; Pritzel, A.; Green, T.; Figurnov, M.; Ronneberger, O.; Tunyasuvunakool, K.; Bates, R.; Žídek, A.;
1525 Potapenko, A.; Bridgland, A.; Meyer, C.: Kohl, S,A,A,; Ballard, A.J.; Cowie, A.; Romera-Paredes, B.; Nikolov, S.; Jain, R.;
1526 Adler, J.; Back, T.; Petersen, S.; Reiman, D.; Clancy, E.; Zielinski, M.; Steinegger, M.; Pacholska, M.; Berghammer, T.;
1527 Bodenstein; S.; Silver, D.; Vinyals, O.; Senior, A.W.; Kavukcuoglu, K.; Kohli, P.; Hassabis, D. Highly accurate protein
1528 structure prediction with AlphaFold. *Nature* **2021**, *596*, 583–589. https://doi.org/10.1038/s41586-021-03819-2.
1529 79. Tunyasuvunakool, K.; Adler, J.; Wu, Z.; Green, T.; Zielinski, M.; Žídek, A.; Bridgland, A.; Cowie, A.; Meyer, C.; Laydon,
1530 A.; Velankar S, Kleywegt GJ, Bateman A, Evans R, Pritzel A, Figurnov M, Ronneberger O, Bates R, Kohl SAA, Potapenko
1531 A, Ballard AJ, Romera-Paredes B, Nikolov S, Jain R, Clancy E, Reiman D, Petersen S, Senior AW, Kavukcuoglu K, Birney
1532 E, Kohli P, Jumper J, Hassabis D. Highly accurate protein structure prediction for the human proteome. *Nature* **2021**, *596*,
1533 590–596. https://doi.org/10.1038/s41586-021-03828-1.
1534 80. David, A.; Islam, S.; Tankhilevich, E.; Sternberg, M.J.E. The AlphaFold Database of Protein Structures, A Biologist's Guide.
1535 *J. Mol. Biol.* **2022**, *434*, 167336. https://doi.org/10.1016/j.jmb.2021.167336.
1536 81. Monzon, V.; Haft, D.H.; Bateman, A. Folding the unfoldable, using AlphaFold to explore spurious proteins. *Bioinform.*
1537 *Adv.* **2022**, *1*, vbab043. https://doi.org/10.1093/bioadv/vbab043.
1538 82. Rettie, S.A.; Campbell, K.V.; Bera, A.K.; Kang, A.; Kozlov, S.; De La Cruz, J.; Adebomi, V.; Zhou, G.; DiMaio, F.;
1539 Ovchinnikov, S.; et al. Cyclic peptide structure prediction and design using AlphaFold. *bioRxiv* **2023**, 26:2023.02.25.529956.
1540 https://doi.org/10.1101/2023.02.25.529956.
1541 83. Xu, T.; Xu, Q.; Li, J.-Y. Toward the appropriate interpretation of Alphafold2. *Front. Artif. Intell.* **2023b**, *6*, 1149748.
1542 https://doi.org/10.3389/frai.2023.1149748.
1543 84. Abramson, J.; Adler, J.; Dunger, J.; Evans, R.; Green, T.; Pritzel, A.; Ronneberger, O.; Willmore, L.; Ballard, A.J.; Bambrick,
1544 J.; Bodenstein SW, Evans DA, Hung CC, O'Neill M, Reiman D, Tunyasuvunakool K, Wu Z, Žemgulytė A, Arvaniti E,
1545 Beattie C, Bertolli O, Bridgland A, Cherepanov A, Congreve M, Cowen-Rivers AI, Cowie A, Figurnov M, Fuchs FB,
1546 Gladman H, Jain R, Khan YA, Low CMR, Perlin K, Potapenko A, Savy P, Singh S, Stecula A, Thillaisundaram A, Tong C,
1547 Yakneen S, Zhong ED, Zielinski M, Žídek A, Bapst V, Kohli P, Jaderberg M, Hassabis D, Jumper JM. Accurate structure
1548 prediction of biomolecular interactions with AlphaFold 3. *Nature* **2024**, *630*, 493–500. https://doi.org/10.1038/s41586-024-
1549 07487-w.
1550 85. Varadi, M.; Bertoni, D.; Magana, P.; Paramval, U.; Pidruchna, I.; Radhakrishnan, M.; Tsenkov, M.; Nair, S.; Mirdita, M.;
1551 Yeo, J.; et al. AlphaFold Protein Structure Database in 2024, providing structure coverage for over 214 million protein
1552 sequences. *Nucleic Acids Res.* **2024**, *52*, D368–D375. https://doi.org/10.1093/nar/gkad1011.
1553 86. Wroblewski, K.; Kmiecik, S. Integrating AlphaFold pLDDT Scores into CABS-flex for enhanced protein flexibility
1554 simulations. *Comput. Struct. Biotechnol. J.* **2024**, *30*, 4350–4356. https://doi.org/10.1016/j.csbj.2024.11.047.
1555 87. Li, X.-Z.; Li, Y.-L.; Zhu, J.-S. Three-dimensional structural heteromorphs of mating-type proteins in *Hirsutella sinensis* and
1556 the natural *Cordyceps sinensis* insect–fungal complex. *J. Fungi.* **2025**, *11*, 244. https://doi.org/10.3390/jof11040244.
1557 88. Yang, X.; Zhu, H.-Q.; Shi, L.-X.; Song, T.-G.; Gong, W.-B.; He, S.-M.; Shan, S.; Xu, C.-F.; Zhou, Z. AlphaFold-guided
1558 structural analyses of nucleosome binding proteins. *Nucleic Acids Res.* **2025**, *53*, gkaf735.
1559 https://doi.org/10.1093/nar/gkaf735.
1560 89. Mariani, V.; Biasini, M.; Barbato, A.; Schwede, T. lDDT, a local superposition-free score for comparing protein structures
1561 and models using distance difference tests. *Bioinformatics* **2013**, *29*, 2722–2728.
1562 https://doi.org/10.1093/bioinformatics/btt473.
1563 90. Baxevanis, A.D.; Bryant, S.H.; Landsman, D. Homology model building of the HMG-1 box structural domain. *Nucleic*
1564 *Acids Res.* **1995**, *23*, 1019–1029. https://doi.org/10.1093/nar/23.6.1019.
1565 91. Thapar, R. Structure-specific nucleic acid recognition by L-motifs and their diverse roles in expression and regulation of
1566 the genome. *Biochim. Biophys. Acta* **2015**, *1849*, 677–687. https://doi.org/10.1016/j.bbagrm.2015.02.006.

1567 92. White, T.J., Bruns, T., Lee, S., Taylor, J.W. Amplification and direct sequencing of fungal ribosomal RNA genes for
1568 phylogenetics. In: Innis, M.A., Gelfand, D.H., Sninsky, J.J., White, T.J. (Eds.), PCR Protocols, A Guide to Methods and
1569 Applications. Academic Press, London, 1990; pp. 315–322.
1570 93. Li, Y.; Hsiang, T.; Yang, R.-H.; Hu, X.-D.; Wang, K.; Wang, W.-J.; Wang, X.-L.; Jiao, L.; Yao, Y.-J. Comparison of different
1571 sequencing and assembly strategies for a repeat-rich fungal genome, *Ophiocordyceps sinensis*. *J. Microbiol. Methods* **2016a**,
1572 *128*, 1–6. https://doi.org/10.1016/j.mimet.2016.06.025.
1573 94. Jin, L.-.Q.; Xu, Z.-.W.; Zhang, B.; Yi, M.; Weng, C.-.Y.; Lin, S.; Wu, H.; Qin, X.-T.; Xu, F.; Teng, Y.; Yuan, S.-J.; Liu, Z.-Q.;
1574 Zheng, Y.-G. Genome sequencing and analysis of fungus *Hirsutella sinensis* isolated from *Ophiocordyceps sinensis*. *AMB*
1575 *Expr.* **2020**, *10*, 105. https://doi.org/10.1186/s13568-020-01039-x.
1576 95. Liu, J.; Guo, L.-N.; Li, Z.-W.; Zhou, Z.; Li, Z.; Li, Q.; Bo, X.-C.; Wang, S.-Q.; Wang, J.-L.; Ma, S.-C.; Zheng J, Yang Y. Genomic
1577 analyses reveal evolutionary and geologic context for the plateau fungus *Ophiocordyceps sinensis*. *Clin. Med.* **2020**, *15*, 107–
1578 119. https://doi.org/10.1186/s13020-020-00365-3.
1579 96. Shu, R.-H.; Zhang, J.-H.; Meng, Q.; Zhang, H.; Zhou, G.-L.; Li, M.-M.; Wu, P.-P.; Zhao, Y.-N.; Chen, C.; Qin, Q.-L. A new
1580 high-quality draft genome assembly of the Chinese cordyceps *Ophiocordyceps sinensis*. *Genome Biol. Evol.* **2020**, *12*, 1074–
1581 1079. https://doi.org/10.1093/gbe/evaa112.
1582 97. Martin, T.; Lu, S.-W.; van Tilbeurgh, H.; Ripoll, D.R.; Dixelius, C.; Dixelius, C.; Turgeon, B.G.; Debuchy, R. Tracing the
1583 Origin of the Fungal a1 Domain Places Its Ancestor in the HMG-Box Superfamily, Implication for Fungal Mating-Type
1584 Evolution. *PLoS ONE* **2010**, *5*, e15199. https://doi.org/10.1371/journal.pone.0015199.
1585 98. Czaja, W.; Miller, K.Y.; Miller, B.L. Complex mechanisms regulate developmental expression of the matA (HMG) mating
1586 type gene in homothallic *Aspergillus* nidulans. *Genetics*. **2011**, *189*, 795-808. doi: 10.1534/genetics.111.131458
1587 99. Angelini, R.M.D.M., Rotolo, C., Pollastro, S., Faretra, F. Molecular analysis of the mating type (*MAT1*) locus in strains of
1588 the heterothallic ascomycete *Botrytis cinerea*. *Plant Pathol*. **2016**, *65*, 1221-1400. https://doi.org/10.1111/ppa.12509.
1589 100. Poveda-Huertes, D., Matic, S., Marada, A., Habernig, L., Licheva, M., Myketin, L., Gilsbach, R., Tosal-Castano S, Papinski
1590 D, Mulica P, Kretz O, Kücükköse C, Taskin AA, Hein L, Kraft C, Büttner S, Meisinger C, Vögtle FN. An Early mtUPR:
1591 Redistribution of the Nuclear Transcription Factor Rox1 to Mitochondria Protects against Intramitochondrial Proteotoxic
1592 Aggregates. *Mol Cell*. **2020**, *77(1)*, 180-188. doi: 10.1016/j.molcel.2019.09.026
1593 101. Hansen, F.T., Madsen, C.K., Nordland, A.M., Grasser, M., Merkle, T., Grasser, K.D. A novel family of plant DNA-binding
1594 proteins containing both HMG-box and AT-rich interaction domains. *Biochemistry*. **2008**; *47*, 13207–13214. doi:
1595 10.1021/bi801772k
1596 102. Rajewska, M., Wegrzyn, K., Konieczny, I. AT-rich region and repeated sequences - the essential elements of replication
1597 origins of bacterial replicons. *FEMS Microbiol Rev*. **2012**, *36(2)*, 408–434. doi: 10.1111/j.1574-6976.2011.00300.x
1598 103. Jackson, D.; Lawson, T.; Villafane, R.; Gary, L. Modeling the structure of yeast MATα1, An HMG-Box motif with a C-
1599 terminal helical extension. *Open J. Biophys.* **2013**, *3*, 1–12. https://doi.org/10.4236/ojbiphy.2013.31001.
1600 104. Zheng, P.; Xia, Y.-L.; Zhang, S.-W.; Wang, C.-S. Genetics of Cordyceps and related fungi. *Appl Microbiol Biotechnol*, **2013a**,
1601 *97*, 2797–2804. doi: 10.1007/s00253-013-4771-7
1602 105. Kim, H.-K.; Jo, S.-M.; Kim, G.-Y.; Kim, D.-W.; Kim, Y.-K.; Yun, S.-H. A large-scale functional analysis of putative target
1603 genes of mating-type loci provides insight into the regulation of sexual development of the cereal pathogen *Fusarium*
1604 *graminearum*. *PLoS Genet.* **2015**, *11*, e1005486. https://doi.org/10.1371/journal.pgen.1005486.
1605 106. Ramšak, B.; Markau, J.; Pazen, T.; Dahlmann, T.A.; Krappmann, S.; Kűck, U. The master regulator MAT1-1-1 of fungal
1606 mating binds to its targets via a conserved motif in the human pathogen *Aspergillus fumigatus*. *G3 Genes Genom. Genet.*
1607 **2020**, *11*, jkaa012. https://doi.org/10.1093/g3journal/jkaa012.
1608 107. Yamamoto, A.; Ando, Y.; Yoshioka, K.; Saito, K.; Tanabe, T.; Shirakawa, H.; Yoshida, M. Difference in affinity for DNA
1609 between HMG proteins 1 and 2 determined by surface plasmon resonance measurements. *J. Biochem.* **1997**, *122*, 586–594.
1610 https://doi.org/10.1093/oxfordjournals.jbchem.a021793. PMID 9348088.

108. Ait Benkhali, J.; Coppin, E.; Brun, S.; Peraza-Reyes, L.; Martin, T.; Dixelius, C.; Lazar, N.; van Tilbeurgh, H.; Debuchy, R. A Network of HMG-box Transcription Factors Regulates Sexual Cycle in the Fungus Podospora anserina. *PLoS Genet.* **2013**, *9*, e1003642. https://doi.org/10.1371/journal.pgen.1003642.
109. Balasubramanian, B.; Lowry, C.V.; Zitomer, R.S. The Rox1 repressor of the *Saccharomyces cerevisiae* hypoxic genes is a specific DNA-binding protein with a high-mobility-group motif. *Mol. Cell Biol.* **1993**, *13*, 6071–6078. https://doi.org/10.1128/mcb.13.10.6071-6078.1993.
110. Zitomer, R.S.; Limbach, M.P.; Rodriguez-Torres, A.M.; Balasubramanian, B.; Deckert, J.; Snow, P.M. Approaches to the study of Rox1 repression of the hypoxic genes in the yeast Saccharomyces cerevisiae. *Methods* **1997**, *11*, 279–288. https://doi.org/10.1006/meth.1996.0422.
111. Zheng, Q.; Hou, R.; Zhang, J.-Y.; Ma, J.; Ma, J.-W.; Wu, Z.-S.; Wang, G.-H.; Wang, C.-F.; Xu, J.-R. The MAT locus genes play different roles in sexual reproduction and pathogenesis in *Fusarium graminearum*. *PLoS ONE.* **2013b**, *8*, e66980. https://doi.org/10.1371/journal.pone.0066980.
112. Kastaniotis, A.J.; Zitomer, R.S. Oxygen Dependent Repression in Yeast. In *Rox1 Mediated Repression*; Advances in Experimental Medicine and Biology; Springer Nature: Cham, Switzerland, 2000; Volume 475, pp. 185–195. https://doi.org/10.1007/0-306-46825-5_18.
113. Kües, U.; Casselton, L.A. The origin of multiple mating types in mushrooms. *J. Cell Sci.* **1993**, *104*, 227–230. https://doi.org/10.1242/jcs.104.2.227.
114. Asante-Owusu, R.N.; Banham, A.H.; Böhnert, H.U.; Mellor, E.J.C.; Casselton, L.A. Heterodimerization between two classes of homeodomain proteins in the mushroom *Coprinus cinereus* brings together potential DNA-binding and activation domains. *Gene* **1996**, *172*, 25–31. https://doi.org/10.1016/0378-1119(96)00177-1.
115. Jacobsen, S.; Wittig, M.; Pöggeler, S. Interaction Between Mating-Type Proteins from the Homothallic Fungus Sordaria macrospora. *Curr. Genet.* **2002**, *41*, 150–158. https://doi.org/10.1007/s00294-002-0276-0.
116. Hancock, S.P.; Cascio, D.; Johnson, R.C. Cooperative DNA binding by proteins through DNA shape complementarity. *Nucleic Acids Res.* **2019**, *47*, 8874–8887. https://doi.org/10.1093/nar/gkz642.
117. Mao, X.-M.; Zhao, S.-M.; Cao, L.; Yan, X.; Han, R.-C. The morphology observation of *Ophiocordyceps sinensis* from different origins. *J. Environ. Entomol.* **2013**, *35*, 343–353.
118. Li, Y.; Yang, R.-H.; Jiang, L.; Hu, X.-D.; Wu, Z.-J.; Yao, Y.-J. rRNA Pseudogenes in Filamentous Ascomycetes as Revealed by Genome Data. *G3-Genes Genom. Genet.* **2017**, *7*, 2695–2703. https://doi.org/10.1534/g3.117.044016.
119. Li, Y.; Jiang, L.; Wang, K.; Wu, H.-J.; Yang, R.-H.; Yan, Y.-J.; Bushley, K.E.; Hawksworth, D.L.; Wu, Z.-J.; Yao, Y.-J. RIP mutated ITS genes in populations of *Ophiocordyceps sinensis* and their implications for molecular systematics. *IMA Fungus* **2020c**, *11*, 18.
120. Li, X.-Z.; Li, Y.-L.; Wang, Y.-N.; Zhu, J.-S. Translations of mutant repetitive genomic sequences in *Hirsutella sinensis* and changes in secondary structures and functional specifications of the encoded proteins. *Int. J. Mol. Sci.* **2024a**, *25*, 11178. https://doi.org/10.3390/ijms252011178.
121. Wang, Y.-B., Wang, Y., Fan, Q., Duan, D-E., Zhang, G.-D., Dai6, R.-Q., Dai, Y.-D., Zeng, W.-B. Chen, Z.-H., Li, D.-D., Tang, D.-X., Xu, Z.-H., Sun, T., Nguyen, T.-T., Tran, N.-L., Dao, V.-M., Zhang, C.-M., Huang, L.-D., Liu, Y.-J., Zhang, X.-M., Yang, D.-R., Sanjuan, T., Liu, X.-Z., Yang, Z.-L., Yu, H. Multigene phylogeny of the family Cordycipitaceae (Hypocreales): new taxa and the new systematic position of the Chinese cordycipitoid fungus *Paecilomyces hepiali*. *Fungal Diversity* **2020**, *103*, 1–46. https://doi.org/10.1007/s13225-020-00457-3.
122. Holliday, J.; Cleaver, M. Medicinal value of the caterpillar fungi species of the genus *Cordyceps* (Fr.) Link (Ascomycetes). A review. *Int. J. Med. Mushrooms* **2008**, *10*, 219–234. https://doi.org/10.1615/IntJMedMushr.v10.i3.30.
123. Stone, R. Improbable partners aim to bring biotechnology to a Himalayan kingdom. *Science* **2010**, *327*, 940–941. https://doi.org/10.1126/science.327.5968.940.
124. Qin, Q.-L.; Zhou, G.-L.; Zhang, H.; Meng, Q.; Zhang, J.-H.; Wang, H.-T.; Miao, L.; Li, X. Obstacles and approaches in artificial cultivation of Chinese cordyceps. *Mycology* **2018**, *9*, 7–9. https://doi.org/10.1080/21501203.2018.1442132.

125. Li, W.-J.; Xia, J.-M.; Li, Q.-P.; Zhang, Z.-Y.; Zhang, W.-W.; Dong, C.-H.; Wei, J.-C.; Liu, X.-Z. Developmental recording of the ghost-moth larvae after ex situ infection by *Ophiocordyceps sinensis*. *Sci. China Life Sci.* **2020a**, *63*, 1093–1095. https://doi.org/10.1007/s11427-020-1686-7. Erratum in Sci. China Life Sci. **2023b**, 66, 892. https://doi.org/10.1007/s11427-022-2232-5.
126. Quandt, C.A., Kepler, R.M., Gams, W., Araújo, J.P.M., Ban, S., Evans, H.C., Hughes, D., Humber, R., Hywel-Jones, N., Li, Z.-Z., Luangsa-ard, J.J., Rehner, S.A., Sanjuan, T., Sato, H., Shrestha, B., Sung, G.-H., Yao, Y.-J., Zare, R., Spatafora, J.W. Phylogenetic-based nomenclatural proposals for Ophiocordycipitaceae (Hypocreales) with new combinations in Tolypocladium. *IMA Fungus.* 2014, **5(***1*), 121–134. doi:10.5598/imafungus.2014.05.01.12.
127. Bennett, R.J.; Johnson, A.D. Completion of a parasexual cycle in *Candida albicans* by induced chromosome loss in tetraploid strains. *EMBO J.* **2003**, *22*, 2505–2515. https://doi.org/10.1093/emboj/cdg235.
128. Sherwood, R.K.; Bennett, R.J. Fungal meiosis and parasexual reproduction--lessons from pathogenic yeast. *Curr. Opin. Microbiol.* **2009**, *12*, 599–607. https://doi.org/10.1016/j.mib.2009.09.005.
129. Seervai, R.N.H.; Jones, S.K.; Hirakawa, M.P.; Porman, A.M.; Bennett, R.J. Parasexuality and ploidy change in *Candida tropicalis*. *Eukaryot. Cell.* **2013**, *12*, 1629–1640. https://doi.org/10.1128/EC.00128-13.
130. Nakamura, N.; Tanaka, C.; Takeuchi-Kaneko, Y. Transmission of antibiotic-resistance markers by hyphal fusion suggests partial presence of parasexuality in the root endophytic fungus Glutinomyces brunneus. *Mycol. Progress.* **2019**, *18*, 453–462. https://doi.org/10.1007/s11557-018-1455-9.
131. Du, X.-H.; Wu, D.-M.; Kang, H.; Wang, H.-C.; Xu, N.; Li, T.-T.; Chen, K.-L. Heterothallism and potential hybridization events inferred for twenty-two yellow morel species. *IMA Fungus* **2020**, *11*, 4. https://doi.org/10.1186/s43008-020-0027-1.
132. Hėnault, M.; Marsit, S.; Charron, G.; Landry, C.R. The effect of hybridization on transposable element accumulation in an undomesticated fungal species. *eLife* **2020**, *9*, e60474. https://doi.org/10.7554/eLife.60474.
133. Samarasinghe, H.; You, M.; Jenkinson, T.S.; Xu, J.-P.; James, T.Y. Hybridization Facilitates Adaptive Evolution in Two Major Fungal Pathogens. *Genes* **2020**, *11*, 101. https://doi.org/10.3390/genes11010101.
134. Mishra, A.; Forche, A.; Anderson, M.Z. Parasexuality of Candida Species. *Front. Cell. Infect. Microbiol.* **2021**, *11*, 796929. https://doi.org/10.3389/fcimb.2021.796929.
135. Steensels, J.; Gallone, B.; Verstrepen, K.J. Interspecific hybridization as a driver of fungal evolution and Adaptation. *Nat. Rev. Microbiol.* **2021**, *19*, 485–500.
136. Kück, U.; Bennett, R.J.; Wang, L.; Dyer, P.S. Editorial, Sexual and Parasexual Reproduction of Human Fungal Pathogens. *Front. Cell Infect. Microbiol.* **2022**, *12*, 934267. https://doi.org/10.3389/fcimb.2022.934267.
137. Yokoyama, E., Yamagishi, K., Hara, A, Heterothallism in *Cordyceps takaomontana*. *FEMS Microbiol Lett*. **2005**, *250(1)*, 145–150. https://doi.org/10.1016/j.femsle.2005.07.004
138. Lee SC, Ni M, Li W, Shertz C, Heitman J. The Evolution of Sex: a Perspective from the Fungal Kingdom. Microbiol *Mol Biol Rev*. **2010**, *74(2),* 298–340. doi: 10.1128/MMBR.00005-10
139. Araújo, J.P.M., Evans, H.C., Kepler, R., Hughes, D.P. Zombie-ant fungi across continents: 15 new species and new combinations within *Ophiocordyceps*. I. Myrmecophilous hirsutelloid species. *Stud Mycol*. **2018**, *90*, 119–160. doi: 10.1016/j.simyco.2017.12.002.
140. Xu M, Ashley NA, Vaghefi N, Wilkinson I, Idnurm A. Isolation of strains and their genome sequencing to analyze the mating system of *Ophiocordyceps robertsii*. *PLoS One*. **2023a**, *18(5)*, e0284978. doi: 10.1371/journal.pone.0284978
141. Zou, J.; Zhang, Y.-T.; Luo, Y.; Fu, M.-H.; Sun, B.-L.; Liu, S.-G. MAT1-1 and MAT1-2 *Ophiocordyceps xuefengensis* and comparison of their chemical composition. methods. *Biol. (Basel)* **2024**, *13(9)*, 686; https://doi.org/10.3390/biology13090686.
142. Zhou, X.W.; Li, L.J.; Tian, E.W. Advances in research of the artificial cultivation of *Ophiocordyceps sinensis* in China. *Crit. Rev. Biotechnol.* **2013**, *34*, 233–243. https://doi.org/10.3109/07388551.2013.791245.